cen2014

may 14–16

Santander (Spain)

Conferencia Española de Nanofotonica

Spanish Nanophotonics Conference

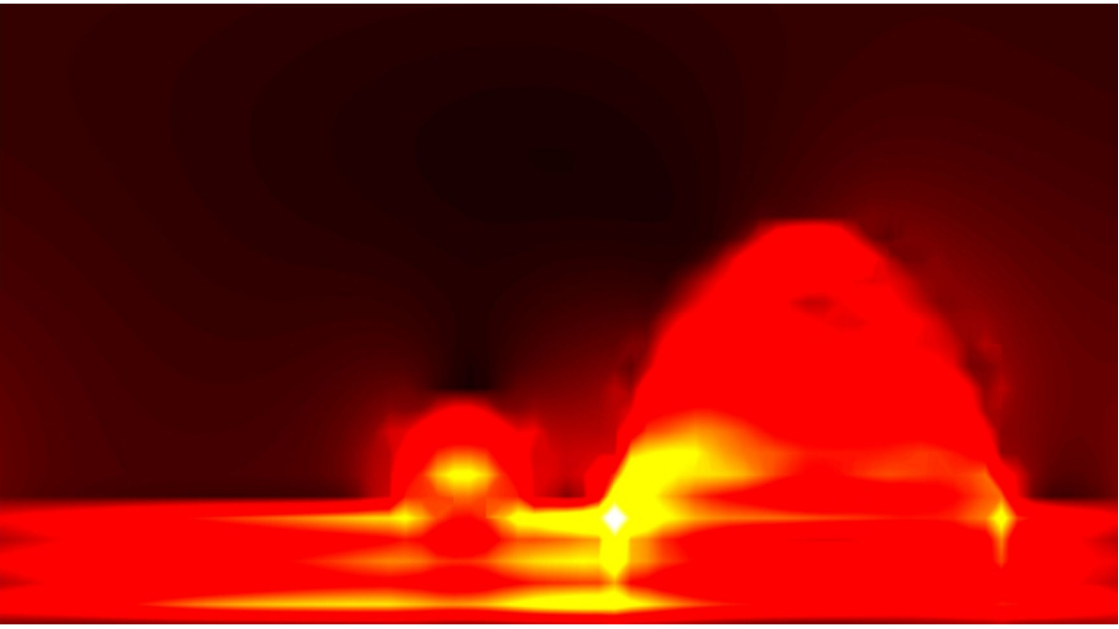

Organisers

CSIC
Consejo Superior de Investigaciones Científicas

Phantoms foundation

ICFO
Institut de Ciències Fotòniques

UAM
Universidad Autonoma de Madrid

UC
Universidad de Cantabria

Universidad de Sevilla

Universitat Rovira i Virgili

Universitat Politècnica de València

TNT2014 Barcelona Spain

October 27-31, 2014

www. tntconf.org/2014

Lead Organiser

PHANTOMS foundation

TENTATIVE PROGRAMME

Mon 27 October	Tue 28 October	Wed 29 October	Thu 30 October	Fri 31 October
Plenary Session	Graphene Plenary Session	Plenary Session		Students Track A / Students Track B
		POSTER SESSION	Plenary Session	Seniors Track A / Seniors Track B
Cocktail Lunch Poster Session				
Plenary Session	Graphene Track A / Graphene Track B	Plenary Session	Plenary Session	Plenary Session

Exhibition

Conference Dinner
Award Ceremony

CONFERENCE FEES

	Before 14 July	After 14 July
Senior	420 € +21% VAT*	505 € +21% VAT*
PhD Student	295 € +21% VAT*	355 € +21% VAT*

*Spanish VAT only applies to Spanish institutions

TNT 2014 Trends in NanoTechnology
Barcelona (Spain)
October 27-31, 2014

Index

Foreword

Following the spirit initiated by the first three editions of the "Conferencia Española de Nanofotónica", held respectively in Tarragona in 2008, Segovia in 2010 and Carmona in 2012, we launch the 4th edition that will be conducted in Santander (Spain) during May 14-16, 2014. The Conference aims to gather all the groups carrying out research in Nanophotonics in Spain (as well as somewhere else with interest in the research in Nanophotonics performed here). It intends to spread the research results achieved by all the different Spanish groups and to promote the establishment or reinforcement of contacts between them, as a mean to help the community to become more visible and dynamic.

The Conference technical program aspires to address a wide area of research related to nanophotonics, metamaterials and subwavelength optics. Topics will include all aspects of the research, ranging from fundamental science to nanofabrication or applications.

The Conference will be organized in thematic sessions composed of Keynotes / invited talks and contributed scientific communications (oral and poster).

The meeting will be structured in the following thematic lines, but interactions among them will be promoted:

1. Magnetoplasmonics and Optomechanical systems
2. Novel synthetic routes: materials aspects of photonic nanostructures
3. Colloidal nanophotonics and nanoplasmonics
4. Photonic nanostructures for energy efficient optoelectronic devices
5. Graphene and silicon photonics
6. New concepts and metamaterials
7. Near Field Optics: nanospectroscopy and nanoimaging
8. Nanophotonics for sensing

Finally, thanks must be directed to the staff of all organising institutions whose hard work has helped the smooth organisation and planning of this conference.

THE ORGANISING COMMITTEE

Organisers

Sponsors

Exhibitors

MICOS IBERIA SL
Plaça de la Vila 15, 1 A
08800 Vilanova i la Geltrú
www.pimicos.es

Micos Iberia is a supplier of high technology, specialized in the field of motion control, photonics and metrology.

The founders of Micos Iberia SL, Physik Instrumente and PI miCos, as well as the Company Qioptiq are well known for their innovative and unique products. Physik Instrumente is a world leader in developing and production of nanopositioning systems, while PI miCos is specialist in the micro positioning field. Also, Qioptic (successor of Spindler & Hoya), offers high quality optics and precision optomechanic components.

Committees

Chair

Fernando Moreno (UC)

Organizing Committee

Antonio Correia (Fundación Phantoms)
María Ujué González (IMM-CSIC)
Cefe López (ICMM-CSIC)
Ricardo Marqués (US)
Lluís Marsal (URV)
Alejandro Martínez (NTC-UPV)
Jordi Martorell (ICFO)
Hernán Míguez (ICMS-CSIC)
Pablo Aitor Postigo (IMM-CSIC)
Juan José Sáenz (UAM)
Niek van Hulst (ICFO)

Technical Committee

José Luis Roldan (Fundación Phantoms)

Local Committee

Francisco González (UC)
Dolores Ortiz (UC)
José Maria Saiz (UC)
Juan Marcos Sanz (UC)

Scientific committee

Ramón Alcubilla (UPC)
Gonçal Badenes (ICFO)
Salvador Balle (UIB)
Alvaro Blanco (ICMM-CSIC)
José M. Calleja (UAM)
Enrique Calleja (UPM)
Francesc Díaz (URV)
Concepción Domingo (IEM-CSIC)
Antonio García Martín (IMM-CSIC)
Laura Lechuga (CIN2)
Javier Marti (CTN-UPV)
Luís Martín Moreno (UZ-CSIC)
Juan Martínez-Pastor (ICMUV)
Francisco Meseguer (UPV-CSIC)
Josep Pallarés (URV)
Roman Quidant (ICFO)
Jose Sánchez-Dehesa (UPV)
José A. Sánchez Gil (IEM-CSIC)
Jan Siegel (IO-CSIC)
Mario Sorolla (UN)
Clivia Sotomayor (ICN-CIN2)
Luis Viña (UAM)

Contributions

Contributions

Index alphabetical order

I: Invited Lecture
K: Keynote Speakers
O: Oral Presentation
P: Poster Presentation

Abstracts

Critical influence of gap morphology in the optical response of ultranarrow gap-plasmonic nanoantennas

G.Aguirregabiria[1], R.Esteban[1], A.G.Borisov[2], G.W.Bryant[3], J.Aizpurua[1]

[1]Material Physics Center CSIC-UPV/EHU and Donostia International Physics Center DIPC, Paseo Manuel de Lardizabal 5, Donostia-San Sebastián 20018, Spain
[2]Institut des Sciences Moléculaires d'Orsay-UMR 8214, CNRS-Université Paris Sud, Bâtiment 351, Orsay Cedex 91405, France
[3]Quantum Measurement Division and Joint Quantum Institute, National Institute of Standards and Technology and University of Maryland, Maryland 20899-8423

garikoitz_aguirregabiria001@ehu.es
aizpurua@ehu.es

Plasmonic nanoantennas are resonant structures that support localized plasmonic modes, typically in the visible and near-infrared range of the electromagnetic spectrum, due to free-electron oscillations[1]. Plasmon resonances can be easily tuned and can concentrate incoming radiation to very small volumes. Notably, when two plasmonic particles are separated by a small gap, Coulomb interaction induces hybridized resonances that localize and enhance the field into the gap region. In this work, we demonstrate that, for very narrow separation distances, the gap morphology strongly affects the optical response. In particular, we consider linear gap antennas comprising two metallic rods, and study the difference in the optical response between spherical and flat gap ends (see sketches in Fig.1). Furthermore, we decrease the gap down to sub-nanometric distances where quantum tunneling plays an important role in the optical response of the system. To study this quantum regime, we use the Quantum Corrected Model [2,3], which enables to include electron tunneling within a classical framework [4] and therefore enables to adress large plasmonic systems.

We first consider a classical treatment of narrow gaps at large enough separation distances where electron tunneling is not present. The spherical-ended antenna (Fig.1a) behaves similarly to a metallic sphere dimer [5]. As the gap narrows, the plasmonic resonances strongly redshift showing a large extinction cross-section and very strong near-field enhancement at the gap. When the gap separation distance is equal to zero, an abrupt change in the modal distribution is clearly observed in the extinction spectrum. Once the two arms are in contact, we observe charge transfer plasmons that blueshift as the overlap increases.

The flat-gap antenna (Fig.1b), the optical response of flat-gap antennas is very different, particularly for very narrow gaps. Several longitudinal antenna modes can be observed in the extinction cross section. The dominant lowest energy mode, which is spectrally broad, also redshifts as the gap distance is reduced but this redshift saturates for very narrow gaps. The spectral position of higher order modes is hardly affected by the gap separation distance. A simple RC model is able to explain the spectral behavior and relates the modes to those of the constituent individual nanorods [5]. After contact, the resulting modes correspond to the resonances of a rod of twice the initial length. In contrast, in the nearfield spectrum at the gap two different sets of modes are clearly appreciable: (i) the longitudinal antenna modes and (ii) a set of spectrally narrow modes that strongly redshift with decreasing gap, identified as cavity modes that radiate very weakly [6,7]. We use a simple analytical expression based on the modes of a Fabry-Pérot resonator to interpret the spectral evolution of these plasmon cavity modes as the gap narrows. High order cavity modes exhibit very fast spatial variation of the fields at the gap. For narrow gaps, the longitudinal antenna modes and the cavity modes can be tuned independently by changing the respective geometrical parameter. The field enhancement is maximum when the resonant energy of a cavity mode coincides with that of an

antenna longitudinal resonance. To access this ultrananarrow gap regime at visible frequencies is very challenging experimentally since distances below 1 nm along extended areas are necessary. A situation experimentally at hand that would reproduce this behavior for larger separation distances could be obtained with use of phononic resonances in the infrared. We therefore apply the same concepts to phononic antennas made of SiC.

For distances smaller than approximately half a nanometer, electron tunneling must be considered. The main effect observed in this tunneling regime is a very strong quenching of the near-field enhancement at the gap [2,3] for both spherical-gap and flat-gap geometries. The cavity modes appear to be quenched for larger separation distances in flat gaps compared to the case of the spherical-gap antennas. Moreover, the effect of the tunneling on the extinction depends on the morphology of the gap. In the spherical case, the tunneling induces a smooth spectral transition between the modes of the nontouching situation and the charge transfer plasmons found in the particle-overlapping situation. The charge transfer plasmons already appear slightly before contact. This continuous spectral transition is in contrast with the unphysical discontinuity found within a classical treatment of the response. For the flatgap antenna however the tunneling does not appreciably change the extinction cross-section found classically.

Our work shows that the gap morphology influences dramatically the optical response of plasmonic gap nanoantennas separated by ultrashort distances not only quantitative but also qualitatively, an influence that should be considered in design strategies for sensing or spectroscopy applications. Importantly, when sub-nanometric gaps are studied, electron tunneling needs to be included in the description.

References

[1] M.Pelton, J.Aizpurua, and G.Bryant, Laser Photonics Rev. 2 (2008) 136.

[2] R.Esteban, A.G.Borisov, P.Norlander and J.Aizpurua, Nature Commun. 3 (2012) 825.

[3] K.J.Savage, M.M.Hawkeye,R.Esteban, A.G.Borisov, J.Aizpurua and J.J.Baumberg, Nature 491 (2012) 574.

[4] F.J.García de Abajo and A.Howie, Phys. Rev. B 65 (2002) 115418.

[5] J.Aizpurua, G.W.Bryant, L.J.Richter, F.J.García de Abajo, B.K.Kelley, and T.Mallouk, Phys. Rev. B 71 (2005) 235420

[6] L.Novotny, Phys. Rev. Lett. 96 (2007) 266802.

[7] B.P.Joshi and Q.-H.Wei, Opt. Express 16 (2008) 10315-10322.

Figures

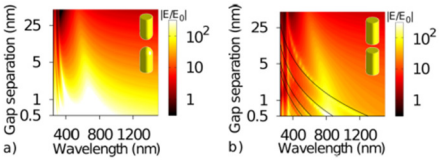

Figure 1: Near-field enhancement at the spherical-gap (a) and flat-gap (b) antennas as a function of distance and wavelength. For the distances considered in these calculations tunneling is not present. In (b), the resonant wavelength of the cavity modes, as predicted by a simple model, is labeled with black lines.

Optoelectronics in plasmonic nanogaps

Javier Aizpurua

Materials Physics Center CSIC-UPV/EHU and DIPC, Paseo Manuel Lardizabal 5, Donostia-San Sebastián, Basque Country, Spain

aizpurua@ehu.es

A plasmonic nanogap is an ideal platform to explore and test quantum effects in the optical response of nanoscale structures. As the separation between interfaces in a nanogap becomes below nanometric distances, the optical response of the system enters a strong nonlocal regime where the quantum nature inherent to the coherent oscillation of interacting electrons becomes apparent (see schematics of a typical plasmonic gap in the figure). We have developed full quantum mechanical calculations within time-dependent density functional theory (TDDFT) to address nonlocal effects in plasmonic gaps [1]. By doing so, we have identified a tunneling regime for separation distances of the interfaces below 0.5 nm, which totally modifies the spectral fingerprints of the cavity [2]. Quantum tunneling screens plasmonic modes localized at the cavity and establishes charge transfer across the gap producing lower energy modes of the optical response, as recently demonstrated experimentally [3]. By applying both a full quantum mechanical framework as well as a semiclassical approach, we explore the interactions between photons and electrons in these subnanometric gaps in a variety of situations of practical interest in plasmonics and in optoelectronics. Among other topics of interest, we consider the presence of an emitter in the nanogap under the strong coupling regime where hybrid plexcitonic modes are produced, identifying the situation where resonant electron transfer (RET) can be established. Moreover, we explore subnanometric gaps produced by novel materials such as rigid organic molecules producing controlled aggregates for field-enhanced spectroscopy [4], or 2D materials such as graphene, MoS_2 or CdSe, where a distinctive optical response is obtained within the nanogap [5]. The results presented here stress the importance of the plasmonic gap as a canonical structure in nanophotonics, giving rise to the emergence of new optoelectronic processes that can be tailored on demand.

References

[1] D.C.Marinica, A.K.Kazansky, P.Nordlander, J.Aizpurua, A.G. Borisov, Nano Lett. 12 (2012) 1333.

[2] R. Esteban et al. Nature Comm. 3 (2012) 825.

[3] K.J. Savage, M.M. Hawkeye, R. Esteban, A.G. Borisov, J. Aizpurua and J.J. Baumberg, NATURE 491 (2013) 574.

[4] R.W. Taylor et al. ACS Nano 5 (2011) 3878; R. Esteban et al. Langmuir 28 (2012) 8881.

[5] J. Mertens et al. Nano Lett. 12 (2012) 5033.

Figures

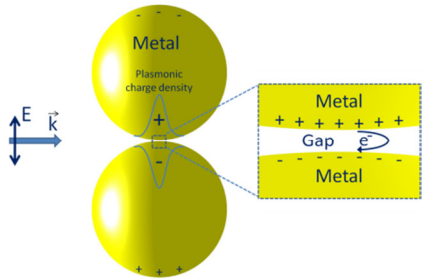

Figure 1: Nanooptics in a plasmonic gap. Sketch of the surface charge density associated to the surface plasmon mode at the nanogap formed by a metallic dimer, excited by a planewave linearly polarized along its axis (E) that propagates with k vector. The interaction between the two nanoparticles localizes and enhances the plasmonic field at the nanogap. For nanometric and subnanometric separation distances (see zoom-in), an interplay between the plasmon charge densities induced by light and electronic states e- shows a rich and complex variety of optoelectronic processes with potential for technological application.

Stability analysis of organic solar cells fabricated with PTB1:PCBM in accordance with established ISOS-D1 protocols

V.S. Balderrama[a], M. Estrada[b], P.L. Han[a], P. Granero[a], J. Pallarés[a], J. Ferré-Borrull[a] and L.F. Marsal[a]

[a]Departament d'Enginyeria Electrònica, Elèctrica i Automàtica, Universitat Rovira i Virgili, Avda. Països Catalans 26, 43007 Tarragona, Spain
[b]Department of Electrical Engineering, Section of Solid-State Electronics, CINVESTAV-IPN, Mexico D.F., Mexico

lluis.marsal@urv.cat

The fabrication of organic solar cells (OSC) in the last ten years has attracted interest due to potential application in the different fields [1, 2]. Actually, the polymers of low-band gap are being used as promised materials to increase the power conversion efficiency (*PCE*). However, the degradation of performance in OSCs such as power conversion is a crucial point and has been seldom studied [3, 4]. ISOS-D1 protocols in the last years have been applied to quantify the lifetime in OSC [5]. Using these protocols is possible to compare the lifetime from other similar devices.

In this work, we fabricated bulk heteterojuction (BHJ) OSC using as polymeric material of low-band gap Poly((4,8-bis (octyloxy) benzo (1,2-b:4,5-b') dithiophene-2,6-diyl) (2-((dodecyloxy) carbonyl) thieno(3,4-b) thiophenediyl)) (PTB1) in combination with [6,6]-phenyl C_{61}-butyric acid methyl ester (PCBM) material. The samples were exposed under nitrogen and air environment and encapsulation conditions. To analyze the degradation process in OSC was applied ISOS-D1 protocols. From the parameters got of current density-voltage characterization (i.e. open circuit voltage (V_{OC}), short circuit current density (J_{SC}), fill factor (*FF*) and *PCE*) were used to follow stability process on the OSC during 5300 h. The normalized *PCE* parameter versus time was studied and they are then related to the possible predominant degradation mechanisms that are present in the device [6].

The OSC structure was manufactured with the stack ITO (120 nm) / PEDOT:PSS (40 nm) / PTB1:PCBM (90 nm) / Ca (25 nm) / Ag (100 nm) as is shown in Fig 1. Three groups of devices were prepared to study the degradation process of their electrical characteristics under 3 different environments: a) in electronic grade 99.999% N_2 (H_2O < 0.1 ppm, O_2 < 0.1 ppm), b) in ambient conditions (60 ± 5% RH) and c) encapsulated. A light intensity of 100 mW/cm^2 was used to test the organic solar cell devices under illumination. In addition *J–V* dark curves were collected for all the photovoltaic devices. Active area used in OSC was 0.09 cm^2.

Fig. 2 is shown the *J–V* curves under illumination for samples under encapsulation. The average performance parameters for all devices such as V_{OC}, J_{SC}, *FF* and *PCE* just after fabrication were 577±8 mV, 11.4±0.7 mA/cm^2, 67.1±3.7% and 4.4±0.2%, respectively. In accordance with ISOS-D1, the lifetime (T_{S80}) for samples under nitrogen, air and encapsulation was 1000 h, 4 h and 48 h, respectively as is shown in Fig. 3. The mechanism responsible for the slow degradation in devices exposed under N_2 was identified to the intrinsic chemical reactions of the polymeric materials. Samples under air environment, the mechanisms responsible for the extremely rapid degradation were associated to chemical reaction of the active layer and/or electrodes with water and oxygen that diffuse into devices. Water was the dominant degradation mechanism. Finally solar cells under encapsulation the main mechanism was associated with the oxygen that takes place product of the encapsulation. The main source of oxygen in these conditions might be the encapsulating/sealing material (EPT-HM), as it contains oxygen in its molecular structure. These results show that the procedure followed in this work under ISOS-D-1 protocols has permitted to gain knowledge of the main degradation mechanisms of the PTB1 donor polymer in the solar cells and thus to improve their reliability and durability.

Acknowledgements

This work was supported by the Spanish Ministry of Economy and competitiveness (MINECO)

under grant number TEC2012-34397, Catalan authority under project 2009 SGR 549 and CONACYT project 127978 in Mexico

References

[1] C.J. Brabec, Sol. Energy Mater. Sol. Cells, 83 (2004) 273.

[2] V.S. Balderrama, M. Estrada, A. Viterisi, P. Formentin, J. Pallarés, J. Ferré-Borrull, E. Palomares, L.F. Marsal, Microelectron. Reliab., 53 (2013) 560.

[3] B. Kippelen, J.L. Bredas, Energy & Environmental Science 2, (2009) 251.

[4] S.A. Gevorgyan, M. Jørgensen, F.C. Krebs, Sol. Energy Mater. Sol. Cells, 92 (2008) 736.

[5] M.O. Reese, S.A. Gevorgyan, M. Jørgensen, E. Bundgaard, S.R. Kurtz, D.S. Ginley, D.C. Olson, M.T. Lloyd, P. Morvillo, E.A. Katz, A. Elschner, O. Haillant, T.R. Currier, V. Shrotriya, M. Hermenau, M. Riede, K. R. Kirov, G. Trimmel, T. Rath, O. Inganäs, F. Zhang, M. Andersson, K. Tvingstedt, M. Lira-Cantu, D. Laird, C. McGuiness, S. Gowrisanker, M. Pannone, M. Xiao, J. Hauch, R. Steim, D.M. DeLongchamp, R. Rösch, H. Hoppe, N. Espinosa, A. Urbina, G. Yaman-Uzunoglu, J.-B. Bonekamp, A.J.J.M. van Breemen, C. Girotto, E. Voroshazi, F.C. Krebs, Sol. Energy Mater. Sol. Cells, 95 (2011) 1253

[6] V.S. Balderrama, M. Estrada, A. Cerdeira, B.S. Soto-Cruz, L.F. Marsal, J. Pallares, J.C. Nolasco, B. Iñiguez, E. Palomares, J. Albero, Microelectron. Reliab., 51 (2011) 597

Figures

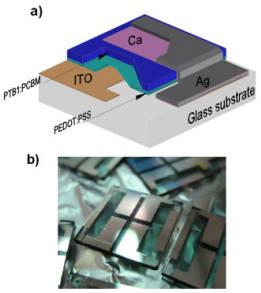

Figure 1: a) Schematic structure PTB1:PCBM of organic bulk heterojunction solar cell, b) physical representation of device.

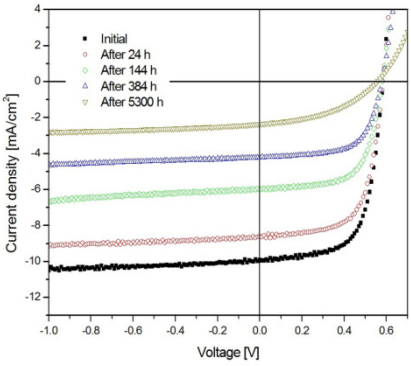

Figure 2: Illuminated J–V curves of PTB1: PCBM solar cells under encapsulation during 5300 h.

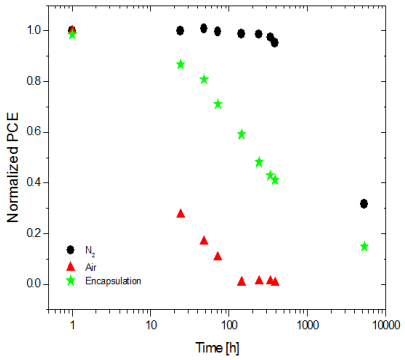

Figure 3: Stability PCE normalized versus time from organic solar cells under N2, air and encapsulation.

Sensing with HRI nanoparticles by means of the linear polarization degree

A.I. Barreda, J.M. Sanz, J.M. Saiz, F. Moreno and F. González*

Grupo de Óptica. Departamento de Física Aplicada, Universidad de Cantabria, Santander, 39005, España

gonzaleff@unican.es

The spectral evolution of the linear polarization degree (PL) at right-angle scattering configuration (θ=90º) is numerically studied for high refractive index (HRI) dielectric nanoparticles. The goal of this research is oriented to sensing purposes. This analysis is performed as a function of the refractive index of the surrounding medium, and it is compared with the more conventional extinction efficiency (Qext) parameter. We focus on the spectral region where quadrupolar magnetic, dipolar electric and dipolar magnetic resonances are located for various semiconductor materials.

Introduction and Methods

Nanotechnology has revolutionized science during the last years by generating important theoretical and practical developments. Particularly, interaction of light with metallic nanoparticles (NP's) has been a very active field in optics with impact in many areas, including sensing applications [1]. When incident light illuminates a metallic NP, free electrons start to oscillate. This generates localized surface plasmons (LSP's). These coherent oscillations of the electronic plasma, which depends on the material properties, the particle size, shape, and also on the wavelength of the incoming radiation, are able to produce some particular surface charge distributions [2]. For certain frequencies, resonances can be observed and strong enhancements of the electric field in the surroundings of the NP's may occur. Although most studies on metallic NP's take advantage of the good response of the plasma in the visible range, their metallic nature is also the cause of their main disadvantage, i.e. the ohmic losses.

High refractive index (HRI) dielectric NP's have been proposed as a solution for this problem because light can travel through these materials without being absorbed [3]. Furthermore, depending on their size and shape, they can show clear resonances in well-defined spectral ranges [4], being whispering gallery-like modes responsible for these resonances. Another important feature is the appearance of a magnetic response that these non-magnetic materials are able to exhibit. During the last years this magneto-dielectric behavior has been vastly explored for some elements, such as Silicon or Germanium [5], while the study of other semiconductor compounds has begun only recently [6,7].

In this research, spherical NP's of Silicon (Si), Germanium (Ge), Aluminum Arsenide (AlAs), Aluminum Antimonide (AlSb) and Gallium Phosphide (GaP) are theoretically analyzed for a set of refractive indices of the surrounding media (next) from 1 to 2. The spectral evolution of the linear polarization degree of the scattered light at right-angle detection, PL(90º) [8], is established as a polarimetric parameter for sensing purposes. Although the study is performed for five materials, general results are shown for Silicon, as representative of their behavior. The most important common feature of these materials is their low absorption. In fact, in a range that varies from VIS to IR their absorption can be considered null in most cases [9].

Results and Discussion

Fig. 1 shows the spectral evolution of PL(90º) for a Silicon NP (R=200nm) as a function of next. As can be seen, the location and magnitude of all resonances evolve with next. In fact, an estimate of next can be obtained from PL(90º), by observing the wavelengths where resonances occur. Although Si has no absorption in the studied wavelength range, there are some materials, such as Ge, that have absorption traces in the NIR region [9]. The right choice of materials and sizes for each sensing application will lead to better results in sensing devices. Nevertheless, even in the worst case, electric resonances are less sensitive with absorption

than magnetic ones [10], so that their fingerprint in PL (90º) can still be followed in sensing.

$$\frac{\partial P_L(90^o)}{\partial m_{ext}} \quad (1)$$

Fig. 2 shows the sensitivity of $P_L(90º)$ to changes in m_{ext} (Eq. 1) at the wavelengths where resonances take place for isolated NP's of Si, Ge, AlAs, AlSb and GaP (always at R=200 nm). It is clear that Ge shows low sensitivity at short wavelengths (where the magnetic quadrupolar resonance appears). Such phenomenon lies in the absorption shown by Ge in this spectral range [9]. Furthermore, the main result is the high sensitivity values obtained for all these materials, regardless of the analyzed resonance. As a consequence, $P_L(90º)$ can be considered as an experimentally feasible indicator for sensing purposes.

Acknowledgements

This research was supported by USAITC-A (United States Army International Technology Center Atlantic) through grant W911NF-13-1-0245

References

[1] P.N. Prasad, Nanophotonics (John Wiley & Sons, Inc., 2004).

[2] K.L. Kelly et al., The optical properties of metal nanoparticles: the influence of size, shape and dielectric environment, The Journal of Physical Chemistry B 107:668-77 (2003).

[3] A. Forouhi et al., Optical properties of crystalline semiconductors and dielectrics, Physical Review B 38:1865 (1988).

[4] Y.H. Fu et al., Directional visible light scattering by silicon nanoparticles, Nature Communications 4:1527 (2013).

[5] L. Shi et al., Monodisperse silicon nanocavities and photonic crystals with magnetic response in the optical region, Nature Communications 4:1904 (2013)

[6] B. García-Cámara et al., Sensing with magnetic dipolar resonances in semiconductor nanospheres, Optics Express 21(20):23007-20 (2013).

[7] J.M. Gefrin et al., Magnetic and electric coherence in forward-and back-scattered electromagnetic waves by a single dielectric subwavelength sphere," Nature Communications 3:1171 (2012).

[8] B. Setién et al., Spectral behavior of the linear polarization degree at right-angle scattering configuration for nanoparticle systems, New Journal of Physics 12:103031 (2010).

[9] E.D. Palik, *Handbook of Optical Constants of Solids* (Academic Press: New York, 1998).

[10] J.M. Sanz et al., Influence of pollutants in the magneto-dielectric response of silicon nanoparticles, Optics Letters (2014), *Accepted*.

[11] C.F. Bohren, and D.R. Huffman, *Absorption and scattering of light by small particles* (Wiley, New-York, 1983).

Figures

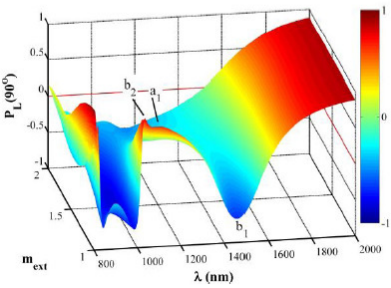

Figure 1: Spectral evolution of PL(90º) for a Silicon nanoparticle (R=200 nm) as a function of m_{ext}. Indicators a1, b_1 and b_2 show the resonances location in the analyzed spectrum [11] (dipolar electric and magnetic, and quadrupolar electric, respectively).

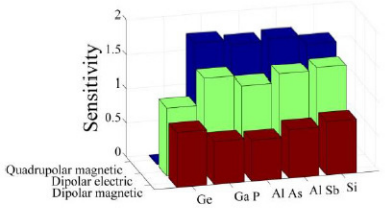

Figure 2: Sensitivity of $P_L(90º)$ with m_{ext} at the wavelengths where resonances take place for isolated nanoparticles of Si, Ge, AlAs, AlSb and GaP (R=200 nm). Sensitivity expressed in RIU^{-1} (RIU stands for Refractive Index Units).

E-beam assisted etching and patterning of few-layer molybdenum disulfide

Ramón Bernardo-Gavito[1], Rodolfo Miranda[1,2,3], Daniel Granados[2]

[1]Dpto. de Física de la Materia Condensada, Universidad Autónoma de Madrid, Facultad de ciencias, Cantoblanco, 28049, Madrid, Spain
[2]IMDEA Nanociencia, Faraday 9, 28049, Madrid, Spain
[3]Instituto de Ciencia de Materiales "Nicolás Cabrera", Universidad Autónoma de Madrid, Cantoblanco, 28049, Madrid, Spain

ramon.bernardo@uam.es

Transition metal dichalcogenides have attracted a huge interest since the isolation of graphene. This interest is based in the fact that these materials develop different properties when their thickness is reduced down to the monolayer or few-layer regime [1]. Among all of them, molybdenum disulfide (MoS_2) is especially interesting because as a bulk it is a semiconductor with an indirect band-gap in the near-infrared region of the spectrum, and this band-gap blue-shifts when reducing the number of layers, resulting in a direct band-gap semiconductor which emits in the visible (1.85eV) when its thickness is reduced to a single layer [1, 2, 3].

During the last years, many different techniques for fabricating MoS_2 single layers have been developed, such as mechanical exfoliation [2, 3], XeF_2 plasma etching [4] and many others [5, 6].

In this work we use mechanical exfoliation to deposit MoS_2 flakes on a SiO_2/Si substrate and use an electron beam with a XeF2 flow to locally etch specific regions of the flake (Fig. 1) without using masks or electron beam lithography resists. We also created point defects using a focused ion beam and visualized on-line the growth of hexagonal holes (Fig. 2) while using the SEM while keeping the XeF_2 flow. This is consistent with the results obtained in [4] using a XeF_2 plasma and graphene as a masking layer.

Using this method we are able to pattern the exfoliated MoS_2 and to selectively etch the material with arbitrary shapes and a good lateral resolution. This will allow us to design complex structures with controlled thicknesses, giving us the possibility to fabricate different kinds of devices such as photonic crystals, quantum dots or transistors.

References

[1] Qing Hua Wang, Kourosh Kalantar-Zadeh, Andras Kis, Jonathan N. Coleman, Michael S. Strano. Nature Nanotechnology, 7 (2012), 699.
[2] Kin Fai Mak, Changgu Lee, James Hone, Jie Shan, and Tony F. Heinz. PRL, 105 (2010), 136805.
[3] A Castellanos-Gomez, N Agraït, G Rubio-Bollinger. App. Phys. Lett., 96 (2010), 213116.
[4] Yuan Huang, Jing Wu, Xiangfan Xu, Yuda Ho, Guangxin Ni, Qiang Zou, Gavin Kok Wai Koon,Weijie Zhao, A. H. Castro Neto, Goki Eda, Chengmin Shen, and Barbaros Özyilmaz. Nano Research, 6 (2013), 200.
[5] Xiao Huang, Zhiyuan Zeng and Hua Zhang. Chem. Soc. Rev., 42 (2013), 1934.
[6] Xin Lu, Muhammad Iqbal Bakti Utama, Jun Zhang, Yanyuan Zhao, Qihua Xiong. Nanoscale, 5 (2013), 8904.

Figures

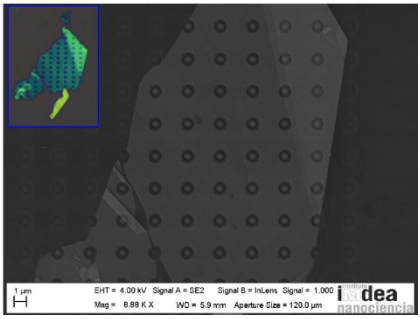

Figure 1: SEM micrograph of a varying-thickness MoS_2 flake deposited on a SiO_x/Si substrate by mechanical exfoliation and patterned using the proposed method. Inset: Optical microscope image of the same flake.

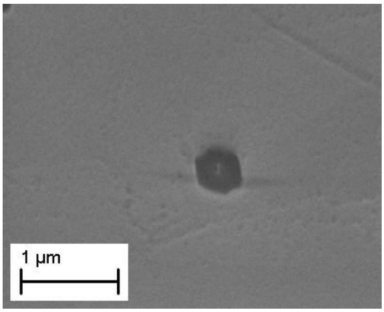

Figure 2: SEM micrograph of a 500nm hexagonal hole grown from a point defect created with a focused ion beam.

In situ characterization of colloidal crystallization

Alvaro Blanco and Cefe López

Instituto de Ciencia de Materiales de Madrid ICMM – CSIC C/Sor Juana Inés de la Cruz 3, 28049, Madrid, Spain

a.blanco@csic.es

Selfassembly has long being used as a successful way to prepare 3d photonic crystals. The formation of silica colloidal crystals by self-assembly, by any of the different ways tested to date [1], is still far from understood. Vertical deposition is the most widely used method and has been studied in more detail in the last few years [2,3]. Hitherto, the understanding of colloidal crystallization early stages is still poor mainly due to the difficulty of direct observations. Recent experiments show small clusters nucleation can direct colloidal crystallization afterwards [4]. However, new experiments on direct visualization of colloidal nucleation with single particle resolution suggest that crystallization may occur from amorphous aggregates rather than from small ordered clusters [5]. We have performed in situ, real-time optical characterization of silica colloidal suspensions during crystallization (sedimentation) that might shine new light on this specific topic supporting the latter mechanism. The understanding of self-assembly at these scales is of paramount importance in modern materials science and we believe our results will help to unveil some of its secrets.

References

[1] J.F. Galisteo-López, M. Ibisate, R. Sapienza, L. Froufe-Pérez, A. Blanco, and C. López, Adv. Mater. 23, 30-69 (2011).

[2] D.J. Norris, E.G. Arlinghaus, L. Meng, R. Heiny, and L.E. Scriven, Adv. Mater. 16, 1393-1399 (2004).

[3] G. Lozano, and H. Míguez, Langmuir 23, 9933-9938 (2007).

[4] K. Hashimoto, A. Mori, K. Tamura, and Y. Suzuki, Jpn. J. Appl. Phys. 52, 030201 (2013).

[5] P. Tang, N. Xu, and L. Xu, Nature Physics 10, 73-79 (2014).

Structural and luminescence properties of silicon-rich oxides and nitrides fabricated by PECVD

J. M. Ramírez[1],* Y. Berencén, J[1]. López-Vidrier[1], **O. Blázquez[1]**, S. Hernández[1], and B. Garrido[1]
J. Hurtado[2], N. Sánchez[2], T. Ivanova[2], F. López-Royo[2], and P. Sanchis**[2]

[1]Department of Electronics, University of Barcelona, Martí i Franquès, 1, 2nd floor, 08028 Barcelona
[2]Nanophotonics Technology Center, Universitat Politècnica de València, Camino de Vera s/n, 46022 Valencia, Spain

jmramirez@el.ub.edu
**pabsanki@ntc.upv.es

During the last two decades, silicon-based light emitters have attracted a lot of attention due to the many benefits envisaged [1]. The implementation of a silicon-based light source using the mainstream CMOS technology is sound and also interesting as it provides an entire new framework for more efficient, sustainable and low-cost devices with full integration capabilities [2]. Thus, several strategies were tackled in order to overcome the poor emitting properties offered by silicon, due to its indirect band gap. In particular, it was in the early nineties when silicon nanocrystals (Si-ncs) came into play, taking advantage of the photoluminescence (PL) enhancement provided by the quantum confinement of trapped excitons within Si-ncs embedded in silicon oxide [3]. From this point on, many research groups focused on the topic, accomplishing major breakthroughs for the scientific community [4]. Noteworthy, there is still a lack for an efficient electrically driven silicon-based light emitter (LED or even a LASER).

Among other drawbacks not solved yet, one has to consider the challenge of injecting electrons into a dielectric material without limiting other key factors such as the reliability or device lifetime [2]. Furthermore, there is a strong trade-off between electrical conduction and emission efficiency in siliconrich oxides (SRO). In terms of PL efficiency, a well passivated material is desired to reduce local defects situated at the nanocrystal-oxide interface and hence diminish the non-radiative paths, although it also makes more difficult the electrical injection. On the contrary, highly defective dielectrics provide good electrical conductivity while displaying low optical efficiency (high non-radiative recombination rates). Consequently, there is only a narrow window of success where both the light efficiency and the electrical injection provide good electrical injection and efficient luminescent emission. Also, other dielectric materials such as silicon nitrides have been investigated as host matrices for Si-ncs [5-7]. Silicon nitride presents several advantages compared to silicon oxide. For instance, it has a larger refractive index and a lower barrier height that makes it suitable for high quality resonant cavities [8] and electrical injection [6]. Moreover, the low two-photon absorption provided in the infrared range stimulates its application in infrared light emitting devices [9].

In this work, we present our roadmap towards the development of efficient silicon nanocrystal-based light emitting devices. In particular, we have centered our efforts in the structural and luminescence properties of silicon-rich oxides and silicon-rich nitrides (SRN) fabricated by plasma-enhanced chemicalvapor deposition (PECVD). The stoichiometry of luminescent layers was sequentially modified in order to introduce a different silicon excess in each sample. Si-nc formation was accomplished after hightemperature annealing samples for 1 h under N2 atmosphere. Different temperature annealing treatments were performed in samples, ranging from 800°C to 1100°C. X-ray photoelectron spectroscopy (XPS) denoted a variable silicon excess in the matrix and the existence of Si-Si bonds in samples annealed at 1000°C or above. Variable angle spectroscopic ellipsometry (VASE) was used to identify

important parameters such as the deposited thickness, the roughness, the refractive index or the extinction coefficient of samples. Layer thickness and roughness were found to be almost independent from the silicon excess, whereas an evident shift of the refractive index and extinction coefficient was displayed in SRO [see figure 1(a)]. On the contrary, only slight differences were observed for SRN, denoting its low sensitivity to silicon excess variations.

The PL of samples excited under 325 nm displayed two different trends. Whereas SRN showed a broad white emission centered at 550 nm, bright red-near infrared emission located around 750 nm was observed in SRO [see figure 1(b)]. Similarly, a different PL lifetime was measured in SRN with respect to SRO. Whereas very fast decay times were identified for all SRN (in the picosecond range), longer values were determined for annealed SRO (few microseconds). Moreover, an evident increase of the decay time was observed for higher annealing temperatures [see figure 1(c)].

The good optical properties of the studied SRO and SRN layers strongly encourage their implementation as luminescent layers in metal-oxide-semiconductor structures to procure the electrical injection and consequently electroluminescence emission. The light emitting device consists of a semitransparent electrode from which electrons are injected (anode), a luminescent layer (SRO or SRN) and finally a cathode to collect injected electrons. Ongoing work is being done in that direction, thus providing an exciting scenario for the progress on the complete integration of the electronic drivers and the optical performance in a silicon CMOS line.

References

[1] L. Pavesi, D.J. Lockwood, "Silicon Photonics", Springer-Verlag (Berlin), 2010..

[2] L. Vivient, L. Pavesi, "Handbook of silicon photonics", Francis & Taylor (Boca Raton), (2013).

[3] H. Takagi, H. Ogawa, Y. Yamazaki, A. Ishizaki, and T. Nakagiri, Appl. Phys. Lett., 56 (1990) 2379.

[4] F. Priolo, T. Gregorkiewicz, M. Galli, and T.F. Krauss, Nat. Nanotech., 9 (2014) 19.

[5] L. Dal Negro, J.H. Yi, L.C. Kimerling, S. Hamel, A. Williamson, and G. Galli, Appl. Phys. Lett., 88,(2006) 183103.

[6] Y. Berencén, J.M. Ramírez, O. Jambois, C. Domínguez, J.A. Rodríguez, and B. Garrido, J. Appl. Phys., 112 (2012) 033114.

[7] A. Zelenina, S. A. Dyakov, D. Hiller, S. Gutsch, V. Trouillet, M. Bruns, S. Mirabella, P. Löper, L. López-Conesa, J. López-Vidrier, S. Estradé, F. Peiró, B. Garrido, J. Bläsing, A. Krost, D.M. Zhigunov, and M. Zacharias, J. Appl. Phys., 114 (2013) 184311.

[8] F. Ferrarese Lupi, D. Navarro-Urrios, J. Monserrat, C. Domínguez, P. Pellegrino, and B. Garrido, Opt. Lett., 36 (2011) 1344.

[9] D.J. Moss, R. Morandotti, A.L. Gaeta, and M. Lipson, Nat. Photon., 7 (2013) 597.

Figures

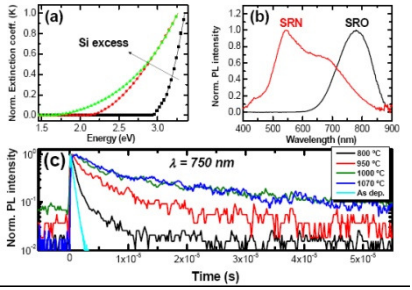

Figure 1: (a) Variation of the extinction coefficient as a function of silicon excess, (b) typical photoluminescence spectra for SRO and SRN, and (c) evolution of PL decay times as a function of the annealing temperature for different SRO samples.

Theoretical study of the Faraday effect in Au-Co-Au membranes in conditions of extraordinary optical transmission

Blanca Caballero[1], Juan Carlos Cuevas[2], Antonio García-Martín[1]

[1]IMM-Instituto de Microelectrónica de Madrid (CNM-CSIC), Isaac Newton 8, PTM, Tres Cantos, E-28760 Madrid, Spain
[2]Departamento de Física Teórica de la Materia Condensada, Universidad Autónoma de Madrid, E-28049, Madrid, Spain

blanca.caballero@imm.cnm.csic.es

In the context of Nanophotonics, Magnetoplasmonics is a field that has become more and more popular during the past few years [1]. It studies the magneto-optical properties of systems combining plasmons and magneto-optically active materials where both interact with each other, enhancing their properties. This kind of systems benefits from the ability of plasmons to localize light in reduced volumes, where the consequent field enhancement results in an amplification of the MO activity of the system. As another result of this synergy, one can also use the electric field to tune the plasmon properties. Those two qualities are very appealing for possible applications and give Magnetoplasmonic devices very promising perspectives.

The extraordinarily high transmission presented in periodically patterned plasmonic structures, when the holes are smaller than the wavelength, has been broadly studied [2,3]. Studies of the magneto-optical response in systems exhibiting extraordinary optical transmission have been carried out in the case of the Kerr effect, mainly considering perforated membranes made of ferromagnetic metals [4,5].

Therefore, it becomes natural to tackle the study of the magneto-optical effect of these systems but considering the transmitted field, rather than the reflected one. In this work we present an analysis of the Faraday polarization conversion through a Au-Co-Au perforated membrane. This combination of materials permits maintaining fairly good plasmonic properties while presenting magneto-optical response due to the presence of a ferromagnetic metal. We will present a systematic analysis of the polarization conversion as a function of the Co layer thickness as well as the Co layer position. Additionally, we will show the effect of the environment by studying the modification that the refractive index of both the incident media and the substrate introduces on the polarization conversion. Following this analysis, we will be able to put forward a clear correlation between the excitation of the SPPs and polarization conversion enhancement.

References

[1] G. Armelles, A. Cebollada, A. García-Martín, M. U. González, Adv. Opt. Mater., 1 (2013) 10.
[2] T.W. Ebbesen, H. J. Lezec, H. F. Ghaemi, T. Thio, and P. A.Wolff, Nature (London), 391 (1998) 667.
[3] F. J. García-Vidal, L. Martín-Moreno, T. W. Ebbesen, and L. Kuipers, Rev. Mod. Phys., 82 (2010) 729.
[4] B. Caballero, A. García-Martín, and J.C. Cuevas, Phys. Rev. B, 85 (2012) 245103.
[5] E. Melander, E. Östman, J. Keller, J. Schmidt, E.Th. Papaioannou, V. Kapaklis, U.B. Arnalds, B.Caballero, A. García-Martín, J.C. Cuevas, and B. Hjörvarsson, Appl. Phys. Lett., 101 (2012) 063107.

Near-field mapping of the electric and magnetic local density of states

R. Carminati[1,*], D. Cao[1], A. Cazé[2], V. Krachmalnicoff[1], R. Pierrat[1] and Y. De Wilde[1] L. Aigouy[3], P. Gredin[4] and M. Mortier[4]

[1] Institut Langevin, ESPCI ParisTech, CNRS, Paris, France
[2] Department of Mathematics, University of Michigan, Ann Arbor, MI, USA
[3] Laboratoire de Physique et d'Etude des Matériaux, ESPCI ParisTech, CNRS, Paris, France
[4] Institut de Recherche de Chimie Paris, Chimie Paristech, CNRS, Paris, France

*remi.carminati@espci.fr

In the first part of the talk, we will present a novel method for mapping the radiative and non-radiative decay rate of a fluorescent emitter in the near-field of a nanostructured sample. The approach is based on the simultaneous mapping of the fluorescence intensity and decay rate of fluorophores with electric dipole transitions [1], and on the rigorous application of the reciprocity theorem of electromagnetism. Experimental data are compared with exact numerical simulations. A quantitative agreement between theory and experiment is demonstrated, proving the validity and the relevance of the method [2].

In the second part, we will report on a similar experimental technique to quantify the relative importance of electric and magnetic dipole luminescence from a single nanosource. By attaching a Eu-doped nanocrystal to a near-field scanning optical microscope tip, we map the branching ratios associated to two electric dipole and one magnetic dipole transitions in three dimensions in the near field. The relative weights of the electric and magnetic radiative local density of states can be recovered quantitatively, based on a multilevel model. This studies paves the way towards the full electric and magnetic characterization of nanostructures for the control of single emitter luminescence.

References

[1] V. Krachmalnicoff, D. Cao, A. Cazé, E. Castanié, R. Pierrat, N. Bardou, S. Collin, R. Carminati and Y. De Wilde, Opt. Express 21, 11536 (2013).

[2] D. Cao, A. Cazé, M. Calabrese, R. Pierrat, N. Bardou, S. Collin, R. Carminati, V. Krachmalnicoff and Y. De Wilde, Mapping the radiative and non-radiative local density of states in the near field of a gold nanoantenna, submitted (2014). arXiv:1401.2858.

[3] L. Aigouy, A. Cazé, P. Gredin, M. Mortier and R. Carminati, Mapping and quantifying electric and magnetic dipole luminescence at the nanoscale, submitted (2014). arXiv:1404.1369 .

Improvement of antigen detection using protein A for the oriented bio-functionalization of integrated photonic biosensor

R. Caroselli[a], J. G. Castelló[a], J. Escorihuela[b], M. J. Bañuls[b], A. Maquieira[b], J. García-Rupérez[a]

[a] Nanophotonics Technology Center, Universitat Politècnica de València, 46022 Valencia, Spain
[b] Centro de Reconocimiento Molecular y Desarrollo Tecnológico, Departamento de Química, Universitat Politècnica de València, 46022 Valencia, Spain

rcaroselli@ntc.upv.es

The objective of this work is to optimize the detection of antigens with integrated photonic sensing structures by using a protein A layer to promote bio-functionalization with specific antibody probes. Protein A allows the oriented attachment of antibody receptors over the sensor surface (see Fig. 1), since they bind to the protein layer through their Fc section and their Fab sections will be oriented towards the sample to be analyzed, thus enhancing the interaction with the target antigens to be detected [1]. The attention was focused on a well-known antigen typically used as model in experimental development: bovine serum albumin (BSA).

Protein A layer can be created over the sensor simply by physical immobilization, by flowing it over the sensor surface. So the delivery of the protein A and the other fluidic samples to the sensing structure was done by flowing using a simple PDMS-based microchannel. This bio-functionalization technique is quite simple and it allows providing specificity to a photonic sensing structure without the need of using other more complex chemical procedures such as those based on organosilanes. Therefore, it is perfect for the implementation of introductory experiments in the field of integrated photonic biosensors.

The photonic sensing structure used for our experiments is a SOI ring resonator (RR) in add-drop configuration, which was fabricated in CEA-LETI in the frame of the cost-share European nanophotonic fabrication platform ePIXfab (see Fig. 2). The basic structural parameters of the sensing device are: silicon thickness, 220 nm; access waveguide width, 450 nm; ring radius, 20 μm; input coupling gap, 170 nm; output coupling gap, 175 nm; free spectral range (FSR), 4 nm. A broadband superluminescent diode (SLD) was used to excite the ring resonator and the transmission spectrum of its through port was continuously measured using an optical spectrum analyzer (OSA).

The experiment consisted in several fundamental steps (see Fig. 3). First of all protein A was flowed over the ring resonator in order to create an intermediate protein layer on the sensing structure surface. By flowing gelatin, chip's areas not coated with protein A were blocked. From now on, PBS 1x with a small concentration of gelatin was used as buffer in order to keep the blocking of the surface. Anti-BSA, which is the antibody specific to the BSA antigen, was flowed over the chip in order to attach the antibody receptors. Finally, to carry out the specific detection, BSA was flowed. After the experiment, the chip can be regenerated by flowing glycine (note that in the regeneration process the antibodies are detached from the protein, so they will need to be attached again in the next cycle).

In order to test the improvement obtained thanks to the use of the protein A, several concentrations of BSA were flowed over the bio-functionalized sensor. For BSA concentrations of 100 ng/ml, 50 ng/ml and 5 ng/ml a wavelength shift of 140 pm, 70 pm and 10 pm has been detected, respectively. These results confirms the good performance in terms of sensitivity that can be obtained using a very simple bio-functionalization design based on the use of an intermediate layer of protein A.

References

[1] Zhanhui Wang, Gang Jin, "Feasibility of protein A for the oriented immobilization of immunoglobulin on silicon surface for a biosensor with imaging ellipsometry", J. Biochem. Biophys. Methods 57, pp. 2'3-211, 2003.

Figures

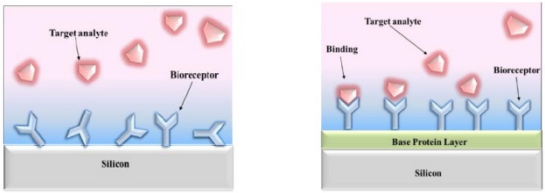

Figure 1: Left: illustration of randomly-oriented antibody receptors on the surface of the sensor; right: illustration of properly-oriented antibody receptors on the surface of the sensor, where an intermediate protein layer has been used.

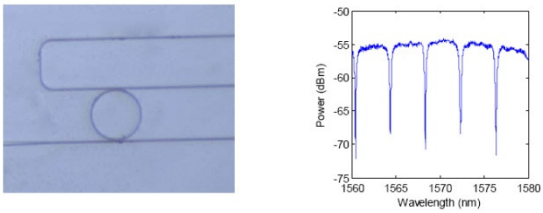

Figure 2: Left: microscope image of the ring resonator used for the experiments; right: transmission spectrum of the through port of the ring resonator.

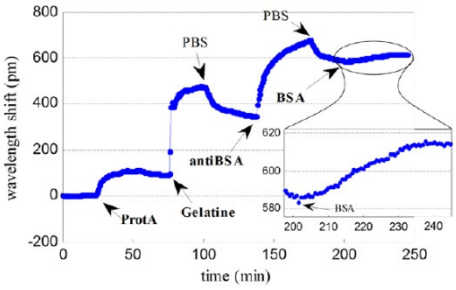

Figure 3: Wavelength shift evolution of the whole experiment; the inset shows a detail of the binding curve for BSA detection.

Optical trapping and manipulation of nano- and micro-objects

S. Carretero Palacios[1,2], L. Osinkina[2], M. Fedoruk[2], S. R. Kirchner[2], S. Nedev[2], T. Lohmüller[2], F. Jäckel[2,3], J. Feldmann[2]

[1]Present Address: Instituto de Ciencia de Materiales de Sevilla (CSIC-Universidad de Sevilla) C/ Américo Vespucio 49, 41092 Sevilla, Spain
[2]Photonics and Optoelectronics Group, Department of Physics and Center for NanoScience (CeNS), Ludwig-Maximilians-Universität München Amalienstaße 54 80799 Munich, Germany
[3]Department of Physics and Stephenson Institute for Renewable Energy, University of Liverpool, Chadwick Building Peach Street, L69 7ZF, Liverpool, UK

sol.carretero@csic.es

Since the discovery of optical trapping by Ashkin [1] in 1970, an ever increasing use of optical tweezers as sensitive tools for the manipulation and observation of isolated nano- and microobjects in aqueous solution has been reported. Optical tweezers employ a focused laser beam to exert small forces on an object of interest, and, depending on the relative contribution of scattering and gradient forces, laser light can be used for either stable optical trapping of the object or for depositing it at desired locations on a substrate. An important advantage of optical trapping is the contactless nature of optical forces, which enables straightforward integration of optical trapping with optical imaging and spectroscopic techniques. Nowadays, optical trapping and optical manipulation of micro- and nanostructures are standard techniques widely used in biology, physics, chemistry, and material sciences. In this talk, we will review some examples of our recent investigations using optical tweezers [2], ranging from the study of DNA-binding events [3], direct optical monitoring of flow generated by artificial dipole-like microobjects or bacterial flagellar rotation [4], to the fine control of heat-induced polymerization reactions at the nanoscale [5].

References

[1] "Acceleration and Trapping of particles by radiation pressure", A. Ashkin, Phys. Rev. Lett. 24, 156 (1970).
[2] "Optical trapping and manipulation of plasmonic nanoparticles: fundamentals, applications and perspectives", A.S. Urban et al. Nanoscale 6, 4458-4474 (2014)
[3] "Tuning DNA Binding Kinetics in an Optical Trap by Plasmonic Nanoparticle Heating", L. Osinkina et al., Nano Lett. 13, 3140 (2013).
[4] "Direct optical monitoring of flow generated by bacterial flagellar rotation", Silke R. Kirchner et al., Appl. Phys. Lett. 104, 9 (2014).
[5] "Nanolithography by Plasmonic Heating and Optical Manipulation of Gold Nanoparticles", Michael Fedoruk et al., ACS Nano 7, 7648 (2013).

Flexible nanoparticle based photonic structures for UV radiation shielding applications

J. R. Castro Smirnov, Mauricio E. Calvo and Hernán Míguez

Instituto de Ciencia de Materiales de Sevilla, Consejo Superior de Investigaciones Científicas-Universidad de Sevilla, Américo Vespucio 49, 41092, Seville, Spain

jrcastro@icmse.csic.es

New porous one dimensional photonic crystals based on ZrO_2 and SiO_2 nanoparticles have been successfully built in order to create hybrid (polymer-nanoparticle) flexible films to protect against UV radiation by optical reflection.[1] These structures are designed to block specific and narrow wavelength ranges of the UVA, UVB, and UVC regions of the electromagnetic spectrum only by interference effects. Also, ZrO_2/SiO_2 system preserves a high transparency in the visible and presents superior optical quality. The inter-linked pore structure of the porous multilayer system leads to prepare thin, flexible, self-standing, transferable, and adaptable selective UV filters by polymer infiltration.[2] These films show a level of protection comparable to that of conventional ones, and at the same time avoiding any unwanted secondary effects, such as photodegradation, increasing of local temperature or, as is the case for organic UV absorbers, formation of free radicals, all of which are a consequence of light absorption.[3].

References

[1] J. R. Smirnov Castro, Mauricio E. Calvo, Herman Miguel. "Selective UV reflecting mirrors based on nanoparticle multilayers." Adv. Funct. Mater., 23 (2013), 2805–2811.

[2] M.E. Calvo, H. Miguez, Chem. Mater., 22, (2010), 3909–3915.

[3] M.E. Calvo, J.R. Castro Smirnov, H. Miguez, J. Pol. Sci part B: pol.Phys, 50, (2012), 945.

Figures

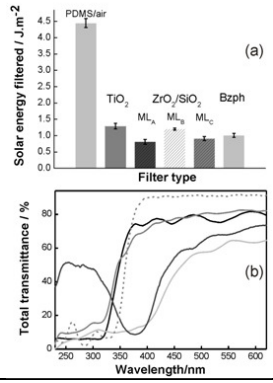

Figure 1: (a) Energy received by identical UV sensitive strips covered with different flexible protective films. Height of the bar represents the media value, black line represents the standard deviation. MLA , MLB , MLC belong to different ZrO_2 /SiO_2 films. (see figure 6b)(b) Total transmittance spectra of the protecting films used in Figure 6a. TiO_2 (black solid line), MLA (light gray solid line), MLB (grey solid line), MLC (dark grey solid line),benzophenone-3 (grey short dashed line).

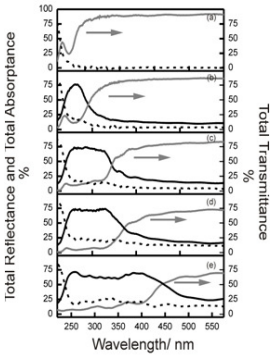

Figure 2: Total reflectance (black solid line), total transmittance (grey solid line) and absorptance (black dotted line) spectra of stacking flexible films prepared from samples shown in figure 4a. The number of stacking samples is 1.

Enhancing the transmittance of a subwavelength aperture close to the focus of a conventional lens

Fernando de León-Pérez[1], F. Villate-Guío[2], L. Martín-Moreno[2]

[1]Centro Universitario de la Defensa de Zaragoza, Ctra. de Huesca s/n, E-50090 Zaragoza, Spain
[2]Instituto de Ciencia de Materiales de Aragón and Departamento de Física de la Materia Condensada, CSIC-Universidad de Zaragoza, E-50009 Zaragoza, Spain

fdlp@unizar.es

One-dimensional light harvesting structures nano-patterned on an opaque metallic film are optimized to render high transmission efficiencies when the system is illuminated by a conventional cylindrical lens. We consider the case of a finite slit-groove array (SGA) with a given number of grooves that are symmetrically distributed with respect to a central slit, see Fig. 1. A total transmittance of 80 % is achieved even for a single slit when (i) Fabry-Perot like modes are excited inside the slit and (ii) the effective cross section of the aperture becomes of the order of the full width at half maximum of the incident beam. A further enhancement is produced by the groove array. The optimal geometry for the groove array consists of a moderate number of grooves at either side of the slit, separated by a distance of half the incident wavelength. Grooves should be deeper than those typically reported for plane wave illumination in order to increase their scattering cross section. Further details can be found in Ref. [1].

References

[1] F. Villate-Guío et al., arXiv: 1403.4968 (2014).

Figures

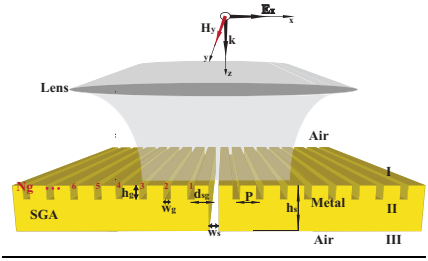

Figure 1: Schematic representation of the system under study.

Fine tuning of light transport in resonant random media

André Espinha, Marta Ibisate, Esther Calle, Álvaro Blanco, Cefe López

Instituto de Ciencia de Materiales de Madrid (ICMM-CSIC), Calle Sor Juana Inés de la Cruz, 3, Cantoblanco, 28049 Madrid, Spain

ablanco@icmm.csic.es

When monodisperse submicron spherical particles assemble, two opposite situations can take place [1]. In the first case, spheres organize into periodic structures originating the well-known photonic crystals. In these materials, the dispersion relation exhibits photonic gaps along determined directions and therefore they behave as three dimensional gratings that Bragg-diffract light. In the other extreme, the spheres assemble into completely disordered structures, giving origin to random media denoted as photonic glasses (PGs) [2]. In these materials, light propagation is described within the diffusive regime, by a random walk with characteristic scattering mean free path. Due to the fact that the building blocks are monodisperse in size and shape, PGs present resonant behavior arising from the collective coupling of Mie modes. In this sense, they present resonant transport parameters namely, the transport mean free path ( ), the diffusion constant and the energy velocity [3]. PGs have allowed the study of interesting phenomena with special emphasis in resonant random lasing [4]. In these systems, the lasing frequency is tuned due to the influence of the material characteristic resonances.

In the present work, we report our latest results concerning the modification of the energy transport mean free path in a PG composed of silica spheres. The glass was stepwise infiltrated with additional conformal layers of silica, by using chemical vapor deposition. The sample was characterized from the structural point of view with scanning electron microscopy (Figure 1). Additionally, total optical transmission allowed us to study the evolution of the transport resonances spectral position. Coherent back scattering was also analyzed, by imaging the backscattering cone emanating from the sample. This allowed the detailed characterization of which revealed an almost tenfold increase, at the end of the process (complete infiltration, see Figure 1b).

We believe that the reported procedure might have impact in further developments of random lasers by allowing to fine tailor the transport properties of the material.

References

[1] J. Galisteo-López, M. Ibisate, R. Sapienza, A. Blanco, C. López, Advanced Materials, 23 (2011) 30.

[2] P. García, R. Sapienza, A. Blanco, C. López, Advanced Materials, 18 (2007) 2597.

[3] R. Sapienza, P. García, J. Bertolotti, M. Martin, Physical Review Letters, 23 (2007) 233902.

[4] S. Gottardo, R. Sapienza, A. Blanco, D. Wiersma, C. López, Nature Photonics, 7 (2008) 429.

Figures

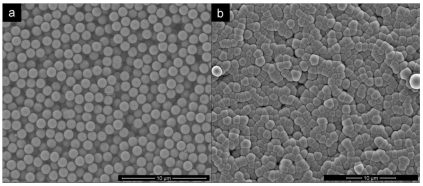

Figure 1: Scanning electron microscopy image of a silica photonic glass (a) and after being infiltrated with silica by chemical vapor deposition (b).

Optical response of metallic nanoparticle heteroaggregates with subnanometric gaps

Christos Tserkezis[1], Richard W. Taylor[2], Jan Beitner[3], **Rubén Esteban[1]**, Jeremy J. Baumberg[3] and Javier Aizpurua[1]

[1]Donostia International Physics Center and Centro de Física de Materiales CSIC-UPV/EHU, Po Manuel de Lardizabal 5, 20018 Donostia-San Sebastián, Spain
[2]Max Planck Institute for the Science of Light, Günther-Scharowsky Strasse 1, Bau 24, 91058 Erlanger, Germany
[3]Nanophotonics Centre, Cavendish Laboratory, University of Cambridge, Cambridge CB3 0HE, U.K.

ruben_esteban@ehu.es

The fabrication and study of the optical properties of metallic nanoparticle (NP) clusters with small particle separations is a key issue in modern nanophotonics. As the interparticle distance becomes smaller, interaction between the hybridised plasmonic modes becomes stronger, large energy shifts are produced, and the local electromagnetic (EM) field at the interparticle gap is enhanced, creating EM "hot spots" [1], which are of great importance for numerous applications in sensing and spectroscopy. Nanolithography is a suitable method for fabricating clusters with a few nanometre separations, but achieving subnanometric gaps is still challenging, and self-assembly techniques are usually preferred. However, most of the molecular linkers used to connect metallic NPs in self-assembled clusters are not very rigid, leading to undesired variations of the gap widths, while they usually restrict access to the generated hot spot. These problems were recently tackled by use of cucurbiturils (CBs) [2]. CBs are rigid, 0.9-nm-long molecular linkers, which form barrel-like cavities that can act as hosts for molecules in sensing applications. The optical response of CB-assisted aggregates of gold (Au) NPs has been interpreted in terms of excitation of long-wavelength modes (Capacitive Chain Plasmons, CCPs) associated with the linear and disordered chains which constitute the clusters [3]. In what follows, we analyse the optical properties of CB-linked heteroaggregates made of admixtures of Au and silver (Ag) nanospheres, in view of the chain model described above.

In Fig. 1a we show extinction spectra of a Au-Ag NP (diameter: 40 nm) dimer in water, illuminated by a plane wave polarised along the dimer's axis, as the width of the interparticle gap, w, decreases from 5 nm to 0.5 nm. For relatively large separations the two peaks at about λ = 410 nm and λ = 540 nm can be identified as hybridised modes originating from the dipole plasmon modes of the Ag and the Au NP, respectively, as can be verified by the corresponding field plots (A and B in Fig. 1b). For smaller w, as the interaction between NPs becomes stronger, the long-wavelength mode redshifts drastically, and it can be described as a CCP mode, with the electric field now equally distributed along the whole dimer (contour plot E in Fig. 1b). On the other hand, the Ag-like mode at first redshifts slightly, until, for very small gaps, it starts blueshifting. These different behaviours can both be explained by the dielectric functions of the two metals: for longer wavelengths, both metals are very similar, free-electron metals with comparably large negative permittivity values. The shorter wavelength regime, on the other hand, is dominated by the plasmonic response, showing larger differences. For example, the resonance of a Au-Ag dimer at about λ = 410 nm has been described as a Fano resonance, originating from the interaction between the sharp silver-like dipole resonance and the continuum of the Au interband transitions [4]. In order to better understand the effect of mixing the two materials, in Fig. 1c we examine how particle order influences the spectra of Au-Ag trimers. In all cases, the behaviour of the CCP mode remains remarkably stable, with only relatively small shifts related to the Au:Ag ratio. On the other hand, for shorter wavelengths, higher-order modes can be less or more effectively excited, depending on NP order. Most notably, when two Ag NPs are placed next to

each other, all the characteristic peaks of a Ag dimer (bonding dipole and higher-order modes) manifest themselves distinctively, as can be verified by the field plots as well (Fig. 1d).

We now focus on the longer linear and disordered chains which can be found as constituents of large self-assembled clusters. It has already been shown that, as the number of NPs in a Au chain increases, the CCP mode redshifts, until, for about 12-16 NPs it reaches a saturation wavelength, while it always retains its dipole-like character and the electric field remains concentrated in the interparticle gaps [3]. In Fig. 2a we gradually replace some of the Au NPs in such a 16-NP chain with Ag ones. As already expected from the trimers studied above, the CCP mode blueshifts as the number of silver spheres increases and the two Drude-like metals are mixed. For shorter wavelengths, various peaks originating mostly from individual Ag NPs and dimers, which have smaller absorptive losses, are also discernible in the extinction spectra, and they produce significant local EM field enhancements, as shown in Fig. 2b. In Figs. 2c and 2d we further explore the applicability of the chain model in the case of hetero-aggregates by gradually introducing spatial disorder in the linear chains. Clearly, both near- and far-field spectra remain very stable, nearly independent of disorder, until the cluster's shape is such that no chain parallel to the incident electric field can be identified.

In summary, we showed that the optical response of Au-Ag NP heteroaggragates can be undestood in terms of excitation of CCP modes within the clusters. These modes are very robust with respect to NP order within the cluster, but can be efficiently tuned by modifying the NP ratio.

References

[1] H. Xu et al., Phys. Rev. E, 62 (2000) 4318.
[2] R. W. Taylor et al., ACS Nano, 5 (2011) 3878.
[3] R. Esteban et al., Langmuir, 28 (2012) 8881.
[4] G. Bachelier et al., Phys. Rev. Lett., 101 (2008) 197401.
[5] C. Tserkezis et al., Part. Part. Syst. Charact., 31 (2014) 152.

Figures

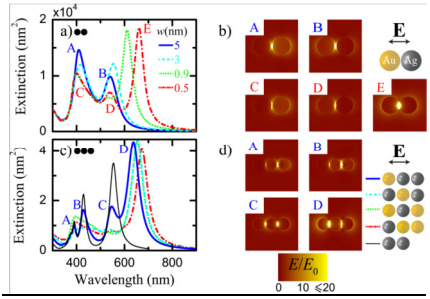

Figure 1: (a) Extinction spectra for an Au-Ag dimer in water as a function of the width of the interparticle gap, w, and (b) contours of the electric field amplitude, *E*, normalised to the incident field, E_0, for *w* = 5 nm (A, B) and w = 0.5 nm (C-E), at the wavelengths denoted by the letters. (b) Extinction spectra for all different realisations of an Au-Ag trimer, and (d) electric field contours for the Au-Ag-Ag (blue line) case.

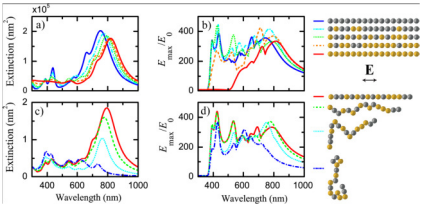

Figure 2: (a) Extinction spectra and (b) maximum electric field enhancement at a gap, for the 16-nanosphere Au-Ag linear chains shown on the right. (c) Extinction spectra and (d) maximum electric field enhancement at a gap, for the disordered chains shown on the right (Au:Ag ratio equal to 1:1).

Magnetoplasmonic nanorings as novel architectures with tunable magneto-optical activity in wide wavelength ranges

Hua Yu Feng[1], Feng Luo[1], Renata Kekesi[2], Daniel Granados[1], David Meneses Rodríguez[2], Jorge M. García[2], Antonio Garcia Martín[2], Gaspar Armelles[2], and Alfonso Cebollada[2]

[1] IMDEA Nanoscience, Faraday 9, Ciudad Universitaria de Cantoblanco, 28049, Madrid, Spain
[2] IMM-Instituto de Microelectrónica de Madrid (CNM-CSIC), Isaac Newton 8, PTM, E-28760 Tres Cantos, Madrid, Spain

huayu.feng@imdea.org

A novel magnetoplasmonic system constituted by Au/Co/Au nanorings fabricated by hole mask colloidal lithography is presented. They exhibit a bimodal resonant behavior in the optical and, more noticeably, in the magneto-optical (MO) properties. We demonstrate that fine control and enhancement of the MO activity can be achieved by modifying ring's structural dimensions such the apex-to-apex distance, and/or the inner and outer ring diameter. This way, large MO activity with moderate optical losses can be achieved in the visible range. Additionally, sizeable MO activity spectrally spans from the visible to the near IR, extending the spectral range over which current magnetoplasmonic structures exhibit MO activity.

References

[1] G. Armelles, A. Cebollada, A. García-Martín, M. U. González, Adv. Optical Mater. 1 (2013) 10.

[2] G. Armelles, A. Cebollada, A. García-Martín, J. M. García-Martín, M.U. González, J. B. González-Díaz, E Ferreiro-Vila, J. F. Torrado, J. Opt. A: Pure Appl. Opt. 11 (2009) 114023.

Figures

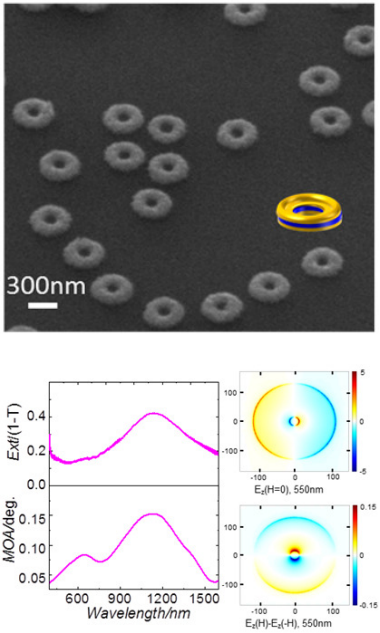

Figure 1: (Up) SEM image and sketch of the fabricated magnetoplasmonic Au/Co/Au nanorings. (Bottom) Typical extinction and polar Kerr MO spectra obtained. Note the clear bimodal resonant nature of the rings' MO activity. (Bottom) Calculated near field intensity of the Ez electric field component for a characteristic nanoring structure in the absence of external magnetic field (up) and corresponding magnetic field induced component (down) corresponding to the high energy MO mode shown in the left.

Polarization plane rotation produced by 3D chiral metamaterial structures in W-band

Oscar Fernández Fernández, Álvaro Gómez Gómez, Angel Vegas García

Universidad de Cantabria, Plaza de la Ciencia s/n, 39005 Santander, Spain

oscar.fernandez@unican.es

Metamaterials are artificial composite materials that exhibit further properties neither available in the nature nor observed in its constituents, or enhancing the composite features relative to the individual properties of its constituents. Among them, we can highlight the Chiral Metamaterials (CMM), which present, besides negative refractive indices, high rotation angles of the polarization plane rotation [1].

Regarding to CMMs manufacturing, several techniques can be found: (i) the traditional one, wherein helical inclusions are dispersed in a dielectric host medium [2] and (ii) the newer based on the Printed Circuit Board Technology [3]. Besides its lower cost of manufacturing, the latest technique is featured by its designability and easiness of characterization using commercial software. In this communication a comparative parametric study focused on the variation of the polarization plane rotation angle (θ) versus different geometric parameters of several plane CMMs is performed.

A. Structures under analysis

Along this work two sets of planar structures implemented in PCB and exhibiting 3D chirality are analyzed in W-band (75-110 GHz). The first one, called mutual twist structure, is composed of chiral [3] (Fig. 1a) or achiral [4] (Fig. 1b) designs printed on both sides of the PCB with a relative rotation angle (φ) between each face. The second set, named specular structures, presents a 2D chiral geometry on one side of the PCB and its enantiomer, with or without rotation, on the other face (Fig. 2) [5]-[7].

B. Structures characterization

Applying the parameter retrieval algorithm published in [8] the aforementioned structures are characterized by obtaining the transmission (t_{++} and t_{--}) and reflection ($r_{++} = r_{--} = r$) coefficients of both right- (+, RHCP) and left- (–, LHCP) handed circularly polarized waves. In t_{++} notation, the first subscript corresponds to the circular polarization type of the transmitted wave, and the second one refers to the circular polarization type of the incident wave. The optical activity introduced by the chiral medium generates a rotation of the polarization plane (θ), which can be calculated from:

$$\theta = \frac{1}{2}\left[\arg(t_{++}) - \arg(t_{--})\right]$$

C. Parametric study

As it was previously mentioned, one of the main features of the CMM is the high values of the polarization plane rotation that they produce. Thus, in our parametric study, we focus our attention on analyzing the CMM structure geometric characteristics dependence on the rotation of the polarization plane. As example, the rosette-type structure will be tested (see Fig. 1).

Fig. 3 shows the variation of θ vs frequency for different values of the most significant parameters of the structure: relative twist between the rosettes (ϕ), line width (w) and unit cell side length (g). At this point, it is important to note that its 3D chirality is due to the relative twist (ϕ) existing between the stamps of each face. From Fig. 3a, it can be seen that, since for ϕ = 0 the polarization plane of the transmitted wave does not rotate (θ = 0), the structure is achiral. In contrast, when ϕ is increased the CMM sample shows chirality. Additionally, Fig. 3b shows that an increasing of w produces an enlarging of the rosette electrical length and, consequently, a reduction of the structure operating frequency. Finally, in Fig. 3c the effects of the unit cell side length are depicted. It can be seen that when the unit cell size length is increased, the distance between neighboring cells enlarges and, consequently, θ is reduced.

In order to go further, the behaviors of same type of structures are compared. Thus, Fig. 4 presents the variation of θ versus frequency for each group of assemblies. In all cases the Rogers

RO3003 dielectric with $\varepsilon_r = 3$, tg $\delta = 0.0013$ and 5 mils (127 µm) thickness is used. From Fig. 4a, it can be seen that, for the same ϕ and dielectric thickness, the crosses provide greater rotation angles than the rosettes do. Meanwhile, the rosettes present the advantage of being a more compact geometry than the crosses. Thus, for a given operating frequency, the rosettes unit cell will be smaller than the crosses one. The reduction of the unit cell geometry allows placing a greater number of rosettes per unit of area. Finally, for the specular structures (see Fig. 4b), a very different behavior is observed between the responses of the squared, L-shaped and wheeled rosettes.

Acknowledgements

This work has been partially supported by the Spanish Government MINECO through the Research Projects CONSOLIDER CSD2008-00066 EMET and TEC2010-21496-C03-01.

References

[1] J. B. Pendry, Science, 306 (2004) 1353-1355.

[2] Á. Gómez, A. Lakhtakia, J. Margineda, G. J. Molina-Cuberos, M. J. Núñez, J.A. Saiz-Ipiña, A. Vegas, and M. A. Solano, IEEE Trans. Microw.Theory Tech., 56 (2008) 2815-2825.

[3] E.Plum, J.Zhou, J.Dong, V. A. Fedotov, T.Koschny, C. M. Soukoulis, and N. I. Zheludev, Phys. Rev. B, 79 (2009) 035407.

[4] J. Zhou, J. Dong, B. Wang, T. Koschny, M. Kafesaki, and C. M. Soukoulis, Phys. Rev. B, 79 (2009) 121104.

[5] J. Li, F. Q. Yang, and J. F. Dong, Progress In Electromagnetics Research, 116 (2012) 395-508.

[6] R. Zhao, L. Zhang, J. Zhou, Th. Koschny, and C.M. Soukoulis, Phys. Rev. B, 83 (2011) 035105.

[7] Y. Ye, X. Li, F. Zhuang, and S. W. Chang, Appl. Phys. Lett., 99 (2011) 031111.

[8] R. Zhao, T. Koschny, and C. M. Soukoulis, "Chiral metamaterials: retrieval of the effective parameters with and without substrate," Opt. Express, vol. 18, no. 14, pp. 14553–14567. Jul 2010.

Figures

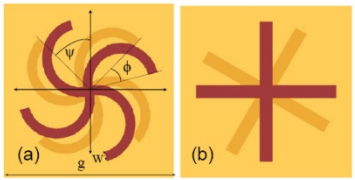

Figure 1: Schematic of mutual twist type structures: (a) rosettes [1] and (b) crosses [3].

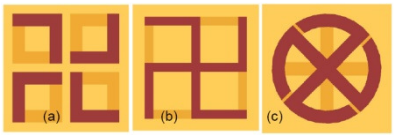

Figure 2: Schematic of specular structures: (a) "L-shaped", (b) conjugated gammadion and (c) wheel.

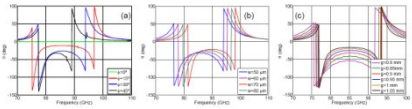

Figure 3: Variation of the polarization plane rotation angle versus frequency for the structure of Fig. 1a for several values of (a) relative twist angle, (b) line width and (c) unit cell side length.

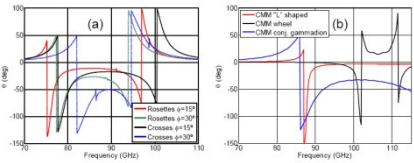

Figure 4: Variation of the polarization plane rotation angle versus frequency for several (a) rosette- and (b) specular- type structures.

Extreme plasmonics in atomically thin materials

F. Javier García de Abajo[1,2]

[1] ICFO - The Institute of Photonic Sciences, Mediterranean Technology Park, 08860 Castelldefels (Barcelona), Spain
[2] ICREA - Institució Catalana de Reserca i Estudis Avançats, Passeig Lluís Companys 23, 08010 (Barcelona), Spain

javier.garciadeabajo@icfo.es

The recent observation [1-4] and extensive theoretical understanding [5-7] of plasmons in graphene has triggered the search for similar phenomena in other atomically thin materials, such as noble-metal monolayers [8] and molecular versions of graphene. [9].The number of valence electrons that are engaged in the plasmon excitations of such thin layers is much smaller than in conventional 3D metallic particles, so that the addition or removal of a comparatively small number of electrons produces sizeable changes in their oscillation frequencies. This can be realized using gating technology, thus resulting in fast optical modulation at high microelectronic speeds. However, plasmons in graphene have only been observed at mid-infrared and lower frequencies, [1-4] and therefore, small molecular structures [9] and atomically thin metals [9] constitute attractive alternatives to achieve fast electro-optical modulation in the visible and near-infrared (vis-NIR) parts of the spectrum. We will discuss several approaches towards optical modulation using atomically thin structures, as well as the challenges and opportunities introduced by these types of materials, including their application to a new generation of quantum-optics and electro-optical devices.

This work has been supported in part by the European Commission (Graphene Flagship CNECT-ICT-604391 and FP7-ICT-2013-613024-GRASP).

References

[1] J. Chen et al., "Optical nano-imaging of gate-tunable graphene plasmons," Nature, vol. 487, pp. 77-81, 2012.
[2] Fei et al., "Gate-tuning of graphene plasmons revealed by infrared nano-imaging," Nature, vol. 487, pp. 82-85, 2012.
[3] Fang et al., "Gated tunability and hybridization of localized plasmons in nanostructured graphene," ACS Nano, vol. 7, pp. 2388-2395, 2013.
[4] Brar et al., "Highly confined tunable mid-infrared plasmonics in graphene nanoresonators," Nano Lett., vol. 13, pp. 2541-2547, 2013.
[5] A. Vakil and N. Engheta, "Transformation optics using graphene," Science, vol. 332, pp. 1291-1294, 2011.
[6] F. H. L. Koppens, D. E. Chang , "Graphene plasmonics: A platform for strong light-matter interactions," Nano Lett., vol. 11, pp. 3370–3377, 2011.
[7] F. J. García de Abajo, "Graphene plasmonics: Challenges and opportunities", ACS Photonics, vol. 1, pp. 135-152, 2014.
[8] A. Manjacacas and F. J. García de Abajo, "Tunable plasmons in atomically thin gold nanodisks,", Nat. Commun., vol. 5, p. 3548, 2014.
[9] A. Manjavacas et al., "Tunable molecular plasmons in polycyclic aromatic hydrocarbons," ACS Nano, vol. 7, pp. 3635-3643, 2013.

Multiband Tunable Large Area Hot Carrier Plasmonic-Crystal Photodetectors

F. Pelayo García de Arquer, Agustín Mihi and Gerasimos Konstantatos

ICFO—Institut de Ciències Fotòniques, Mediterranean Technology Park, 08860 Castelldefels, Barcelona, Spain)

pelayo.garciadearquer@icfo.es

We report highly tunable and multispectral photodetectors based on plasmonic hot-carriers, fabricated via a facile, low cost and large area – soft nano-imprinting technique. We provide optical and electrical characterization of our devices to showcase the feasibility of this architecture in optoelectronics including photodetection and light harvesting.

Optical sensing at visible and infrared wavelengths is of paramount importance for a vast number of applications. To accomplish that task, solid-state photodetection has been vastly employed during the last decades, based on semiconductor materials. In semiconductors, the process upon which photons are converted to electrons relies on photon band-to-band absorption, i.e. only photon energies above the bandgap of the semiconductor can be detected [1]. In the last years, a novel metal-based architecture, free from these frequency restrictions, has been proposed that exploits in one hand, the tunable absorption range provided by a nanostructured metal and, on the other hand, the favorable electronic barrier established in the junction of a metal and a semiconductor to separate carriers [2-5]. This makes possible to take advantage of the plasmon decay into electron-hole pairs generating a photocurrent, which will ultimately depend on the absorption of the metal nanostructure itself. Based on that process, visible [2, 3] or IR-sensitive [4, 5] hot carrier devices have been reported, mostly accomplished by complex and costly nanostructuring of the metal, using e-beam nanofabrication techniques. This methodology poses intrinsic problems for scalability and practical applications. A large-area compatible fabrication method, also capable of producing higher performance, is therefore needed in order to fully exploit the advantages of plasmonic hot-carrier devices. In this work we report a multispectral and highly tunable architecture for visible and near-infrared photodetection (see Figure 1). We study the plasmonic and photonic properties of our architecture and by comparing both experimental spectra and FDTD simulations, shed light on the underlying mechanisms responsible for the high degree of tunability of our devices. Our fabrication approach, based on a low cost and large area compatible soft nano-imprinting lithography, facilitates the way for the implementation of this technology in a great variety of optoelectronic devices.

References

[1] Sze, S. M. Physics of Semiconductor Devices, 2nd ed.; John Wiley & Sons: New York, 1981; p 868.

[2] Lee, Y. K.; Jung, C. H.; Park, J.; Seo, H.; Somorjai, G. A.; Park, J. Y."Surface Plasmon-Driven Hot Electron Flow Probed with Metal-Semiconductor Nanodiodes" Nano Lett. 2011, 11,4251– 4255.

[3] F. Pelayo García de Arquer, Agustín Mihi, Dominik Kufer, and Gerasimos Konstantatos, "Photoelectric Energy Conversion of Plasmon-Generated Hot Carriers in Metal–Insulator–Semiconductor Structures" ACS Nano 2013 7 (4), 3581-3588.

[4] M.W. Knight, H. Sobhani, P. Nordlander and N.J. Halas, "Photodetection with Active Optical Antennas Science 2011, 332, 702–704.

[5] Y. Nishijima, K. Ueno,Y. Yokota, K. Murakoshi, H. Misawa, H. "Plasmon-Assisted Photocurrent Generation from Visible to Near-Infrared Wavelength Using a Au-Nanorods/TiO2Electrode" J. Phys. Chem. Lett. 2010, 1, 2031– 2036.

[6] A. Sobhani, M.W. Knight, Y. Wang, B. Zheng, N.S. King, L.V. Brown, Z. Fang, P. Nordlander, and N.J. Halas. Narrowband photodetection in the near-infrared with a plasmon-induced hot electron device. Nat. Commun. 4, 1643 (2013).

Figures

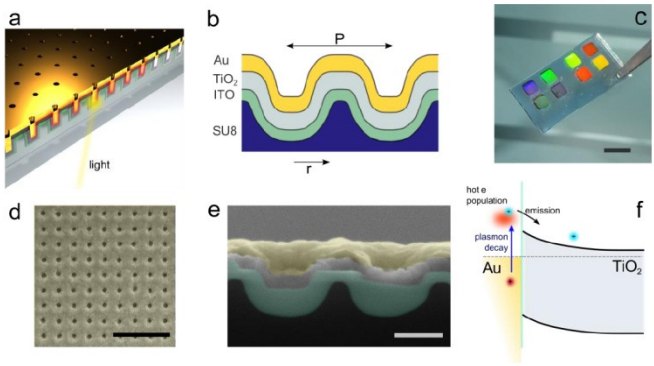

Figure 1: device architecture and principle of operation. (a) Representation of the plasmonic crystal photodetector. Light impinges from the bottom (ITO/glass) exciting resonant modes responsible for the hot electron generation. (b) Schematic of the device architecture: a square array of cylindrical voids in photorresist is coated with 40nm of ITO, followed by 60nm of TiO_2 and 150nm of Au. Different geometries are fabricated varying both lattice parameter (L) and / or the cylinder radius (r). (c) Photograph of a substrate containing eight 9 mm^2 devices; the reflected colors are indicative of the nanostructured metal electrodes. Scale bar is 1 cm. (d) 45° angle view SEM image of the periodic arrays. Scale bar is 2 µm. (e) Cross sectional SEM artificially colored to portray the different layers of the architecture. Scale bar 400 nm. (f) Schematic representation of the photocurrent generation process after light excitation: hot electrons derived from plasmonic damping are emitted over the Au/TiO_2 Schottky barrier into the TiO_2 conduction band.

Magnetically controlled optical nanoantennas

[1]**A. García-Martín**, [2]N. de Sousa and [3]L.S. Froufe-Pérez

[1]IMM-Instituto de Microelectrónica de Madrid (CNM-CSIC), Isaac Newton 8, PTM, E-28760 Tres Cantos, Madrid, Spain.
[2]Departamento de Física de la Materia Condensada,Universidad Autónoma de Madrid, 28049 Madrid, Spain.
[3]Soft Matter and Photonics Group, University of Fribourg, Switzerland.

a.garcia.martin@csic.es

The study of light emission through optical nanoantennas has been a matter of intense research during the last decade. They allow to control and manipulate optical radiation at subwavelength, with applications in photodetection [1, 2], sensing [3], heat transfer [4, 5] or spectroscopy [6], among others. A fluorescent molecule, as a first approximation, can be regarded as a dipole nanoantenna. The emission properties of these molecules, essentially lifetime and angular radiation pattern, depend not only on the intrinsic properties but also on the environment where they are embedded. This phenomenon, initially described by Purcell [7], has been observed in emitters placed close to photonic crystals [8] and more recently in plasmonic [9, 10] and magnetoplasmonic structures [11]. The possibility of creating and manipulate nanostructured materials encouraged the exploration of new strategies to control the electromagnetic properties with an external agent. A possible approach is combining magnetic and plasmonic materials, where it is feasible control the optical properties with magnetic fields [12-14].

In this work we present a fundamental study of the properties of an emitter in two different situations: in the presence of a single magneto-plasmonic nanoparticle and inside a cavity formed by two magneto-plasmonic nanoparticles.

We analyze the effect of the magneto-optical activity both in the decay rate (inverse lifetime) and in the radiated far field patterns.

We will show that the decay rate of an emitter experiments a weak dependence on the magneto-optical effect, both in the presence of a single particle and within a cavity. This weak modification is in contrast to the large modification of the far field pattern for a given range of distances between the emitter and the scatterers. This implies that the radiated field pattern can be dramatically distorted while causing a small modification on the dynamics of the emitter. In the particular case of absorptionless particles, the situation is radically different and there is a region in which also the decay rate is largely affected by the magneto-optical effect.

References

[1] L. Tang, et al., Nature Phot. 2, 226 (2008).
[2] L. Cao, et al., Nano Lett. 10, 1229 (2010).
[3] J.N. Anker, , et al., Nature Mat. 7, 442 (2008).
[4] Y. De Wilde, et al., Nature 444, 740 (2006).
[5] J.A. Schuller, et al., Nature Phot. 3, 658 (2009).
[6] L. Novotny, et al., Annu. Rev. Phys. Chem. 57, 303 (2006).
[7] E.M. Purcell, Phys. Rev. 69, 681 (1946).
[8] P. Lodahl, et al., Nature 430, 654 (2004).
[9] R. Carminati, et al., Optics Comm. 261, 368 (2006).
[10] E. Castanié, et al., Opt. Lett. 37, 3006 (2012).
[11] D. Nikolova, and A. J. Fisher, Phys. Rev. B 88,125136 (2013).
[12] G. Armelles, et al., Adv. Opt. Mat. 1, 10 (2013).
[13] G. Armelles, et al., Opt. Express 21, 27356 (2013).
[14] N. de Sousa, et al., submitted

Fine tuning of size and polydispersity of hollow carbon spheres

Luz Carime Gil-Herrera,[a] Beatriz H. Juárez,[b,c] Cefe López[a]

[a]Instituto de Ciencia de Materiales de Madrid, Consejo Superior de Investigaciones Científicas (CSIC), C/Sor Juana Inés de la Cruz 3, 28049 Madrid (Spain).
[b]IMDEA Nanociencia, Faraday 9, Campus de Cantoblanco, 28049 Madrid (Spain).
[c]Departamento de Química-Física Aplicada, Universidad Autónoma de Madrid, Cantoblanco, 28049 Madrid (Spain)

luzkar12@icmm.csic.es

Due to their morphology, low density and high surface area hollow carbon spheres have attracted much attention in several fields for applications in catalysts, energy storage-media, or drug delivery. Furthermore, their use as building blocks to produce high ordered structures is also an appealing feature in photonics. [1, 2]

In this work the optimized conditions for the preparation of hollow carbon spheres have been studied by means of a 2-step method. This method involves the use of polystyrene beads as seeds and glucose as precursor in a hydrothermal treatment [3] followed by further carbonization at high temperatures. [4] The concentration of polystirene beads, size, polystyrene/glucose ratio, hydrothermal and carbonization temperatures as well as reaction time allow for a fine tuning of the size (100-1000 nm) and monodispersity (<4%) of the final carbon shell structures. Figure 1a show a SEM image of carbon spheres produced with initial 260 nm polystyrene beads as seeds where broken spheres evidence the empty cores (Figure 1b).

References

[1] T. Zhang, Q. Zhang, J. Ge, J. Goebl, M. Sun, Y. Yan, Y. Liu, C. Chang, J. Guo, and Y. Yin, J. Phys. Chem. C., 113 (2009) 3168.
[2] M. Goodman, K. Arpin, A. Mihi, N. Tatsuda, K. Yano, and P. Braun, Adv. Optical Mater., 1 (2013) 300.
[3] R. White, K. Tauer, M. Antonietti, and M. Titirici, J. Am. Chem. Soc., 132 (2010) 17360.
[4] Q. Wang, H. Li, L. Chen, X. Huang, Carbon, 39 (2001) 2211.

Figures

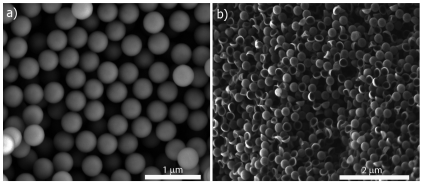

Figure 1: 1a) Hollow carbon spheres obtained from polystyrene beads as seeds. b) Broken spheres evidencing empty cores.

Magnetic Field Modulation of Chirooptical Effects in Magnetoplasmonic Structures

Gaspar Armelles, Blanca Caballero, Patricia Prieto, Fernando García, Alfonso Cebollada, **María Ujué González**, Antonio García–Martin

IMM-Instituto de Microelectrónica de Madrid (CNM-CSIC), Isaac Newton 8, PTM, E-28760, Tres Cantos, Madrid, Spain

gaspar@imm.cnm.csic.es
maria-ujue.gonzalez@csic.es

Chirality is an important property in biology and pharmacology, since a significant proportion of the molecules of interest within these fields show it and their function is determined by the chiral configuration. In the last years, new chiral materials based on metallic nanostructures have been developed, presenting high values of optical activity due to plasmon excitation [1,2]. Due to the high values of chirooptical effects obtained, these systems have allowed the realization of structures with negative refraction behavior [3] and sensors with enhanced chiral sensitivity [4].

At the same time, structures with plasmon resonances and magneto-optical (MO) activity, the so-called magnetoplasmonic systems, have also been studied [5]. In this case, it has been shown that high values of MO activity may be achieved upon plasmon excitation, and that the plasmonic properties may be modulated under the action of an external magnetic field because of the MO activity. These two effects find application niches for example in sensing or telecommunications.

A magnetic field applied along the propagation direction of a circularly polarized light propagating in a chiral medium does not modify the polarization state of the light and thus it induces no coupling between the eigenmodes of the chiral media. Therefore, plasmonic structures presenting simultaneously optical activity and magneto-optical properties are potential candidates to develop tunable chiral structures whose properties could be controlled by a magnetic field. We have recently proved this concept by analyzing magnetoplasmonic chiral structures based on gammadion crosses [6].

In particular, the structures consist of two-dimensional arrays of Au gammadions in which thin layers of Co have been inserted (see sketch in Fig. 1). Due to the magnetic properties of the Au/Co interface, the structures have perpendicular magnetic anisotropy which favors magnetic saturation along the surface normal, allowing magnetic field modulation of the chirooptical response with moderate magnetic fields. The structures present two main resonances in the spectral range of 400nm-1100nm (Fig. 2a), with different chirooptical response and magnetic field induced effects. The resonance at 850 nm has a larger chirooptical response than the resonance at 650 nm, which, on the other hand, exhibits a larger magnetic field modulation of its chirooptical response (Fig. 2b). This dissimilar behavior is due to the different physical origin of the chirooptical and magneto-optical responses. Whereas the chirooptical effects are due to the geometry of the structures, the magneto-optical response is related to the intensity of the electromagnetic field in the magnetic (Co) layers. We also show that the optical chirality can be modulated by the applied magnetic field, which suggests that magnetoplasmonic chiral structures could be used to develop new strategies for chirooptical sensing

References

[1] A. Guerrero-Martinez, J. L. Alonso-Gomez, B. Auguie, M. M. Cid, and L. M. Liz-Marzan, Nano Today, 6 (2011) 381.

[2] M. Hentschel, M. Schäferling, T. Weiss, N. Liu, and H. Giessen, Nano Lett., 12 (2012) 2542.

[3] Z. Li, M. Mutlu and E. Ozbay, J. Opt., 15 (2013) 023001.

[4] E. Hendry, T. Carpy, J. Johnston, M. Popland, R. V. Mikhaylovskiy, A. J. Lapthorn, S. M. Kelly, L. D. Barron, N. Gadegaard, and M. Kadodwala, Nat. Nanotechnol., 5 (2010) 783.

[5] G. Armelles, A. Cebollada, A. García-Martín and M. U. González, Adv. Opt. Mater. 1, (2013) 10.

[6] G. Armelles, B. Caballero, P. Prieto, F. García, A. Cebollada, M.U. González, and A. García-Martín, Nanoscale, 6 (2014) 3737.

Figures

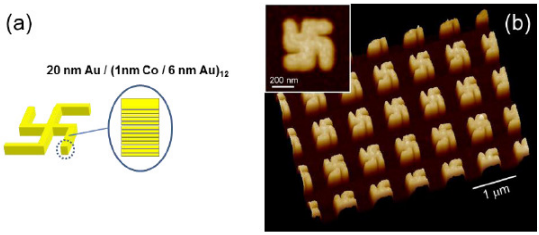

Figure 1: (a) Schematic of the internal layers configuration of a magnetoplasmonic gammadion. (b) AFM image of one of the fabricated arrays.

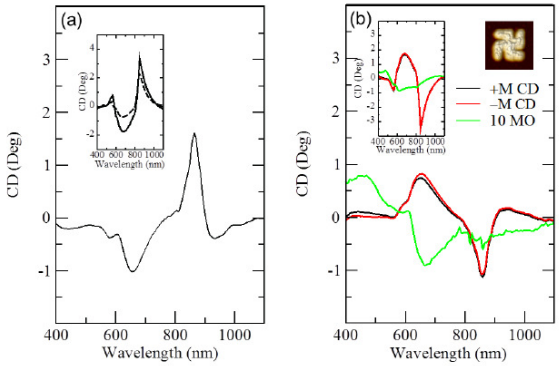

Figure 2: (a) Experimental (main graph) and theoretical (inset) circular dichroism spectra of right handed Au/Co gammadions arrays. (b) Experimental (main graph) and theoretical (inset) circular dichroism spectra of left handed Au/Co gammadions arrays, magnetized along the positive (black curves) and negative (red curves) direction of the z-axis, respectively. The green curves correspond to the magnetic circular dichroism (MCD) spectra. The MCD signal has been multiplied by 10.

Resolving light spin via angular-to-linear moment conversion in a silicon microdisk nanoantenna

Francisco J .Rodríguez-Fortuño, Isaac Barber-Sanz, Daniel Puerto, **Amadeu Griol** and Alejandro Martínez*

Nanophotonics Technology Center, Universitat Politècnica de València, Camino de Vera, s/n, 46022, Valencia, Spain

*amartinez@ntc.upv.es

It has been recently shown that the propagation direction of guided waves can be properly selected just by using as an excitation source a circularly-polarized dipole put in close proximity to a waveguide [1]. Although in Ref. [1] the concept was experimentally demonstrated for plasmonic waves (visible wavelengths), it can be extended to other kinds of waveguides and technological platform. In this work, we have used this concept to demonstrate experimentally at telecom wavelengths that a silicon microdisk nanoantenna can resolve the handedness (or spin) of an incoming light.

The idea is briefly sketched in Fig. 1. A circular microdisk resonator is known to support resonant whispering gallery modes displaying angular momenta given by $\pm l\hbar$, where *l* is the azimuthal number. Unlike higher-order modes that can display ultrahigh Q factors, the fundamental mode (*l*=1), which is essentially a dipolar resonance, is highly radiative. Under normal incidence with circularly polarized light (CPL), one of the two degenerate fundamental modes, with an angular momentum per photon equal to $+\hbar$ (for left-handed circular polarization, LCP) or $-\hbar$ (for right-handed circular polarization, RCP), is excited. This means that there is an angular momentum transfer and match between the incoming CPL light beam and the microdisk nanoantenna.

Now let us consider that the microdisk nanoantenna is implemented on a silicon photonics platform close to a waveguide. It is well known that the resonant modes of a microdisk can be excited on-chip by introducing light through an optical waveguide which at some point is in close proximity to the microdisk, and the direction of propagation of light along the waveguide (or the direction of the linear momentum of the guided photons) will define the direction of rotation of the fields inside the microdisk at the resonance frequencies, due to local phase matching in the interacting region, and as a consequence, will define the sign of the excited angular momentum. In accordance to reciprocity, the reverse approach is also true: if a given resonance in the microdisk is excited from free space using CPL, part of the angular momentum transferred to the microdisk will be finally converted into linear momentum, which will result in light propagation along one or another direction of the waveguide depending on the handedness of incident light. Such unidirectional excitation of waveguided modes depending on the handedness of the microdisk resonant mode can also be easily interpreted as near-field interference, which inspired us to pursue this result. Therefore, the device will be capable of discerning between LCP and RCP without employing chiral structures. Notice that the placement of the microdisk with respect to the waveguide will determine the sorting direction of each handedness. The x-asymmetry achieved in the amplitude of excitation of the two waveguide outputs is only possible thanks to the broken y-symmetry in the full (microdisk + waveguide) structure, which constitutes a fundamental requirement of this approach.

Experimental results are in close agreement to numerical results which predict an extinction ratio over 18 dB in a 20 nm bandwidth, which by far outperforms other approaches for resolving light spin. Importantly, the device is reciprocal, so in a transmitting configuration it can radiate right or left circular polarization depending on the chosen feeding waveguide chosen.

This work complements the results shown in Ref. [2] in which a rectangular nanoantenna was used to sort linearly polarized photons. As in Ref. [2], feeding by both input waveguides simultaneously our device can generate any polarization state on the Poincaré sphere [3],

which could be a disruptive step in the field of optical nanoantennas.

Acknowledgement

This work has been supported by Spanish Government and European Union (EU) funds under contracts CSD2008-00066 and TEC2011-28664-C02-02, and Universitat Politècnica de València.

References

[1] F. J. Rodríguez-Fortuño, G. Marino, P. Ginzburg, D. O'Connor, A. Martínez, G. A. Wurtz, and A. V. Zayats, Science 340, 328 (2013).

[2] F. J. Rodríguez-Fortuño, Daniel Puerto, Amadeu Griol, Laurent Bellieres, Javier Martí, and Alejandro Martínez, "Sorting linearly polarized photons with a single scatterer," Opt. Lett. 39, 1394-1397 (2014).

[3] F. J. Rodríguez-Fortuño, D. Puerto, A. Griol, L. Bellieres, J. Martí, and A. Martínez, "Universal method for the synthesis of arbitrary polarization states radiated by a nanoantenna," to appear in Laser Photon. Rev. (2014).

Figures

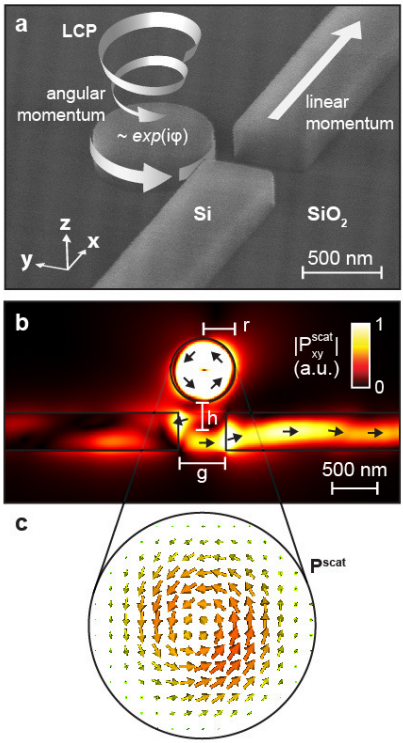

Figure 1: Scheme of the silicon circular nanoantenna that resolves the spin of a normally incident circularly polarized light beam. (a) Scanning electron microscope (SEM) image of the fabricated microdisk and silicon waveguide, annotated with arrows describing the fundamental idea of this approach. (b) Magnitude of the in-plane component of the Poynting vector of the scattered fields in the midplane of the silicon structure when a left-handed circularly polarized (LCP) plane wave is incident (scattering is obtained by subtraction of the background fields in a straight waveguide to the total fields obtained in numerical simulations), and (c) a vector plot of the Poynting vector of the scattered fields in the midplane inside the nanodisk. It is evident from symmetry that an incident right-handed circularly polarized (RCP) wave will excite the microdisk and waveguide with an x-mirror-symmetry, directing the light into the left output waveguide.

Theory of absorption-induced transparency

Sergio G. Rodrigo[1,2] F.J. García-Vidal[3], and L. Martín-Moreno[2]

[1]Centro Universitario de la Defensa, Carretera de Huesca, E-50090 Zaragoza, Spain
[2]Instituto de Ciencia de Materiales de Aragón and Departamento de Física de la Materia Condensada,CSIC-Universidad de Zaragoza, E-50009, Zaragoza, Spain
[3]Departamento de Física Teórica de la Materia Condensada, Universidad Autónoma de Madrid, E-28049 Madrid, Spain

sergut@unizar.es

Absorption induced transparency (AIT), roughly speaking, is a peak seen in the transmission spectrum of a holey metal film when a molecular dye is deposited on top of it [1]. The AIT peak appears unexpectedly close to one of the absorption energies of the molecules, hence its name. Tentative explanations of AIT pointed to strong-coupling interactions between Surface-Plasmon-Polaritons (SPPs) and molecules, when they are close by the metal surface (not inside the holes) [1].

Here we present our findings and extend our recent theoretical work on AIT [2]. We show the actual physical mechanism behind AIT. This takes place through a strong modification of the propagation constant of holes, kz, so the holes must be at least partially filled. The spectral position of an AIT peak, its intensity and full width is mainly controlled by the spectral features of kz. Therefore AIT has a localized character, which also explains that it occurs in single holes. In addition, we demonstrate that hole arrays in the AIT regime behave like a metamaterial characterized by a dielectric constant composed by a Drude plasma term (geometric origin) plus a Lorentz term due to the molecules. We also show that AIT peaks are nonplasmonic in character, so they are expected to occur at frequency regimes different than the optical, which opens the door for detection spectroscopy of chemical compounds with sharp absorption lines in the THz or microwave regimes.

To illustrate how AIT depends on the amount of molecular dye in the holes, we show in Fig.1(b) three transmission curves as a function of the wavelength, calculated with the Finite-Difference Time-Domain method (see caption for details). We choose the parameters in our model so the results best match the ones in Ref. [1], the dielectric constant of the molecules characterized by a Lorentz function. When the molecules are present and filling the holes (solid line) transmission clearly displays an AIT peak around 710nm, which is absent both without the molecules (dotted line) and even when they are not allowed to fill the holes, but deposited within a thin layer of polymer (dashed line). The rest of transmission features are Extraordinary Optical Transmission (EOT) peaks, boosted by the excitation of SPPs.

References

[1] J.A. Hutchison, D.M. O'Carroll, T. Schwartz, C. Genet, and T.W. Ebbesen, "Absorption-induced transparency", Angew. Chem. Int. Ed. 50, 2085 (2011).

[2] S.G. Rodrigo, F.J. García-Vidal, and L. Martín-Moreno,"Theory of absorption-induced transparency", Phys. Rev. B 88, 155126 (2013).

Figures

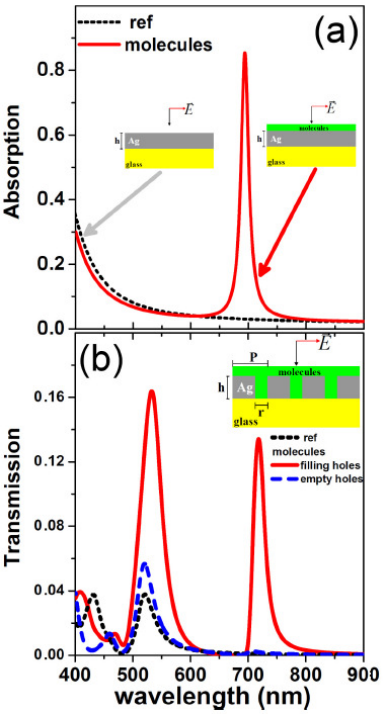

Figure 1: (a) An optically thick silver film is illuminated from the top, the absorption spectrum calculated then for two different "covering" media: air (dotted line) and molecules embedded within a polymer (solid line). (b) Transmission through a hole array covered and filled with molecules (solid line), just covered - no molecules inside- (dashed line) and without molecules (dotted line). Two EOT peaks are observed at wavelengths shorter than 650nm. The "filled" configuration shows an "extra" feature around 710nm, an AIT peak, apparently appearing at the absorption energy of the molecules. Hole array parameters: circular holes (*radius* = 70 nm), period P = 250 nm, and 200nm metal film thickness. The polymer layer is 30 nm in width.

Metallic arrays for directional light-emitting devices

Gabriel Lozano[1,*,#], Said R. K. Rodríguez[1], Marc A. Verschuuren[2], Jaime Gómez Rivas[1,3]

[1] Center for Nanophotonics, FOM Institute AMOLF, The Netherlands
[2] Philips Research, The Netherlands
[3] COBRA Research Institute, Eindhoven University of Technology, The Netherlands
present address: Institute of Materials Science of Seville, Spanish Research Council (CSIC)

*g.lozano@csic.es

The development of efficient light sources based on light-emitting diodes (LEDs) is a central goal for solid-state lighting (SSL). The most widely employed route to achieve white light using LEDs consist in combining an electrically driven blue LED and a material, usually known as a phosphor that absorbs part of the blue light and emits in the green-to-red region of the electromagnetic spectrum. The critical role played by this emitting material in SSL has guided most of material research efforts in this field. With the advent of stable and ultra-high efficient emitters, research in SSL is shifting towards the use of nanostructures that allows an accurate control over the intensity, color content, directionality and polarization of the emission. Nanostructuring strategies represent a versatile approach to tailor the emission characteristics of the phosphor without changing its intrinsic structural properties or chemical composition.

Metal nanoparticles provide unique ways of controlling light at length scales smaller than the wavelength through the excitation of surface plasmons. Herein, we demonstrate that the emission of a phosphor-converted LED can be boosted by aluminum nanoparticles that enhance the directionality of the emitted light such that it is preferably emitted straight from the surface, rather than toward the side. The emission in this direction is enhanced by more than a factor of 60 for a specific color. This directional enhancement is the result of the plasmonic enhanced excitation of the phosphor and its decay into collective resonances supported by the array of nanoparticles. These lattice-induced resonances arise from the coupling of localized surface plasmon polaritons to photonic modes induced by the array. In contrast to localized surface plasmon resonances, collective resonances have a large spatial extension and can couple very efficiently to free space radiation due to their hybrid photonic-plasmonic character. These features lead to a highly directional emission in defined directions which can be controlled by the shape and dimensions of the particles and by the lattice geometry. This demonstration opens a new path for fundamental and applied research in SSL in which plasmonic nanostructures are able to mold the emission with unprecedented precision.[1].

References

[1] G. Lozano, D. J. Louwers, S. R. K. Rodríguez et al., Light: Sci. Appl. 2, e66 (2013).

High-sensititive magnetoplasmonic label-free sensing using Ni nanodisks

N. Maccaferri[1], K. Gregorczyk[1], T. V. A. G. De Oliveira[1], M. Kataja[2], S. van Dijken[2], Z. Pirzadeh[3], A. Dmitriev[3], M. Knez[1,4], and P. Vavassori[1,4]

[1]CIC nanoGUNE Consolider, 20018 Donostia-San Sebastián, Spain
[2]Aalto University School of Science, 00076 Aalto, Finland
[3]Chalmers University of Technology, 41296 Gothenburg, Sweden
[4]IKERBASQUE, Basque Foundation for Science, 48011 Bilbao, Spain

n.maccaferri@nanogune.eu

Plasmonic sensors based on the environment sensitivity of localized surface plasmon resonances (LSPRs) excited in metallic nanoparticles are attracting a lot of attention. Pure ferromagnetic (FM) nanostructures are not usually considered for sensing purposes, due to their highly damped plasmonic behavior [1]. FM nanostructures show intrinsically higher LSPRs refractive index sensitivity ($S_{RI}=\Delta\lambda_{SPR}/\Delta n$) than noble metals. However, the broad and low intensity plasmonic peak result in a figure of merit (FoM, defined as SRI normalized to the FWHM of the LSPR peak) much lower than that for noble metal nanostructures. Pure FM plasmonic nanostructures supporting LSPRs and magneto-optical (MO) activity [2-4] have been investigated. By taking advantage of the magneto-optical Kerr effect (MOKE), phase-sensitive measurements of LSPRs are enabled by looking at the spectral position of the Kerr ellipticity ε_K vanishing point (zero crossing) [4]. Using this concept we show that pure FM nanostructures provide unprecedented sensitive detection capabilities, having significantly higher SRI than standard noble metals [5]. In addition and more important, the high precision tracking of the ellipticity vanishing point results in FoMs exceeding 10^2, even higher than the maximum values measured for noble metal nanostructured systems based on LSPRs reported in literature [6]. This really opens the pathway to an entirely unused class nanostructured materials for sensing applications.

References

[1] J. Chen et al., Small 7 (2011) 2341.
[2] V. Bonanni et al., Nano Lett., 11 (2011) 5333.
[3] N. Maccaferri et al., Optics Express 21 (2013) 9875.
[4] N. Maccaferri et al., Phys. Status Solidi A, in press (2014).
[5] N. Maccaferri et al., Phys. Rev. Lett. 111 (2013) 167401.
[6] N. Maccaferri et al., submitted (2014).
[7] Y. Shen et al., Nat. Comm. 4 (2013) 2381.

Figures

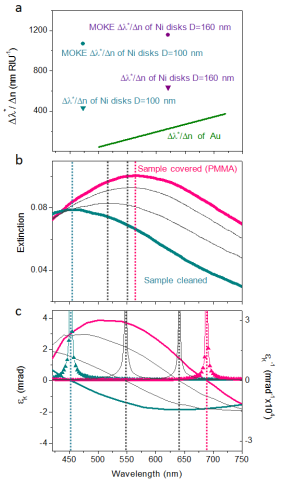

Figure 1: a Comparison between the optical sensitivity of Au nanostructures and the optical and magneto-optical sensitivities of Ni nanostructures. b Extinction spectra of Ni nanodisks before and after PMMA spin-coating (grey lines correspond to intermediate steps of covering). c Magneto-optical Kerr effect (MOKE) measurements of the Kerr ellipticity ε_K and of its inverse ε_K^{-1} before and after PMMA spin-coating.

Plasmonic phase tuning of magneto-optics in ferromagnetic nanostructures

Nicolò Maccaferri[1], Andreas Berger[1], Stefano Bonetti[2], Valentina Bonanni[3], Mikko Kataja[4], Sebastiaan van Dijken[4], Josep Nogués[5,6], Johan Åkerman[7], Zhaleh Pirzadeh[8], Alexandre Dmitriev[8], and Paolo Vavassori[1,9]

[1]CIC nanoGUNE Consolider, Spain
[2]SIMES, SLAC National Accelerator Laboratory, USA
[3]University of Florence & INSTM, 50019 Florence, Italy
[4]NanoSpin, Aalto University, FI-00076 Aalto, Finland
[5]ICN2, Campus UAB, 08193 Bellaterra (Barcelona), Spain
[6]ICREA, Spain
[7]Materials Physics, School of Information and Communication Technology, KTH Royal Institute of Technology, Electrum 229,16440 Kista, Sweden and Physics Department, University of Gothenburg, 41296 Gothenburg, Sweden
[8]Chalmers University of Technology, Sweden
[9]IKERBASQUE, Spain

n.maccaferri@nanogune.eu

Electromagnetic scattering from metallic nanometer-scale particles is currently a topic of huge interest. The vast majority of these studies is performed on noble-metal nanostructures and is focused on the effects on the scattered field due to the nano-confinement of electric fields caused by the excitation of localized plasmon resonances in single nanoparticles. In the last years the research efforts moved on magnetoplasmonic nanostructures, viz., nanostructures that combine magnetic and plasmonic functionalities [1]. These systems could be the building block of a new class of magnetically controllable optical nanodevices for future biotechnological and optoelectronic applications.

Very recently it was shown how the concerted action of localized plasmon resonances in single nanoparticles and magnetization can be exploited to actively manipulate the reflected light's polarizati on (i.e., to induce and control Kerr rotation/ellipticity reversal) of pure ferromagnetic nanostructures beyond what is offered by intrinsic material properties [2], even if plasma oscillations in ferromagnetic materials typically exhibit a stronger damping than in noble metals [3]. While most of the investigations carried out before were focused on the achievement of substantial enhancement of magneto-optical Kerr effect here we study the polarizability of nanoferromagnets to understand the role of the phase of localized plasmon resonances on their magneto-optical activity. We demonstrate that these systems can be described as two orthogonal damped oscillators coupled by the spin-orbit interaction, as shown in Fig. 1. We prove that only the spin-orbit induced transverse plasmon plays an active role on the magnetooptical properties by controlling the relative amplitude and phase lag between the two oscillators [4]. A formalism to compute the polarizability, as well as the far-field magneto-optical spectra, of large magnetic ellipsoidal nanoelements, i.e., exceeding the Rayleigh limit (electrostatic regime) is presented [5]. This approach can be applied to real samples of optically non-interacting flat disks with circular and elliptical sections, and size up to a few hundred nanometers. We find a surprisingly excellent quantitative agreement between calculated and experimental magneto-optical spectra both for circular and elliptical nanodisks, as shown in Fig. 2. In spite of its approximations and simplicity, the formalism developed captures the essential physics of the interplay between magneto-optical activity and localized plasmon resonances in ferromagnetic nanostructures.

References

[1] G. Armelles et al., Adv. Optical Mater. 1 (2013), 10.

[2] V. Bonanni et al., Nano Lett. 11(12) (2011), 5333.

[3] J. Chen et al., Small 7(16) (2011), 2341.

[4] N. Maccaferri et al., Phys. Rev. Lett 111(16) (2013), 167401.

[5] N. Maccaferri et al., Optics Express 21(8) (2013), 9875.

Figures

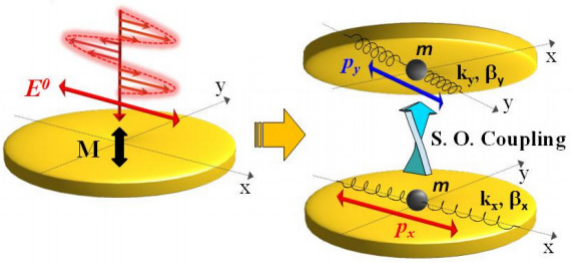

Figure 1: .A ferromagnetic disk modeled with two orthogonal damped harmonic oscillators coupled by the spin-orbit (SO) interaction; m represents the mass of the conduction electrons; the spring constants k_x and k_y originate from the electromagnetic restoring forces due to the displacements of the conduction electrons;β_x and β_y are the damping constants.

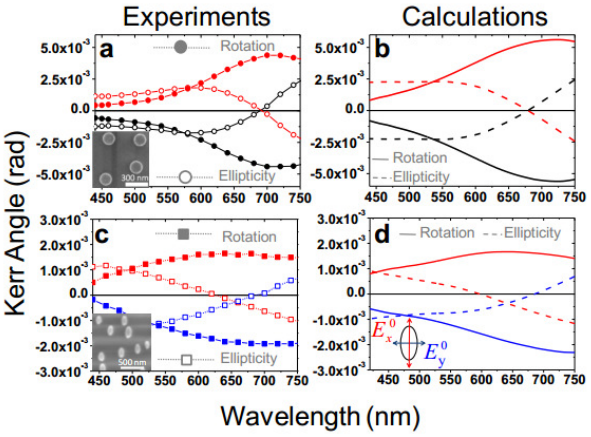

Figure 2: .Experimental magneto-optical spectra for Ni disks with diameter of 160 nm (a) and elliptical disks with in-plane dimensions of 180 nm and 100 nm. The thickness is 30 nm in both cases. Calculated spectra for circular (b) and elliptical (d) disks. Insets: Scanning Electron Microscopy images of a portion of the samples.

Nanoporous anodic alumina based photonic structures for sensing applications

L.F. Marsal, G. Macias, J. Pallarès, J. Ferré-Borrull

Departament d'Enginyeria Electrònica, Elèctrica i Automàtica, Universitat Rovira i Virgili, Avda. Països Catalans 26, 43007 Tarragona, Spain

lluis.marsal@urv.cat

Nanoporous anodic alumina (NAA) has generated considerable attention in nanoscience and nanotechnology due to its cost-effective fabrication process, self-assembled, densely packed and nanoscale-ranged porous structure. The nanopores are straight through the film thickness, parallel to each other and with diameters in the range of 10 to 300 nm. The structural characteristics of the NAA such as pore diameter, interpore distance, porosity, film thickness and barrier layer thickness can be tuned by modifying the anodization conditions [1, 2]. In addition, NAA has demonstrated to be excellent material for producing optical devices by their outstanding set of properties. Optical and photonic properties as reflectance, transmittance, absorbance and photoluminescence can be structurally engineered by modifying the effective medium of the NAA [3, 4]. Furthermore, further chemical functionalization endows NAA platforms with chemical selectivity for detection of specific analytes.

In this work, we introduce new different techniques developed in our group for the structural engineering of nanoporous anodic alumina. We show different examples of engineered NAA for sensing: the definition of photonic barcodes from photoluminescence or reflectance spectra of NAA, the improvement of sensitivity in two-layer NAA structures and the refractive index sensing device using the central wavelength of a rugate filter stop band, etc [5-8]. Finally, we analyze and discuss different detection techniques such as reflectometric interference spectroscopy, photoluminescent spectroscopy and test their performance in the detection of proteins and heavy metal ions.

Acknowledgements

This work was supported by the Spanish Ministry of Economy and competitiveness (MINECO) under grant number TEC2012-34397 and Generalitat de Catalunya under project 2009 SGR 549.

References

[1] Santos, A., Ferré-Borrull, J., Pallarès, J., Marsal, L.F., Physica Status Solidi (A) 208 (2011) 668.

[2] Santos, A., Vojkuvka, L., Alba, M., Balderrama, V.S., Ferré-Borrull, J., Pallarès, J., Marsal, L.F., Physica Status Solidi (A) 209 (2012) 2045.

[3] Maksymov, I., Ferré-Borrull, J., Pallarès, J., Marsal, L.F., Photonics and Nanostructures - Fundamentals and Applications 10 (2012) 459.

[4] Santos, A., Alba, M., Rahman, M.M., Formentin, P., Ferre-Borrull, J., Pallarès, J., Marsal, L.F., Nanoscale Research Letters 7 (2012) 228.

[5] Santos, A., Balderrama, V. S., Alba, M., Formentín, P., Ferré-Borrull, J., Pallarès, J., Marsal, L. F. Advanced Materials 24 (2012) 1050.

[6] Santos, A., Macias, G., Ferré-Borrull, J., Pallarès, J., Marsal, L.F., ACS Applied Materials and Interfaces 4 (2012) 3584.

[7] Macias, G., Hernández-Eguía, L.P., Ferré-Borrull, J., Pallarès, J., Marsal, L.F., ACS Applied Materials and Interfaces 5 (2013) 8093.

[8] Rahman, M.M., Marsal, L.F., Pallarès, J., Ferré-Borrull, J., ACS Applied Materials and Interfaces 5 (2013) 13375.

Refractive index sensor based on a curved biconical tapered fiber

S. Mas[1], J. Palací[1], R. Caroselli1, D. Zurita[1], J. García-Rupérez[1], D. Monzón-Hernández[2], and J. Martí[1]

[1]Valencia Nanophotonics Technology Center, Universitat Politècnica de València, 46022 Valencia, Spain
[2]Centro de Investigaciones en Óptica A.C., 37150 Guanajuato, México

smasg@ntc.upv.es

Biconical tapered fibers have been widely used to modify the propagation characteristics of standard fiber in optical communication systems. They are obtained by a heating and stretching process along the propagation axis that results in a uniform waist between two transition regions [1]. Depending on the geometry of these tapered regions adiabatic and non-adiabatic tapered fibers with gradual and abrupt transitions, respectively, can be distinguished. In the non-adiabatic case the fundamental mode couples into two modes, one propagating in the core of the waist and another traveling through the air-cladding interface. Each mode experiences different propagation conditions because of their distinct effective indexes. The interference between these two modes creates a spectral fringe pattern whose visibility and periodicity depends on the waist length and the effective indexes of the modes.

Different devices based on optical technology have been developed to perform sensing. Those based on optical fiber are especially convenient because they provide high mode confinement with little losses. Fiber-based sensors have been developed to detect, among others, changes in temperature, strain or refractive index. For the latter, the air-cladding mode interacts with the outer medium shifting the sensor response thus providing an indirect measurement of the medium refractive index. Depending on the technology employed different sensitivity values have been achieved [2], including those based on tapered fibers [3].

In this work we propose a simple way to carry out refractive index measurements through bending of a tapered fiber. Low-loss sharp curves can be made in the tapered fiber when the refractive index of the sensed medium is considerably lower from that of the cladding. In this case the mode simply suffers from propagation losses. However, when the outer refractive index becomes similar to the index of the cladding a sharp curve will result in high radiation losses because the mode is poorly confined. It is therefore possible to estimate the refractive index of the outer medium through measurement of the radiated power.

Figure 1(a) shows the profile of the straight (i.e. without any introduced curvature) tapered fiber used in the experiment, where τ_t = 1 mm, L_w = 13 mm and ρ = 18 μm. Figure 1(b) shows an schematic of the same tapered fiber after being curved. The refractive index sensor is characterized by means of a broadband optical source and an optical spectrum analyzer. Three different surrounding mediums were considered to characterize the sensor: air, deionized water (DIW) and 10% ethanol concentration in DIW being their refractive indexes n_{air} = 1, n_{DIW} = 1.3173 [4] and $n_{Ethanol10\%}$≈1.338 [5], respectively. All these values are inferior to the cladding effective index which exceeds 1.4. The transfer function of the tapered fiber for the different external indexes is plotted in Fig. 2. It can be seen how losses for the straight taper do not change considerably despite the different absorption coefficient of the ethanol. In this case the refractive index must be deduced from variations in the period of the spectral fringes. However, when the same tapered fiber is curved an increasingly high amount of radiation losses are introduced for outer refractive indexes getting closer to the fiber cladding index. In this case an average power of 0.2 mW becomes 0.05 mW for an estimated increase in the refractive index of 0.0207. Careful interpretation of these results must be made since the relationship between radiated losses and refractive index is not necessarily linear.

In conclusion, a simple technique to fabricate refractive index sensors using curved tapered

fibers is presented. It is based on converting changes in the confinement of the air-cladding mode into optical losses through bending of the tapered fiber. A prototype of the device show good sensitivity in terms of losses per refractive index variation. The whole subsystem can be built using cheap broadband optical sources as LEDs instead of expensive CW lasers required by current approaches.

References

[1] J. Villatoro, D. Monzón-Hernández, and E. Mejía, Appl. Optics, 42(2003) 2278-2283.

[2] I.M. White, and X. Fan, Opt. Express, 2(2008) 1020-1028.

[3] K.Q. Kieu, and M. Mansuripur, IEEE Photonic. Tech. L., 21(2006) 2239-2241.

[4] J. García-Rupérez, V. Toccafondo, M.J. Bañuls, J.G. Castelló, A. Griol, S. Peransi-Llopis, and A. Maquieira, Opt. Express, 23(2010) 24276-24286.

[5] M.P. Duggan, T. McCreedy, and J.W. Aylott, Analyst 128(2003) 1336-1340..

Figures

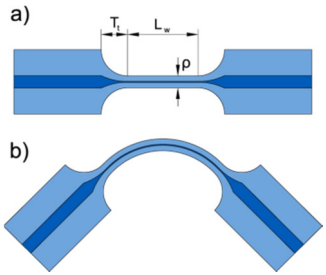

Figure 1: (a) Straight and (b) curved biconical tapered fiber

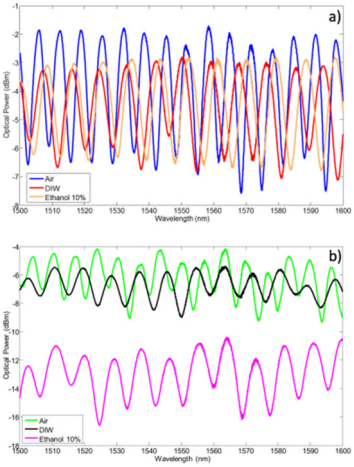

Figure 2: Experimental transfer function of the (a) straight and (b) curved tapered fiber

Hybrid Light Emitting Diodes as novel alternative to traditional light sources

Eugenia Martínez-Ferrero and Alberto Quintana

CETEMMSA, Avda. Ernest Lluch 36, Mataró, Spain

emartinez@cetemmsa.com

Hybrid Light Emitting Diodes (HyLEDs) are novel electro-optic devices in which organic lumophores are combined with inorganic transition metal oxides that act as charge transport layers. The use of the metal oxides results in increased robustness, lower turn-on voltages, enhanced charge transport properties and stability in air of the devices. The enhanced resistance to air and oxygen moisture eliminates the need of encapsulating layers under operation making these devices very interesting for technological applications.

First reported in 2006,[1] research has revealed the potential of these type of devices which behave at the same performance level that the polymer organic light emitting diodes. Furthermore, the organic/inorganic interface has been improved through the reduction of the current leakage, the improvement of the charge injection or the enhancement of the exciton recombination rates.[2,3] Moreover, tuning the organic layer has resulted in light emission at different wavelengths. However, the transition from the laboratory to the industrial devices is hampered by the use of high sintering temperatures that impedes deposition on flexible substrate.

In this communication, we will analyze the potential of these hybrid LEDs and how they can be developed to reach better functionalities. Experimental results will be evaluated in view of the influence played by the morphology of the polymer and the changes at the organic-inorganic interface which are reflected in the luminance and efficiency values.

References

[1] K. Morii, M. Ishida, T. Takashima, T. Shimoda, Q. Wang, M. K. Nazeeruddin and M. Gratzel, Applied Physics Letters, 89, (2006) 183510/183511

[2] M. Sessolo and H. J. Bolink, Advanced Materials, 23, (2011) 1829.

[3] E. Martinez-Ferrero, A. Forneli, C. Boissière. D. Grosso, C. Sanchez and E. Palomares, ACS Applied Materials & Interfaces, 3, (2011) 3248.

Novel photonic configurations in thin film photovoltaics to enhance light absorption

Jordi Martorell

ICFO–Institut de Ciencies Fotoniques, 08860 Castelldefels (Barcelona), Spain

jordi.martorell@icfo.es

Thin film solar cells and, more in particular, organic solar cells present unique properties, such as flexibility, low fabrication cost, or an inherent visible semi-transparency of the active layer that make them an ideal technology for many different applications were the traditional Si based technology cannot be used. However, the use of extremely thin active layer prevents an efficient sunlight harvesting in such kind of devices.

In the current paper we present several approaches to enhance such light harvesting: 1) Using non-ordered one-dimensional photonic crystals to limit the loss in performance when the back metal electrode is thinned down to make the solar cell transparent. We will show 30% visible transparency cells with a 5.6% power conversion efficiency (PCE) equivalent to 72% the PCE of the opaque cell. 2) In an alternative approach we enclosed the active material in between two metal electrodes forming an optical cavity designed to optimize photon trapping inside the cell. We will report experimental results demonstrating that it is possible to obtain 20% visible transparency cells with a PCE equivalent to 92% the PCE of the corresponding opaque cell. 3) We will also report on a cell where the substrate instead of being a planar transparent glass is formed by an array of transparent fibers (See Figure 1). In that configuration photons from the Sun are "longitudinally" coupled into the absorber material along the long axis of the active layer. In other words, photons to be absorbed by such material may travel a distance close to half the perimeter of the fiber, potentially increasing photon absorption probability to 1 at all wavelengths. This longitudinal light coupling or the efficiency of the cell becomes better as we increase the angle of incidence, reaching a maximum value at 55º. 4) Finally we will consider cases where plasmonic nano-particles are embedded in the device architecture to increase light scattering in the active layer.

References

[1] Betancur R., Romero-Gomez P., Martinez-Otero A., Elias X., Maymó M. & Martorell J. Transparent polymer solar cells employing a layered light-trapping architecture. Nature Photon. 7 995-1000 (2013).

Figures

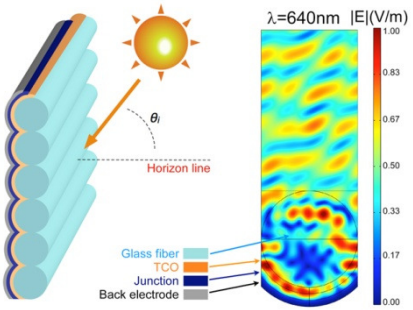

Figure 1: Left: Schematic view of the of a fiber array cell architecture (very thin buffer layers are omitted for simplicity of the figure). Right: Field distribution when the light is incident at 55º.

Low Cost and Large Area Photonic Architectures for Enhanced Light Trapping in Solution Processed Solar Cells

Agustín Mihi[1,2], F. J. Beck[2], T. Lasanta[2], A. K. Rath[2] and G. Konstantatos[2]

[1] Universitat Rovira i Virgili. DEEEA, Escuela Técnica Superior de Ingeniería. Tarragona (Spain)
[2] ICFO. Instituto de Ciéncias Fotónicas. Barcelona (Spain)

agustin.mihi@urv.cat

Emerging photovoltaic technologies cells (dye sensitized, organic and quantum dot based cells) focus in low cost and large area manufacturing and present typical thicknesses ranging from 100nm until several microns, imposed by efficient carrier collection constraints. Therefore, there is a necessity for new light trapping schemes that can be applied to these thin solar cells and at the same time, compatible with industrial manufacturing processes (roll to roll, solution processing, etc.). As opposed to geometric optics approaches where all light wavelengths are treated equally, emerging wave optics based structures target certain ranges where the light harvesting enhancement can be the most beneficial for the cell. Dielectric and metallic photonic architectures can enhance light matter interaction by concentrating the electric field through resonances, increasing the light optical path by diffraction and many other interesting phenomena that cannot be achieved with traditional lenses and mirrors. In this presentation, I will describe how low cost and large area photonic architectures coupled to solution processed PbS quantum dot solar cells [1] facilitate enhanced light trapping within the active layer while being fully compatible with current manufacturing processes [2].

Figures

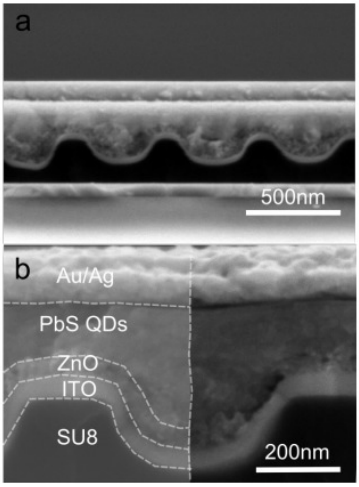

Figure 1: Cross-sectional SEM image of a ZnO-PbS solar cell built on top of a photonic electrode.

References

[1] McDonald, S. A., et al. (2005). Solution-processed PbS quantum dot infrared photodetectors and photovoltaics. Nature Materials, 4(2), 138–42.

[2] Mihi, A., et al. (2014). Imprinted electrodes for enhanced light trapping in solution processed solar cells. Advanced Materials, 26(3), 443–8. .

Photonic forces with random fields. From optics of partially coherent light to Van der Waals and Casimir interactions

Manuel Nieto-Vesperinas and Juan Miguel Auñón

Instituto de Ciencia de Materiales de Madrid, Consejo Superior de Investigaciones Científicas. Campus de Cantoblanco, Madrid, 28049, Spain

mnieto@icmm.csic.es

We describe the consequences of the mechanical action on matter of electromagnetic fields emitted by three-dimensional randomly fluctuating, statistically homogeneous, and isotropic sources. At the selected wavelengths, (visible and near-infrared), the Planck energy is equivalent to that of the vacuum fluctuations. This has important consequences: employing a quasi-monochromatic optical source, the photonic forces on nanoparticles may be tailored at will. In particular, one may create with light forces equivalent to those of Casimir-Polder and Van der Waals interactions. Thus allowing a control studying these forces and beyond them.

We shall discuss the different contributions (electric, magnetic and interference) of the forces, showing how this scenary is ruled by the interplay of the evanescent (conservative) and propagating (non-conservative) modes of both the random field emitted by the fluctuating source and of the wavefields radiated by the electric and magnetic dipoles randomly induced on particles.

In particular, the asymptotic behavior of these stochastic forces close to the source, assesses and goes beyond the current approximations taken in previous studies of Casimir interactions and their relatives.

References

[1] J.M. Auñón, C.W. Qiu and M. Nieto-Vesperinas. “Tailoring photonic forces on a magnetodielectric nanoparticle with a fluctuating optical source”. Phys. Rev. A, 88, 043817 (2013).

[2] A. García-Etxarri et al. “Strong magnetic response of submicron Silicon particles in the infrared”. Optics Express, 19, 4815 (2011).

[3] M. Nieto-Vesperinas et al. “Angle-suppressed scattering and optical forces on submicrometer dielectric particles”. Journal of the Optical Society of America A, 28, 54 (2011).

[4] A. Novitsky et al. “Single Gradientless Light Beam Drags Particles as Tractor Beams”. Physical Review Letters, 107, 203601 (2011).

Optical Response of Nanosculptured Bragg Microcavities Prepared by Physical Vapor Deposition at Glancing Angles

M. Oliva-Ramírez, F. Yubero, A. Barranco, A.R. González-Elipe

Nanotechnology on Srufaces laboratory. Instituto de Ciencia de Materiales de Sevilla (CSIC-Univ. Sevilla), c/ Américo Vespucio nº49, Sevilla, Spain.
www.sincaf-icmse.es

manuel.oliva@icmse.csic.es

This paper reports the fabrication, characterization and study of the optical properties of porous Bragg microcavities formed by the stacking of a series of porous nanocolumnar layers of different refraction index materials (SiO_2 and TiO_2) which are deposited by physical vapor deposition at glancing angles (GLAD) [1, 2]. Nanosculptured microcavities with different optical properties and formed by tilted nanocolumns can be obtained by adjusting the stacking sequence of porouos TiO_2 and SiO_2 layers with well defined thickness and porosities. Both the refraction index and the thickness of the individual layers can be controlled by changing the zenithal evaporation angle and the azhimutal orientation of the substrates with respect to the evaporation target [3]. Figure 1 (a) (b) shows a series of selected SEM micrographs of some microstructures attainable by this method, as well as some schemes describing the organization of the nanocolumns in the different layers. Differences in the optical response of the different microcavities have been related both with the thickness of the layers and the different growth mode (i.e. orientation of the nanocolumns) of the stacked layers. Figure 1c) shows a typical transmission spectrum of one of these microcavities. The azimuthal and zenithal optical responses of these colored devices (Figure 1d)) have been studied and related with their particular microstructure. These Bragg microcavities experienced changes in their optical behavior when they were infiltrated with liquids (Figure 1c) and have resulted ideal for optofluidic applications and as liquid sensors to determine the concentration of different solutions.

References

[1] González-García, L.; Lozano, G.; Barranco, A.; Míguez, H.; González-Elipe, A.R., Journal of Materials Chemistry, 20 (2010), 6408

[2] Gonzalez-García, L.; Parra-Barranco, J.; Sanchez-Valencia, J.R.; Barranco, A.; Borras, A.; Gonzalez-Elipe, A.R.; Garcıa-Gutierrez, M.C.; Hernandez, J.J.; Rueda, D.R.; Ezquerra, T.A., Nanotechnology, 23 (2012), 205701

[3] Oliva-Ramírez, M.; González-García, L.; Parra-Barranco, J.; Yubero, F.; Barranco, A; González-Elipe, A.R.; ACS Appl Mater Interfaces, 5 (2013), 6743.

Figures

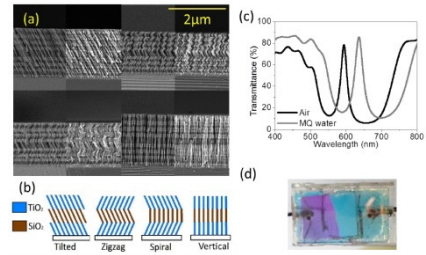

Figure 1: a) Selected SEM micrographs obtained for Bragg microcavities prepared by physical vapor deposition at glancing angles of successive SiO_2 and TiO_2 layers. b) Scheme describing the arrangement of the nanocolumns depending on the evaporation geometry. c) Transmission spectrum of a microcavitiy empty and full with water. D) Aspect of the microcavities when a liquid is filling their pores.

Time domain simulation of optical comb generation in microresonators

Jesús Palací, Sara Mas and Javier Martí

Valencia Nanophotonics Technology Center, Universitat Politècnica de València, 46022 Valencia, Spain

jespalpe@ntc.upv.com

Optical frequency combs (OFCs) are light sources whose spectrum is made of equidistant modes [1]. Because of their remarkable stability and spectral purity these lasers have found application in almost every field that uses optics technology, from metrology to coherent optical communications and terahertz spectroscopy. Initial designs used nonlinear modulators to generate many spectral sidebands that expand the resulting spectrum [2]. Recently, the generation of OFCs using optically pumped microresonators where parametric processes generate an initial set of modes that expand the spectrum through nonlinear mixing has been reported [3]. Whispering-gallery mode resonators were used to demonstrate the concept [3, 4] although similar results were obtained later with integrated microresonators that compensate for lower Q factors using materials with a higher nonlinear index [5]. Microresonator combs show advantages in terms of size and compatibility with integrated technology while being the best choice to generate combs with repetition frequencies exceeding 100 GHz.

There are basically two different approaches to simulate OFC generation in microresonators. One uses a set of coupled-mode equations (CMEs) [6] that represent the interaction among the different modes while the other makes use of the Lugiato-Lefever equation (LLE) [7] that models the time evolution of the optical field in the microresonator. Although CMEs provide direct frequency description of the comb and allow for frequency dependent absorption and coupling coefficients the LEE is more popular because it resembles the well-known nonlinear Schrödinger equation (NLSE).

Accurate and efficient simulations are necessary to study the influence of vacuum fluctuation noise on the generated combs and to identify potential instabilities that may be mistaken during experiments as instabilities in the measuring system. Here we show how to simulate the LEE by optimization of the simulation parameters to obtain short execution times and accurate results. We explain similarities and differences between the LEE and generalized NLSE and show simulation results that agree with those reported in the literature.

Figure 1 illustrates the generation of OFCs by pumping a microresonator with a single wavelength. A tapered fiber is depicted as the coupling element. The NLSE [8] can be used to solve propagation inside of the microresonator. However, the structure imposes boundary conditions: in the *m+1*th roundtrip the light in a given point will be the one in the mth roundtrip plus the newly injected light. By considering a low-loss (high-Q) resonator these conditions can be included in the NLSE, resulting in the LEE as shown in Fig. 1. The LEE is numerically solved by generating a pump signal with its corresponding vacuum noise fluctuation as a vector of random values. This signal is used as the algorithm seed and is injected into the microresonator every roundtrip. The pump and cavity field envelopes are E_{in} and E, respectively. t and τ account for waveform variations within and during successive roundtrips. Relevant microresonator parameters include roundtrip losses α, dispersion coefficients βi, nonlinear coefficient γ and transmission power coefficient θ. The phase tuning between the pump frequency and the closest cavity resonance is included through δ. The split-step Fourier method (SSFM) is used to solve propagation for one roundtrip before applying boundary conditions. The process is repeated until the simulation time is over.

To achieve efficient simulation of the structure the simulation time window is fixed to 2 roundtrips. The field is sampled with 496 points in both time and spectrum for the spectral samples to fall on each resonator's FSR and in

between. The spatial step is one roundtrip although more than one could be used to further reduce the computation time. The simulation time depends on the microresonator and varies between a few microseconds and tens of nanoseconds. These parameters allow for short execution times (below 10 seconds using a laptop computer) while providing reliable results. Simulation results that correspond with those reported in the literature [7] are shown in Fig. 2.

To sum up, we have demonstrated efficient time domain simulation of microresonator comb generation. The relationship between the LLE and generalized NLSE is analyzed and explained. Short time window, low number of spectral discretization points and large spatial steps were identified to be the most important requirements to reduce simulation time. The program is validated through simulations that fit results reported in the literature using the same parameters.

References

[1] A. E. Siegman, Lasers, University Science Books, 1986.

[2] J. Ye and S. T. Cundiff, Femtosecond optical frequency comb: principle, operation, and applications, Springer. 2004.

[3] P. Del'Haye, A. Schliesser, O. Arcizet, T. Wilken, R. Holzwarth and T. J. Kippenberg, Nature, 450 (2007) 1214–1217.

[4] A. A. Savchenkov, A. B. Matsko, V. S. Ilchenko, I. Solomatine, D. Seidel and L. Maleki, Phys. Rev. Lett. 101 (2008) 093902.

[5] J. S. Levy, A. Gondarenko, M. A. Foster, A. C. Turner-Foster, A. L. Gaeta and M. Lipson, Nat. Photonics 4 (2010) 37–40.

[6] T. Hanssonn, D. Modotto and S. Wabnitz, Opt. Comm., 312 (2014) 134–136.

[7] S. Coen, H. G. Randle, T. Sylvestre and M. Erkintalo, Opt. Lett., 38 (2013) 37-39

[8] G. P. Agrawal, Nonlinear fiber optics, 3rd edn., Academic Press, 2001.

Figures

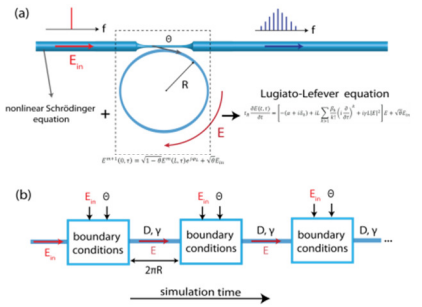

Figure 1: (a) Generation of optical frequency combs in microresonators and (b) its simulation.

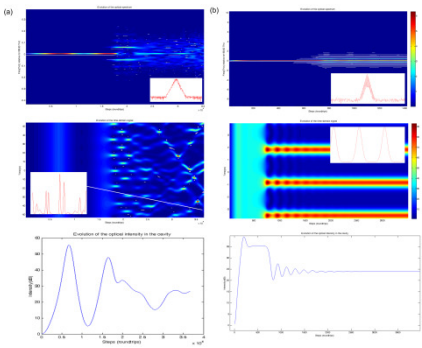

Figure 2: Simulation of (a) amplitude varying OFC and (b) soliton generation. Top to bottom: frequency/time evolution of the comb and power evolution inside the cavity. Parameters from [7].

Enhancing and directing light emission in semiconductor nanowires through leaky/guided modes

R. Paniagua-Domínguez[1], G. Grzela[2], T. Barten[2], Y. Fontana[2], J. Gómez Rivas[2,3], J.A. Sánchez-Gil[1]

[1] Instituto de Estructura de la Materia, Consejo Superior de Investigaciones Científicas, IEM-CSIC, Serrano 121, 28006 Madrid, Spain
[2] FOM Institute for Atomic and Molecular Physics (AMOLF), c/o Philips Research Labs, High-Tech Campus 4, 5656 AE Eindhoven, The Netherlands
[3] COBRA Research Institute, Eindhoven University of Technology, PO Box 513, 5600 MB Eindhoven, The Netherlands

ramon.paniagua@iem.cfmac.csic.es

In the present work, photoluminescence from finite semiconductor nanowires is theoretically [1,2] and experimentally [3] investigated, exploring and predicting their antenna-like properties for light emission in a variety of configurations of interest in Nanophotonics. The theoretical analysis is based on the leaky/guided mode dispersion relation of equivalent infinite nanowires, which governs the local density of electromagnetic states (LDOS). Light emission from finite nanowires is then numerically investigated in various scenarios with regard to its enhancement and directionality. A simple analytical model based on currents flowing in a cavity is derived that, upon tuning leaky/guided mode coupling through dipole position/orientation and nanowire geometry (radius and length), allows us to predict their antenna-like behavior and thus to tailor photoluminescence at will, with regard to both enhancement/inhibition of the total radiated power and associated radiation patterns, as shown in Figure1.

On top of the theoretical results, direct experimental evidence of this so-called nanoantenna effect in vertically standing single Indium Phosphide (InP) nanowires (see Figure 2) will be presented. The experimental setup, based on Fourier microscopy [3], allows one to study the angular photoluminescence pattern from isolated nanowires, as shown in Figure 2, thus providing means to directly test predictions from theory.

The authors acknowledge support from Spanish M.E.C (projects Consolider-Ingenio EMET CSD2008-000666, NANOPLAS+ FIS2012- 31070) and C.A.M. (MICROSERES network S-2009/TIC1476). We also acknowledge the research program of the "Stichting voor Fundamenteel Onderzoek der Materie (FOM)", which is financially supported by the "Nederlandse organisatie voor Wetenschappelijk Onderzoek (NWO)" and is part of an industrial partnership program between Philips and FOM.

References

[1] R. Paniagua-Domínguez, G. Grzela, J. Gómez Rivas and J. A. Sánchez-Gil, Nanoscale, 5 (2013) 10582-10590.
[2] R. Paniagua-Domínguez, G. Grzela, J. Gómez Rivas, and J. A. Sánchez-Gil, Proc. SPIE 8808, Active Photonic Materials V (2013) 88080J.
[3] G. Grzela, R. Paniagua-Domínguez, T. Barten, Y. Fontana, J. A. Sánchez-Gil, and J. Gómez Rivas, Nano Lett., 12 (2012) 5481-5486.

Figures

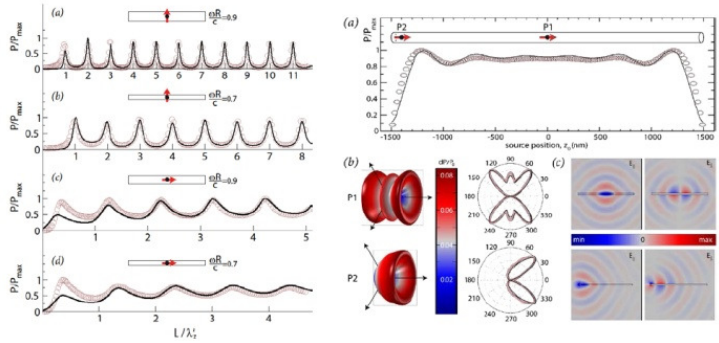

Figure 1: (left) Full numerical simulations (hollow symbols) and model predictions (solid lines) of the normalized total radiated power P/P_{max} as a function of the NW length L, rescaled by the corresponding guided mode wavelength $\lambda'z = 2\pi/k'z$: HE_{11} for the perpendicular dipoles, (a) and (b), and TM01 for parallel dipoles, (c) and (d). (right) (a) Normalized radiated power (hollow symbols) as a function of (parallel) dipole position z at the NW axis for a finite (L=3 μm, R=50 nm) InP NW at λ=880 nm (at which only the TM_{01} leaky mode is excited). Model predictions are also shown (solid black curves). (b) Far-field intensities of the light emitted by two dipoles, located at either the NW center (P1) or close to the NW edge (P2, at a distance d=100 nm), together with model predictions. (c) The corresponding emission snapshots in the near-field map.

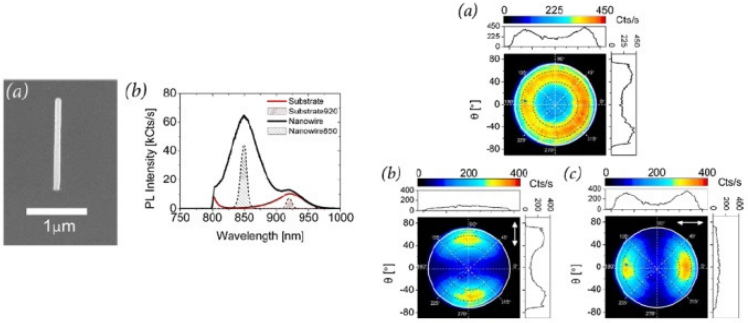

Figure 2: (left) (a) SEM image of the isolated InP nanowire studied and (b) its photoluminescence spectrum. (right) Experimental Fourier images of the emission from InP nanowires at λ =850 nm. Fourier images of the unpolarized (a) emission and with a polarizer with the transmission axis along the vertical (b) and horizontal (c) directions.

Optimization of the active layer thickness in QD-LEDs based on delaminated layered double hydroxides and CdTe quantum dots

Elena Pérez-Barrado[1,2,3], Magdalena Aguiló[2], Yolanda Cesteros[1], Fabio Cucinotta[4] , Francesc Díaz[2], Leonardo Marchese[4], Josep Pallarès[3], Maria Cinta Pujol[2], Pilar Salagre[1], Lluís F. Marsal[3*]

[1]Dept. Química Física i Inorgànica, EMAS, Univ. Rovira i Virgili (URV), Spain.
[2]Física i Cristal·lografia de Materials i Nanomaterials (FICMA-FiCNA), EMAS, Univ. Rovira i Virgili
(URV), Spain.
[3]Dept. d'Enginyeria Electrònica, Elèctrica i Automàtica. EMAS, Univ. Rovira i Virgili (URV), Spain.
[4]Dipartimento di Scienze e Innovazione Tecnologica and Nano-SISTEMI Interdisciplinary Centre, Università del Piemonte Orientale ", Italy.

*lluis.marsal@urv.cat

The use of colloidal quantum dots as semiconductors in light emitting diodes has increased in recent years. The unique properties of the nanoparticles, such as size-dependant optical properties, make quantum dots as valid materials in display technologies [1]. The architecture of quantum dots light emitting diodes (QD-LEDs) typically consists of a hole transporting layer and an electron transporting layer separated by a thin quantum dots interlayer. However, it has been reported that quantum dots can be embedded in layers of delaminated inorganic clays to build a QD-LED and function similarly to a p-n junction [2]. Layered double hydroxides (LDH), also known as inorganic anionic clays, have general formula $[M(II)_{1-x}M(III)_x(OH)2]^{x+}(A^{n-}{}_{1/n})\cdot mH_2O$, where M(II) and M(III) are the divalent and trivalent cations and An- the anion. They consist of positively charged octahedral layers with the anion and the water molecules in the interlayer space [3]. After delamination of the LDH in the appropriate solvent, the layers remain positively charged and can be used for a variety of purposes in nanotechnology applications [4].

The aim of this work is to build luminescent devices following a similar procedure than reported for Bendall et al. [2], where alternated layers of quantum dots and delaminated LDHs define the active layer of the device, based on a p-n junction. CdTe capped nanoparticles, which are negatively charged, are used as quantum dots. Two kinds of LDH have been tested: i) hydrocalumite, where Ca/Al are the divalent and trivalent metals, respectively, (hereafter Ca/Al-LDH) and ii) takovite, where Ni/Al are the divalent and trivalent metals, respectively, (hereafter Ni/Al-LDH). In order to facilitate swelling of the layers, nitrate is the anion for both samples.

The LDHs have been synthesized by co-precipitation method [5,6] and later characterized by XRD, N2 physisorption, FT-IR and TEM microscopy. Delamination was performed following a similar procedure than in [4], using formamide as solvent and ultrasounds to delaminate the sheets, and the resulting material was characterized by XRD, Tyndall effect and AFM microscopy. The architecture of the device was as follows: ITO/PEDOT:PSS/$(dLDH/CdTe)_n$/Ca/Al, where n is the number of alternated layers of delaminated LDH and quantum dots. It has been studied different n optima to achieve the best currentvoltage characteristics (I/V) and luminance response, and ranged between 3 and 7. Substrates were thoroughly cleaned before starting the deposition of the layers. Before cathode evaporation, the devices were heated to promote homogenization of the layers and prevent from aggregation. The cathode was thermally evaporated with a thickness of Ca/Al 10 and 90 nm respectively. The (I/V) and the optical performance were characterized for all devices.

The diffractograms for Ca/Al-LDH and Ni/Al-LDH samples are shown in Fig. 1(a) and (b), respectively. It was possible to identify the hydrocalumite (a) and takovite (b) phases. The intense (00l) reflections are related to the typical layered structure of these materials. After delamination of the LDHs, it was possible to identify delaminated sheets by AFM technique. The corresponding cross-sectional data (Fig. 2(a)) (1.6 nm) is in agreement with the expected height for two single layers after delamination. The micrograph (Fig. 2(b)) shows a detail of delaminated layers for Ca/Al-LDH sample.

The current density-voltage characteristics for devices based upon delaminated Ca/Al-LDH and CdTe are shown in Fig. 3. For all samples, the threshold voltage ranges between 1.5 and 1.7 V. The I/V characteristics demonstrates that the active layer works as a p-n junction. The maximum current density was 0.37 A/cm2 for the device with 3 alternated depositions. It is possible to see a correlation between the number of layers in the extreme of the chosen range (3 and 7 alternated layers). When the value is 7 probably there is some loss in the homogeneity of the CdTe layers. Additionally, as it has been reported before [2], there is a compromise between the thickness of the active layer and the I/V response. When the active layer thickness exceeds 120 nm the efficiency of the device decreases due to an increase in the resistance. Differences between 4 and 6 layers could be associated to the homogeneity of the layers and/or some degree of nanoparticle aggregation that affects the conductivity. From these results, it was possible to build QD-LED devices that operate at low voltages (1.5-3.7 V).

Acknowledgements

The authors are grateful for the financial support of Ministerio de Economía y Competitividad of Spain, FEDER funds (CTQ2009-12520-C03-02, CTQ-2011-24610, TEC2012-34397, MAT2011-29255-C02-02), Catalan authority under projects (2009SGR549 and 2009SGR235) and from Universitat Rovira i Virgili scholarship program for PhD grant.

References

[1] Y. Shirasaki, G. J. Supran, M.G. Bawendi, V. Bulović, Nature Photonics, 1 (2013) 13.

[2] J.S. Bendall, M. Paderi, F. Ghigliotti, N. Li Pira, V. Lambertini, V. Lesnyak, N. Gaponik, G. Visimberga, A. Eychmüller, C.M. Sotomayor Torres, M.E. Welland, C. Gieck, L. Marchese, Advanced Functional Materials, 19 (2010) 3298.

[3] F. Cavani, F. Trifirò, A. Vaccari, Catalysis Today, 2 (1991) 173.

[4] Q. Wang, D. O'Hare, Chemical Reviews, 7 (2012) 4124.

[5] E. Pérez-Barrado, M.C. Pujol, M. Aguiló, Y. Cesteros, F. Díaz, J. Pallarès, L.F. Marsal, P. Salagre, Applied Clay Science, 80-81 (2013) 313.

[6] F. Prinetto, G. Ghiotti, P. Graffin, D. Tichit, Microporous and Mesoporous Materials, 1-2 (2000) 229.

Figures

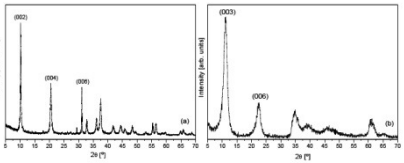

Figure 1: XRD diffractograms of (a) Ca/Al-LDH and (b) Ni/Al-LDH.

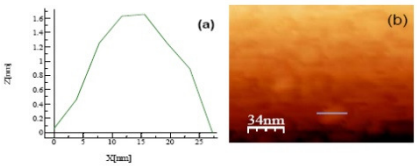

Figure 2: (a) Cross-section of a delaminated sheet of Ca/Al-LDH; (b) Detail of an AFM micrograph of delaminated sheets of Ca/Al-LDH.

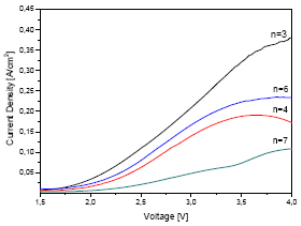

Figure 3: I/V plot for devices based upon delaminated Ca/Al-LDH and CdTe. Alternated layers range: 3n, 4n, 6n, 7n.

Excitation of interacting 2D Dirac fermion systems on a thin film by a localized probe.

M. Ameen Poyli[1,2], Ilya Nechaev[2], Ruben Esteban[1,2], P. M. Echenique[1,2,3], V. M. Silkin[2,3,4] and J. Aizpurua[1,2]

[1]Center for Materials Physics, CFM (CSIC/UPV-EHU), P. Manuel de Lardizabal 5, 20018, San Sebastian, Spain.
[2]Donostia International Physics Center, DIPC, P. Manuel de Lardizabal 4, 20018, San Sebastian, Spain.
[3]Departamento de Fisica de Materiales, Facultad de Químicas, UPV/EHU, 20080, San Sebastian, Spain.
[4]IKERBASQUE, Basque Foundation for Science, 48011, Bilbao, Spain.

mohamedameen_poyli@ehu.es / aizpurua@ehu.es

Metals and doped semiconductors can support quantized collective oscillations of free carriers, called plasmons. These excitations are also supported by two-dimensional (2D) Dirac fermion systems like graphene [1,2], where tight confinement, long propagation distance and tunability of the excitations via electrical gating can be achieved [2].

We study the optical response of materials that support a 2D Dirac fermion gas. We combine many-body theory calculations with classical electrodynamics to obtain the optical response of the electron gas supported on a dielectric substrate. The dielectric response of the 2D Dirac fermions obtained through the many-body theory calculations is used in the classical electrodynamical calculations to obtain the plasmon dispersion relations. In the electrodynamical calculations, the 2D Dirac fermion system is treated as an in-plane conductivity $\sigma(q,\omega)$, which is a function of the incident energy (ω) and the in-plane momentum (q).

In the case of a thin-film, where there are two 2D Dirac fermion gases located on top and bottom surfaces, we obtain the response of the interacting 2D systems. Figure 1 shows the dispersion curves for a single 2D Dirac fermion system supported on a substrate of dielectric constant ε=25, as well as for two interacting ones in a 5 nm thin film, both within local and nonlocal treatments. For the low-energy plasmon mode in the film, a notable difference can be observed between the local and nonlocal treatments for large q values. It can be noticed from the dispersion relations that the plasmons in these systems appear at very low energies (below 0.1 eV) and are extremely confined (far from the light dispersion curve).

Furthermore, we study how these interacting 2D Dirac fermion systems are excited by an electromagnetic localized probe such as an electric dipole in their proximity. Distribution of near-field associated with the excitation will be shown.

The optoelectronics of the considered systems shown here provide a versatile nano-system to control subwavelength optics.

References

[1] Frank H. L. Koppens, et. al., Nano Lett., 11 (2011) 3370-3377.
[2] J. Chen, et. al., Nature, 487 (2012) 77-81.

Figures

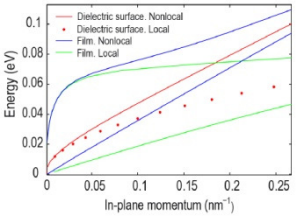

Figure 1: The dispersion relationship of surface plasmons in a two-dimensional Dirac fermion gas supported on a substrate of dielectric constant ε=25. The red solid and dotted curves represent the nonlocal and local dispersions, respectively. The symmetric and antisymmetric modes of dispersion for a 5nm thin film that contains two interacting Dirac fermion systems residing on opposite surfaces of the film are also shown. The blue curves represent the nonlocal dispersion while the green curves give the local dispersion.

Label-free biosensors based on organic distributed feedback lasers

Aritz Retolaza[1,2], Santos Merino[1,2], Marta Morales-Vidal[3], Pedro G. Boj[4], José M. Villalvila[3], José A. Quintana[4], María A. Díaz-García[3]

[1]CIC microGUNE, Goiru Kalea 9 Polo Innovación Garaia, 20500 Arrasate-Mondragón, Spain
[2]Micro and Nano Fabrication Unit, IK4-Tekniker, C/ Iñaki Goenaga 5, 20600 Eibar, Spain
[3]Dpto. de Física Aplicada and Instituto Universitario de Materiales de Alicante (IUMA), UA, 03080 Alicante, Spain
[4]Dpto. de Óptica and IUMA, UA, 03080 Alicante, Spain

aretolaza@cicmicrogune.es

In order to have an impact on the most challenging detection applications, label-free biosensors must simultaneously provide high sensitivity, large dynamic range and resolution sufficient for detection of mass density changes less than < 1 pg/mm^2 [1]. Label-free resonant optical sensors generally detects shifts in resonant wavelength caused by the interaction between the target molecule and the evanescent portion of resonant modes and where the amount of wavelength shift is proportional to the density of immobilized biomaterial on the sensor surface. The narrow spectral linewidth achieved by using Q-factor (>10^5) passive optical resonators enables sensor systems to resolve smaller wavelength shifts associated with the detection analytes at low concentration, or detection of biomolecules with low molecular weight, such as drug compounds [2,3]. While detection resolution can be substantially improved through the use of high Q-factor passive resonators, the sensitivity and dynamic range of the system is generally decreased, although certain examples of passive resonators have achieved high Q-factor and high sensitivity simultaneously [4]. In addition, the implementation of high Q-factor optical resonators typically requires high precision alignment for evanescent light in/out coupling, providing potential limits to their practical application. One way to solve this problem is to use distributed feedback (DFB) lasers. These laser biosensors are simultaneously capable of a high sensitivity and a high degree resolution, since they operate with single mode, narrow linewidth emission [5-7].

This work provides a framework for designing optimized DFB laser biosensors. For that, vertically emitting second order 1D DFB lasers based on organic waveguide films as active laser media and gratings engraved by nanoimprint lithography, have been fabricated. Two types of devices have been studied: (i) with DFB gratings over SiO2 substrates, over which active films are deposited; and (ii) with DFB gratings imprinted directly over the active films. We studied the laser wavelength shift experienced when a liquid or solid layer of material is deposited on top of the device, analyzing the influence on the sensor sensitivity of changing the thickness of the active film. In order to obtain higher sensitivities [8], devices with a top layer of a high refractive index material, such as TiO_2, have also been prepared.

Acknowledgements
This work has been funded by the "Ministerio de Ciencia e Innovación" through the grant MAT2011-28167-C02.

References

[1] X. Fan, I. White, S.I. Shopova, H. Zhu, J.D. Suter, and Y. Sun, "Analytica Chimica Acta", 620 (2008) 8.

[2] I.M. White, X.D. Fan. "Opt. Express", 16 (2008) 1020.

[3] C.Y. Chao, W. Fung, L.J. Guo, "IEEE J. Sel. Top. Quantum Electron. 12 (2006) 134.

[4] I.M White, H. Oveys, X.D. Fan, "Op. Lett." 31 (2006) 1319.

[5] M. Lu, S. Choi, C.J. Wagner, J.G. Eden, B.T. Cunningham, "Appl. Phys. Lett." 92 (2008) 261502.

[6] M. Lu, S.S. Choi, U. Irfan, B.T. Cunningham. "Appl. Phys. Lett." 93 (2008) 111113.

[7] C. Ge, M. Lu, W. Zhang, B.T. Cunningham. "Appl. Phys. Letters" 96 (2010) 163702.

[8] C. Vannahme, M.C. Leung, F. Richter, C.L.C. Smith, P.G. Hermannson, A. Kristensen, "Laser Photonics Rev.", 7 (2013) 1036.

Figures

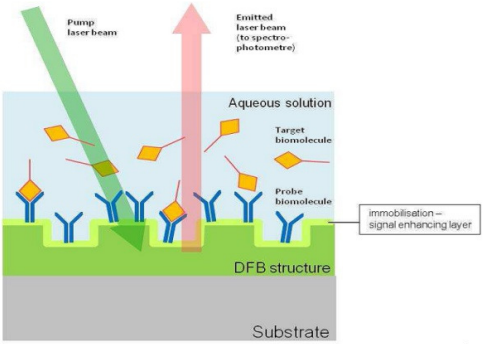

Figure 1: Schematic representation of a DFB laser device working as biosensor.

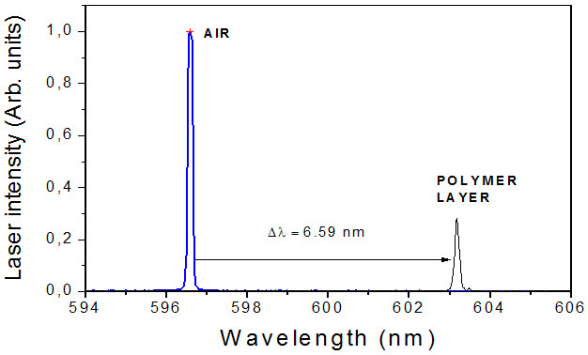

Figure 2: Laser wavelength shift experienced by a TiO_2-coated second-order 1D organic DFB laser, upon the addition of polymer layer.

Silicon Colloids. Fundamentals and applications

I. Rodriguez [1,2], R. Fenollosa[1,2], L. Shi [1,2] X. Lu[3], B. A. Korgel[3], A. Ribes-Greus[4] R. A. Alvarez-Puebla[4,6], and F. Meseguer[1,2]

[1] Unidad Asociada ICMM/CSIC-UPV, Universidad Politécnica de Valencia, 42022 Valencia (Spain)
[2] Instituto de Ciencia de Materiales de Madrid (CSIC), Cantoblanco, 28049 Madrid (Spain).
[3] Department of Chemical Engineering.The University of Texas, Austin, Texas 78712-1062, USA
[4] Instituto de Tecnología de los Materiales (ITM), Universidat Politécnica de Valencia (UPV), Spain
[5] Departamento de Quimica Fisica e Inorganica, Universitat Rovira i Virgili and Centro de Tecnología Química de Catalunya, Carrer de Marcel•lí Domingo s/n, 43007 Tarragona, Spain
[6] ICREA, Passeig Lluís Companys 23, 08010 Barcelona, Spain

mirodrig@upvnet.upv.es

We have developed a completely new type of Silicon we call it as Silicon Colloids (SCs). They are polydisperse [1] or monodisperse [2,3] micro and nanoparticles, ranging from 400 nm to 7 micrometres with a perfect spherical shape. Silicon Colloids constitute the new material platform that could bring together several areas of research as colloidal sciences, metamaterials and semiconductor science. Moreover, metallurgical grade silicon colloids can lead to technological application where neither high purity nor regular shape is required.
We will report on the applications and properties of silicon colloids:

1) Silicon Colloids based sun light management [4]
2) Silicon colloids for Mie-assisted Raman scattering amplification [5]
3) Silicon colloids based metamaterials [3,6]

References

[1] R. Fenollosa, F. Meseguer, M. Tymczenko, Adv. Mater. 20, 95 (2008).
[2] J. T Harris, J. L Hueso, and B. A Korgel, Chem. Mater., 22, 6378-6383 (2010)
[3] L. Shi, J. T. Harris, R. Fenollosa, I. Rodriguez, X. Lu, B. A. Korgel, and F. Meseguer Nature Communications, 4, 1904 (2013)
[4] (a) I. Rodriguez, R. Fenollosa, A. Perez-Roldan, and F. Meseguer, 2011 Patent Ref. WO2011/09236841.(b) I. Rodriguez, R. Fenollosa, A. Perez-Roldan, and F. Meseguer, 2012 Patent WO2012/101306A1
[5] I. Rodriguez, L. Shi, X. Lu, B.A. Korgel, R. A. Alvarez-Puebla and F. Meseguer, Nanoscale 2014, DOI: 10.1039/c4nr00593g
[6] L. Shi, T. U. Tuzer, R. Fenollosa, and F. Meseguer Adv. Mater. 24, 5934 (2012).

Resonant metal-semiconductor nanostructures as building blocks of low-loss negative- and zero-index metamaterials

D. R. Abujetas*, R. Paniagua-Domínguez, L. Froufe-Pérez, J. A. Sánchez-Gil

Instituto de Estructura de la Materia (CSIC), Serrano 121, 28006 Madrid, Spain

diego.romero@iem.cfmac.csic.es

Artificial materials showing electromagnetic properties not attainable in naturally occurring media, the so called metamaterials, are among the most active fields of research in optical and material physics. One of the major challenges found is to obtain truly bulk isotropic negative index metamaterials (NIM) at optical frequencies [1]. Recently, we reported [2] the possibility to use a certain class of core-shell (CS) nanospheres as building blocks of 3D isotropic NIMs, operating in the near infrared. These CS, made of a metallic core and a high permittivity shell, are doubly-resonant (see Fig. 1), allowing for a spectral overlap of their first electric and magnetic dipolar resonances. Since the responses do not depend on the interaction between constituents, no particular arrangement is needed to build the metamaterial, which is, moreover, broadly isotropic, though polarization dependent. Nonetheless, such 3D NIMs exhibit moderate losses, and their fabrication is somewhat challenging.

Therefore, we have extended our study to metallo-dielectric core-shell nanowires (NWs), revealing similar properties when incident light wavevector and polarization are both normal to the nanowire axis (see Fig. 2). We show that, for certain geometrical parameters and filling fractions, metamaterials composed by such CSNWs can have simultaneously negative permittivity and permeability between 1.2-1.5 mm [3]. The resulting metamaterial, at the expense of reduced dimensionality and fixed polarization, then behaves as a 2D isotropic NIM (see Fig. 3) with extremely low losses [3] (f.o.m. up to 200, about one order of magnitude better than previously proposed designs).

Also, the same metamaterials design is shown to yield either negligible dielectric permittivity (ENZ) or negligible magnetic permeability (MNZ), thus leading to a negligible refractive index, manifest fascinating optical properties [4]; specially interesting is the case of zero-index metamaterials (ZIM) with similarly small dielectric permittivity and magnetic susceptibility (impedance Z~1) for obvious reasons. Strictly speaking, unlike for NIMs, no strong resonances are required to achieve such effective ZIM parameters, the only condition being an overlap of the tails of both resonances. Thus we will show [5] that simpler nanostructures, such as solid dielectric cylinders with relatively large refractive index, can actually satisfy such condition in order to behave as a ZIM (see Fig. 4). Moreover, broad spectral regions are also found where the effective index nearly vanishes, while matching vacuum impedance; such zero-index metamaterials are shown to beautifully exhibit the rich phenomenology formally expected.

The authors acknowledge financial support from the Spanish "Ministerio de Economía y Competitividad" (CSD2008-00066 and FIS2012-31070), and European Social Fund and CSIC (JAE-Pre and JAE-Doc grants).

References

[1] C. Soukoulis, M. Wegener, Optical metamaterials--more bulky and less lossy, Science 330: 1633-1634, 2010.

[2] R. Paniagua-Domínguez, F. López-Tejeira, R. Marqués J. A. Sánchez-Gil, Metallo-dielectric core–Shell nanospheres as building blocks for optical three-dimensional isotropic negative-index metamaterials, New. J. Phys. 13: 123017, 2011.

[3] R. Paniagua-Domínguez, D. R. Abujetas, and J. A. Sánchez-Gil, Ultra low-loss, isotropic 2D optical negativeindex metamaterial based on hybrid metal-semiconductor nanowires, Sci. Rep. 3: 1507, 2013.

[4] R.W. Ziolkowski, Propagation in and scattering from a matched metamaterial having a zero index of refraction, Phys. Rev. E 70: 046608 (2004).
[5] R. Paniagua-Domínguez, D. R. Abujetas, L. S. Froufe, J. A. Sánchez-Gil, preprint.

Figures

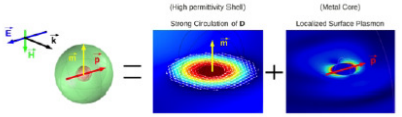

Figure 1: Illustration of the double (electric and magnetic) resonance in core-shell nanospheres [3].

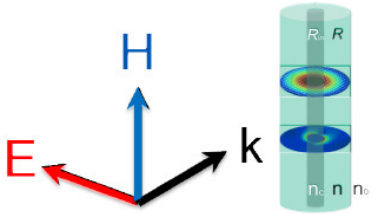

Figure 2: Illustration of the scattering geometry (TE polarization) for a doubly-resonant, single (Ag@Si) core-shell nanowire.

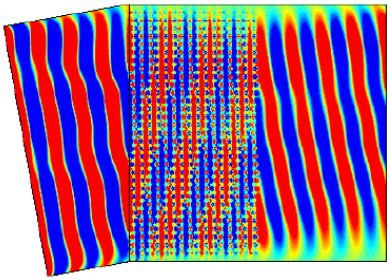

Figure 3: Negative-refraction-index slab made of coreshell (Ag@Si) NWs operating at λ=1.35 μm (TE polarization).

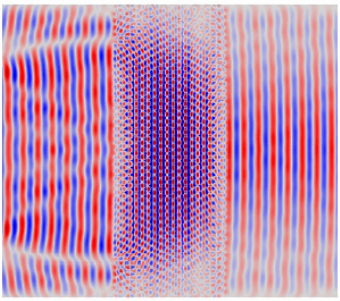

Figure 4: Nearly-zero refraction-index slab made of TiO_2 NWs operating at λ=780 nm (TE polarization).

Design of lumped electrodes for silicon Mach-Zehnder Interferometer switches

Álvaro Rosa[+], Ana María Gutierrez, Antoine Brimont, Pablo Sanchis*

Nanophotonics Technology Center, Universitat Politècnica de València Camino de Vera s/n, 46022 Valencia, Spain

alroes3@ntc.upv.es+
pabsanki@ntc.upv.es*

The emergence of intra-chip optical interconnects on a silicon photonics platform is gradually expected to overwhelm copper based-interconnects. As a result, significant research efforts have been made to realize low drive voltage, low power and fast switching devices featuring high throughput bandwidth. This work deals with the design of lumped-electrodes for silicon Mach-Zehnder Interferometer (MZI) switches with active performance based on carrier-depletion. Carrier depletion has been largely used for implementing silicon modulators [1] however no switches based on carrier depletion have been demonstrated so far despite the perspective of achieving faster switching times and lower power consumption with respect to carrier injection.

Figure 1(a) shows the MZI switch with lumped-electrodes. The active region design has been designed relying on a shallow etched waveguide configuration. Figure 1(b) depicts the cross-section of the active region with electrodes. The chosen semiconductor structure is a vertical PN junction, which on one hand achieves larger effective index change than horizontal PN junctions and on the other hand is more tolerant to potential mask alignment errors since its formation is dictated by the implantation energy rather than the resolution of the optical lithography. Additionally, the combination of a slightly lower modal confinement and wider PN junction leads to a higher interaction between the propagating light and charge carriers.

The active (doped) region has been optimized with ATHENA and ATLAS, respectively process and device simulation software from SILVACO. The fractional change in effective index will depend on holes/electrons density ratio. According to Soref's equations [2], holes are more efficient than electrons in changing the refractive index for carrier concentrations up to 10^{19} cm^{-3}, and absorb less light than electrons. As a result, our PN junction has been designed in such a way that the high intensity region of the optical mode interacts mostly with holes. Static and transient performance of the optimized vertical PN junction has also been analysed. The obtained figures of merit are much lower (<0.55 V.cm from 1 to 10V) than typical values obtained from horizontal PN junction schemes (from 2 to 4 V.cm). The phase shifter insertion loss is 1.55 dB/mm when no bias is applied. For increasing voltages, the losses decrease because the charge carriers are removed from the waveguiding region. The intrinsic rise and fall times (90 % of the maximum effective index change) derived from the transient analysis are both around 30 ps thus confirming the ultra-fast response of the switch.

Lumped-electrodes have been designed taking into account the proposed active region. Electrodes are based on a symmetrical coplanar microwave strip. The main parameters to be optimized are the ground and signal electrodes width (W), the gap between both contacts (G) and the length of the electrode (L). The optimization should be carried out to avoid that electrodes restrict the switching time and power consumption. The optimum gap depends on the drive voltage and the propagation losses. A small electrode gap is required to increase the switching efficiency and so minimizing the required drive voltage. However, the gap should be sufficiently wide to avoid the interaction of the optical mode with the metallic contacts which would drastically increase propagation losses. In the proposed switch, an optimum gap of ~3.5µm has been designed. The optimum length has been designed based on a trade-off between the drive voltage and the insertion losses and switching time. A longer length will decrease the required drive voltage at expenses of increasing the insertion losses and reducing the bandwidth. An optimum electrode length of

around 1mm has been chosen to keep the drive voltage below 4V and the insertion losses below 1.5dB. The switching time will be limited by the electrical bandwidth of the lumped-electrode.

The bandwidth in lumped-electrodes is usually limited by the electrode capacitance, C, and load resistance, R. The electrode capacitance depends basically on the W/G ratio [3]. Several simulations were carried out taking into account the silicon substrate in order to obtain the capacitance per unit length as a function of the W/G ratio. Figure 2(a) shows the obtained results. The corresponding bandwidth-length product is also shown taking into account R= 50Ω. As expected, a small W/G ratio results on a higher electrical bandwidth. Therefore, the electrode width, W, can be reduced to increase the bandwidth. However, the width must also be sufficiently wide to ensure that the static electric resistance does not become a limiting factor in the achievable bandwidth [4]. The static electric resistance will be inversely proportional to the electrode width and the electrode thickness. The maximum electrode thickness depends partly on the fabrication process and in our case values around 1µm are expected to be achieved. Therefore, an optimum electrode width of ~20µm has been designed. Such a value will give rise to W/G~5.7 which ensures a bandwidth-length product above 1GHz·cm. Hence, the bandwidth will be around 10GHz for the designed electrode length (L=1mm) that will allow switching times below 35ps and therefore will not limit the ultra-fast time response achieved thanks to the carrier-depletion effect. Finally, a higher bandwidth could also be achieved by using a parallel resistance of 50 Ω to allow broadband matching to the impedance of the driving source. However, it is also important to notice that in that case it would be needed twice the drive voltage thus penalizing the power consumption of the switch.

Acknowledgments

Financial support from TEC2012-38540 LEOMIS project is acknowledged. Álvaro Rosa also acknowledges the Spanish Ministry of Economy and Competitiveness for funding his grant.

References

[1] G. T. Reed, G. Mashanovich, F. Y. Gardes, and D. J. Thomson, "Silicon optical modulators," Nat Photon., vol. 4, pp. 518-526, 2010.

[2] R. Soref and B. Bennett, "Electrooptical effects in silicon," IEEE J. Quantum Electron., vol. 23, pp. 123–129, 1987.

[3] N. Dagli "High-speed photonic devices," CRC Press, 2007.

[4] R.C. Alferness, "Waveguide electrooptic modulators", IEEE Trans. Microwave Theory Tech., vol. MTT-30, pp. 1121-1137, 1982.

Figures

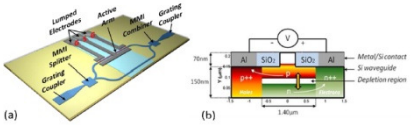

Figure 1: Schematic of (a) the MZI switch with lumped-electrodes and (b) cross-section of the active region with electrodes.

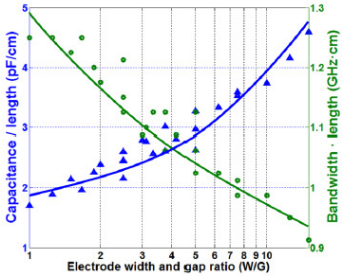

Figure 2: Capacitance and corresponding bandwidth-length product as a function of the W/G ratio.

Magneto-optical Kerr effect in resonant subwavelength nanowire gratings

H. Marinchio[1], R. Carminati[1], A. García-Martín[2] and **J.J. Sáenz** [3,4]

[1] Institut Langevin, ESPCI ParisTech, CNRS, 1 rue Jussieu, F-75238 Paris Cedex 05, France
[2] IMM-Instituto de Microelectrónica de Madrid (CNM-CSIC), Madrid, Spain
[3] Condensed Matter Physics Center (IFIMAC) and Dep. de Física de la Materia Condensada, UAM, Spain
[4] Donostia International Physics Center (DIPC), Donostia-San-Sebastián, Spain

juanjo.saenz@uam.es

Multiple scattering theory can be used to obtain a full analytical description of complex resonant phenomena arising in sub wavelength nanowire gratings or in single mode waveguides with small defects. The strong coupling between the dipolar field scattered by small particles and the evanescent modes (in a waveguide) or evanescent diffracted beams (in a grating) can lead to a number of interesting resonant effects.

Here we analyze the optical response of sub-wavelength nanowire gratings made of arbitrary anisotropic materials [1]. For transparent dielectric nanorods it is possible to obtain very large local field enhancements at specific resonant conditions [2]. These structures would lead to enhancement of molecular fluorescence signals without quenching. In the presence of absorption, it is possible to derive the conditions to tune the absorption/thermal emission and extinction resonances [2].

For magneto-optical dielectrics we show that there is a complex interplay between the geometric resonances of the grating and the magneto-optical Kerr effects (MOKE) response [1]. As we will show, for a given polarization of the incident light, a resonant magneto-optical response can be obtained by tuning the incidence angle and grating parameters to operate near the resonance condition for the opposite polarization.

A completely equivalent analysis was applied to study electromagnetic forces on neutral particles in hollow waveguides [3]. At the geometric resonance, the effective scattering cross section of a very small particle can be made as large as the wavelength even far from any localized plasmon-polariton resonance. A small particle can then be strongly accelerated along the guide. The presence of the two particles splits the resonance leading to a nontrivial oscillating interaction. The existence of stable, optically bound dimers under two counter-propagating (non-correlated) light modes was also discussed. In analogy with these findings, we will discuss some interesting radiation pressure effects on subwavelength nanorod gratings.

References

[1] H. Marinchio, R. Carminati, A. García-Martín and J.J. Sáenz, Magneto-optical Kerr effect in resonant subwavelength nanowire gratings, New J. Phys. 16, 015007 (2014).
[2] M. Laroche et al., Tuning the optical response of nanocylinder arrays, Phys. Rev. B 74, 245422 (2006); Optical Resonances in One-Dimensional Dielectric Nanorod arrays: Field-induced fluorescence enhancement, Opt. Lett. 32, 2762 (2007).
[3] R. Gómez-Medina et al., Resonant radiation pressure on neutral particles in a waveguide, Phys. Rev. Lett 86, 4275 (2001); Unusually strong optical interactions between particles in quasi-one-dimensional geometries, Phys. Rev. Lett 93, 243602 (2004).

Controlling light emission, scattering and propagation at the nanoscale with metal, semiconductor and hybrid nanowires

R. Paniagua-Domínguez, D. R. Abujetas, **J. A. Sánchez-Gil**

Instituto de Estructura de la Materia Consejo Superior de Investigaciones Científicas (IEM-CSIC) Serrano 121, 28006 Madrid, Spain

j.sanchez@csic.es

In this talk, a variety of configurations of interest in Nanophotonics will be described that exploit the resonant optical properties of metal, semiconductor and hybrid nanowires, to control light emission, scattering and propagation at the nanoscale.

First, we investigate photoluminescence from finite semiconductor nanowires, theoretically and experimentally demonstrating their behavior as efficient optical nanoantennas [1], with directional emission of polarized light given by the material and also by the nanowire geometry and dimensions, which determine the Fabry-Perot-like guided/leaky mode resonances [2]. We anticipate the relevance of these results for the development of nanowire photon sources with optimized efficiency and controlled emission.

Second, the spectral properties of similar Fabry-Perot-like resonances occurring in metal nanorods (of plasmonic nature in this case) are shown with emphasis on the corresponding line-shapes, revealing theoretically and experimentally that their asymmetry is governed by mode parity [3]: Surface plasmon resonances of odd mode parity present Fano interference in the scattering cross-section resulting in asymmetric spectral lines. Contrarily, modes with even parity appear as symmetric Lorentzian line-shapes. The emergence of either constructive or destructive mode interference is explained with a semi-analytical 1D line current model. This simple model directly explains the mode-parity dependence of the Fano-like interference. Plasmonic nanorods are widely used as half-wave optical dipole antennas. Our findings offer a perspective and theoretical framework for operating these antennas at higher order modes [4].

Finally, hybrid metal-semiconductor core-shell nanowires are proposed as building blocks (meta-atoms) of 2D optical metamaterials [5]. The concept of overlapping dipolar electric and magnetic resonances occurring at core-shell nanospheres, stemming from, respectively, plasmon (metal core) and lowest-order magnetic (high-index dielectric shell) resonances, was proposed to achieve 3D isotropic optical negative-index metamaterials (NIMs) [6]. Recently, it has been extended to hybrid core-shell nanowires, leading to 2D isotropic optical NIMs which exhibit extremely low-losses (at the expense of the reduced dimensionality and polarization dependence) [5]. Note that, in this configuration, the resonances involved in the NIM behavior occur in the plane perpendicular to the nanowires, and no mode bouncing (Fabry-Perot-like) at the nanowire ends is required, unlike in the previous ones.

References

[1] G. Grzela, R. Paniagua-Domínguez, T. Barten, Y. Fontana, J. A. Sánchez-Gil, and J. Gómez Rivas, "Nanowire Antenna Emission," Nano Lett., 12 (2012) 5481.

[2] R. Paniagua-Domínguez, G. Grzela, J. Gómez Rivas and J. A. Sánchez-Gil, "Enhanced and directional emission of semiconductor nanowires tailored through leaky/guided modes," Nanoscale, 5 (2013) 10582.

[3] F. López-Tejeira, N. Verellen, R. Paniagua-Domínguez, D. Vercruysse, D. Denkova, L. Lagae, P. Van Dorpe, V. V. Moshchalkov, and J. A. Sánchez-Gil, "Mode Parity-controlled Fano and Lorentz Resonances Arising in Plasmonic Nanorods," Nano Lett., (2012) accepted.

[4] F. López-Tejeira, R. Paniagua-Domínguez, J. A. Sánchez-Gil, "High-Performance Nanosensors Based on Plasmonic Fano-like Interference: Probing Refractive Index with Individual Nanorice and Nanobelts," ACS Nano, 6 (2012) 8989.

[5] D. R. Abujetas, R. Paniagua-Domínguez, and J. A. Sánchez-Gil, "Ultra low-loss, isotropic 2D optical negative-index metamaterial based on hybrid metal-semiconductor nanowires," Sci. Reports, 3 (2013) 1507.

[6] R. Paniagua-Domínguez, F. López-Tejeira, R. Marqués and J. A. Sánchez-Gil, "Metallo-dielectric core–shell nanospheres as building blocks for optical three-dimensional isotropic negative-index metamaterials," New. J. Phys., 13 (2011) 123017.

Optical Response of High Refractive Index Nanoparticles with Metallic Impurities

J. M. Sanz, R. Alcaraz de la Osa, A. I. Barreda, J. M. Saiz, F. González, F. Moreno

Grupo de Óptica, Dpto. Física Aplicada, Universidad de Cantabria, Avda. Los Castros s/n, 39005 Santander, Spain

sanzjm@unican.es

The influence of the degree of purity of a high refractive index nanoparticle (silicon or other semiconductor material in the VIS-NIR) on its resonances, either electric or magnetic, is assessed by using Mie theory as well as finite-element simulations. In particular, it is shown that the main effect of the increase of absorption due to metallic pollutants is observed in the magnetic resonances. Concerning directionality conditions (zero backward/forward conditions) of electromagnetic scattering, it is found that they are spectrally shifted when the material's purity is varied. Resistive losses confirm the quenching of magnetic resonances, showing that the region of influence in the magnetic dipole resonance is much larger than in the electric one, although, for instance, for silicon, it has been found that losses are not critical when its purity is over 99.50%.

Introduction and Methods

The resonant response of nanoparticles as a reaction to an external electromagnetic field, makes them attractive for a wide range of applications, such as real-time sensors, surface enhanced Raman spectroscopy (SERS), light energy guiding, nanolensing or electromagnetically induced transparency, among others [1]. The theoretical behavior of small particles exhibiting both electric and magnetic dipolar resonances was predicted several decades ago [2]. These particles scatter with coherent effects between both dipoles, thus enabling control of the scattered radiation [3].

Currently, ohmic losses in metallic nanoparticles have turned attention to dielectric materials and, in particular, to high-permittivity low-loss nanoparticles and nanoparticle structures, for instance, made of silicon (Si) [4, 5, 6]. These researches have been done under the assumption that those high refractive index materials, apart from not having ohmic losses at all, they do not contain any sort of contamination, i.e. they have a purity of 100 %. However, materials with 100% of purity are non-realistic cases since industry can provide pure materials under certain conditions only and massively increasing manufacturing costs. From an industrial point of view, pure Si can be obtained with metallurgical-grade (MG-Si, < 98%) and upgraded up to solar-grade (SG-Si, > 99.999%) [7] with the corresponding increased price.

In this research, Si particles of size smaller than the incident wavelength are studied. Specifically, the influence of the material's degree of purity on both electric and magnetic resonances is analyzed. The main metallic contaminants in Si powder are usually metals, like Fe, Al and Ti [7, 8]. In order to evaluate their influence, the composition of an industrial sample of Si powder (provided by Elkem [8]) was taken as a starting point, varying the Si content of the particle from 99.0% to 100.0%. The resulting dielectric function was obtained by performing a weighted average, by simply taking into account the relative concentration of each pollutant and their optical constants, which, due to their metallic nature, show important absorption losses. Near- and far-field computations were done by using Mie theory [9] as well as finite-element simulations [10].

Results and Discussion

Fig. 1 shows the spectral extinction (top) and absorption (bottom) efficiencies (in the interval [900; 2100] nm) for an isolated spherical particle of Si (radius a=230 nm) as the purity grade is reduced from 100.0% to 98.98%. Obviously, the Si fingerprint can be observed as an absorption peak for multipolar resonances in the visible region. The well-known spectral pattern of a pure Si sphere is distorted when the purity grade is reduced. Initially (for high purity grades), this effect only slightly affects magnetic resonances (b1 and b2 peaks) but it is spread through the

entire spectrum when the purity grade is further reduced. Accordingly, absorption efficiency peaks (especially the magnetic ones) grow and broaden when purity decreases, with the overall absorption efficiency background rising as well.

Fig. 2 shows maps of the norm of the electric near-field and resistive losses of the magnetic (top) and electric (bottom) dipole resonances at the wavelength they occur for several purity grades. As can be seen, the electric dipole resonance only shows slight changes, even for low purity grades. On the other hand, the magnetic dipole resonance dramatically changes for Si purity grades < 99.50%. Resistive losses summarize these two situations: while the maximum value of the losses is similar in both dipolar resonances, the area of influence in the magnetic dipole resonance is much larger than in the electric one.

Acknowledgements

The authors thank the United States Army International Technology Center Atlantic (USAITC-A) for financial support through grant W911NF-13-1-0245. We also thank Elkem [8] for providing Si data and samples.

References

[1] P. N. Prasad, Nanophotonics. John Wiley & Sons, Inc., 2004.

[2] M. Kerker, D.-S. Wang, and C. L. Giles, "Electromagnetic scattering by magnetic spheres," J. Opt. Soc. Am., 73-6 (1983) 765.

[3] J. M. Geffrin, B. García-Cámara, R. Gómez-Medina, et al., "Magnetic and electric coherence in forward- and back-scattered electromagnetic waves by a single dielectric subwavelength sphere," Nat. Commun., 3 (2012) 1171.

[4] L. Shi, J. T. Harris, R. Fenollosa, et al., "Monodisperse silicon nanocavities and photonic crystals with magnetic response in the optical region," Nat. Commun., 4 (2013) 1904.

[5] A. Garcia-Etxarri, R. Gómez-Medina, L. S. Froufe-Perez, et al., "Strong magnetic response of submicron silicon particles in the infrared," Opt. Express, 19- 6 (2011) 4815.

[6] Y. H. Fu, A. I. Kuznetsov, A. E. Miroshnichenko, et al., "Directional visible light scattering by silicon nanoparticles," Nat. Commun., 4 (2013) 1527.

[7] N. Yuge, M. Abe, K. Hanazawa, et al., "Purification of metallurgical-grade silicon up to solar grade," Progress in Photovoltaics: Research and Applications, 9-3 (2001) 203.

[8] Elkem AS Silicon Materials: http://www.elkem.com/Global/ESM/qualitysafety/product-data-sheets/siliconproducts/silgrain/Silgrain-pds.pdf.

[9] C. Bohren and D. Huffman, Absorption and Scattering of Light by Small Particles, 2nd ed. Wiley-VCH, 2010.

[10] Comsol Multiphysics 4.3a, Comsol Inc., Burlington, MA.

Figures

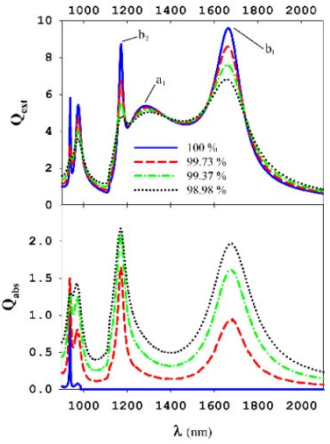

Figure 1: Spectral extinction (top) and absorption (bottom) efficiencies (λ in [900; 2100] nm) for an isolated spherical particle of Si (radius a = 230 nm) as the purity grade is reduced from 100.0% to 98.98%.

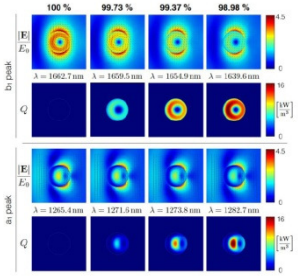

Figure 2: Maps of the near-field norm and resistive losses of the magnetic (top) and electric (bottom) dipole resonances at the wavelength they occur for several purity grades.

UV Plasmonic behavior of various metals

D. Ortiz[a], **J. M. Sanz[a],** R. Alcaraz de la Osa[a], J. M. Saiz[a], F. González[a], A. S. Brown[b], M. Losurdo[c,] H. O. Everitt[d,e] and F. Moreno[a]

[a] Group of Optics, Department of Applied Physics, University of Cantabria, Spain.
[b] Department of Electrical and Computer Engineering, Duke University, United States.
[c] Institute of Inorganic Methodologies and of Plasmas-CNR, and INSTM, Via Orabona, 4-70126 Bari,Italy.
[d] U.S. Army Aviation & Missile RD&E Center, Redstone Arsenal, AL 35802 USA.
[e] Department of Physics, Duke University, USA.

ortizd@unican.es

Plasmonics generally considers the electrodynamics of the electronic plasma confined in nanometer-sized metallic structures. The interaction with electromagnetic radiation in either visible or near-infrared, generates very fast plasma oscillations and can lead to localized surface Plasmon resonances (LSPRs) when the frequency of the incident field is properly tuned. LSPRs localize and strongly enhance the electromagnetic field near the nanostructure at dimensions much smaller than the incident wavelength. Exploiting these characteristics, plasmonics-based solutions have interesting practical applications in areas such as chemical sensing, health monitoring, therapeutics, optical communications, information storage, and enhanced spectroscopy [1, 2].

The ability to tune the LSPR by adjusting the composition, shape, and size of nanometer scale metallic structures has been actively investigated over the last decade [3, 4]. Nevertheless, these research studies have been performed on structures whose LSPRs occur in the visible and near infrared, in part because of the performance of the most accepted metals for plasmonics, Gold and Silver [5]. In response to an increasing demand to detect, recognize, and/or destroy biological toxins, to enhance biological imaging, and to characterize semiconductor devices at the nanometer scale, interest in UV plasmonics is growing [6-8]. This has enhanced the need to explore other metals that might be nanostructured and are suitable for UV applications.

In this research, the discrete dipole approximation (DDA) has been used to assess the performance and efficacy of various metals for use in UV plasmonics (3-6 eV). The metals investigated were aluminum, chromium, copper, gallium, gold, indium, magnesium, palladium, platinum, rhodium, ruthenium, silver, titanium, and tungsten. The plasmonic behavior of these elements is analyzed for two basic geometries: single nanometer-sized spheres and hemispheres located on flat dielectric substrates (Figure 1). For both basic geometries, the substrate was chosen to be, Sapphire to mimic typical experimental conditions [9]. For the selected metals, near-field and far-field electromagnetic analysis have been performed, from which interesting conclusions of their plasmonic performance for UV plasmonic applications, may be ascertained [10]. Some of the most important results are summarized in Figure 2. For instance, it shows that the change from spherical to hemispherical geometry produces a redshift of the plasmonic resonance. For both geometrical configurations, the interaction between the nanoparticle and the sapphire substrate also redshifts the LPSR peak and affects its strength. The combination of these effects redshifts the LSPR of some candidate metals like Ag out of the UV. The most promising metals identified for UV plasmonics are Mg, Al, Ga, In, and Rh, plus Ag in the border of the UV-VIS region. Finally, for practical applications, like SERS or SEF, the maximum “hot-spot” values of the surface-averaged intensity have been found to occur at

the easily accessible contact points between metal hemispheres and the substrate.

Acknowledgements

This research was supported by the U.S. Army's USAITIC-A office in London and the AMRDEC inhouse laboratory innovative research program (project # W911NF-13-1-0245).

References

[1] Stockman, M. Opt Express 19 (2011) 22029.
[2] Prasad P.N., Nanophotonics, Wiley-Interscience, John Wiley & Sons, 2004
[3] Zeman, E.J., Schatz, G.C. J Phys Chem 91 (1987) 634.
[4] Noguez, C. J Phys Chem C 111 (2007) 3806.
[5] Pelton, M., Aizpurua, J., Bryant, G.W. Laser Photon Rev 2 (2008) 136.
[6] Anker, J.N., Hall, W.P., Lyandres, O., et al. Nature Mater 7 (2008) 442.
[7] Chowdhury, M.H., Ray, K., Gray, S.K., et al. Anal Chem 81 (2009) 1397.
[8] Taguchi, A., Hayazawa, N., Furusawa, K., et al. J Raman Spectrosc 40 (2010) 1324.
[9] Albella, P., García-Cueto, B., González, F., et al. Nano Lett 11 (2011) 3531.
[10] Sanz J.M., Ortiz D., Alcaraz de la Osa R. et al. J. Phys. Chem. C 117 (2013) 19606

Figures

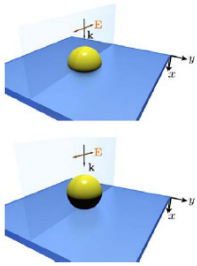

Figure 1: a) The two scattering configurations analyzed: hemispherical (top) and spherical (bottom) nanoparticles on a sapphire substrate. Calculations were done for normal incidence and s-polarization (i.e. z-direction).

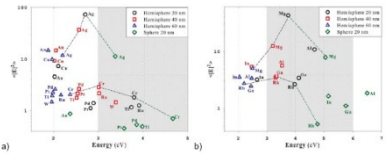

Figure 2: Spectral evolution of the surface-averaged intensity peak, $<|E|^2>$, for hemispherical (R= 20 nm, 40 nm and 60 nm) and spherical (R= 20 nm) for metal nanoparticles on sapphire (a) without and (b) with good UV coverage and performance..

Encoded Nanospheres as Biomarkers for the Early Detection of Cystic Fibrosis.

Iván Castelló Serrano, **Georgiana Stoica,** Alba Matas Adams, Emilio Palomares

Institute of Chemical Research of Catalonia (ICIQ), Avinguda del Països Catalans 16, 43007 Tarragona, Spain

gstoica@iciq.es

Cystic fibrosis (CF) is an autosomal recessive genetic disorder characterized by abnormal transport of chloride and sodium across an epithelium, leading to thick secretions, affecting lung, pancreas, liver and intestine. Current methods for the diagnosis of CF require long time analysis and further experimentation to provide accuracy. Such methods do not allow the determining the genotype of the patient.

We have developed a new sensitive biomarker in such a way that the optical response of the system upon light irradiation, when treated with faeces samples, can be directly correlated to trypsin concentration in the sample, an indicator of the genotype of the patient.1 Our biomarker consists of two silica nanospheres arranged concentrically, one embedding a core of CdSe nanocrystals (CdSe660) with luminescence emission maximum at λ=660 nm, and the other one embedding the second type of CdSe nanocrystal with luminescence emission maximum at λ=540 nm (CdSe540). The outer silica surface is conjugated to a trypsin-specifically sensitive peptide which is labelled with a dye capable of absorbing the light emitted at 540 nm and emits a fluorescence signal via a FRET (Förster Resonance Energy Transfer) process. Upon excitation at λ=405 nm, both types of CdSe quantum dots undergo fluorescence emission and the FRET process takes place. In the presence of trypsin, the proteolytic enzyme activity leads to the peptide cleavage and the FRET process is disrupted. Thus, by measuring the signal increase at λ=540 nm, that corresponds to the CdSe540 emission once the peptide is cleaved, it is possible to correlate the changes in the emission intensity with the enzyme activity and amount using the constant emission intensity of CdSe660 as internal reference. Using our nanospheres in real samples, four participants to the study were confirmed homozygotic, while the other seven were heterozygotic for cystic fibrosis.

References

[1]]. E. Palomares, G. Stoica, I. Castelló Serrano. Ratiometric assay for hydrolytic enzyme quantification (2013), EP13382239.

Figures

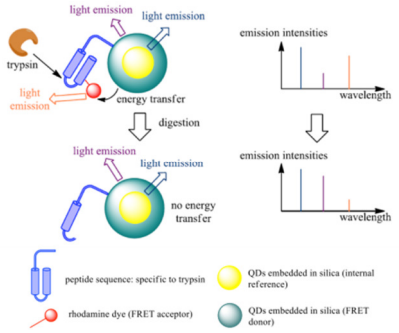

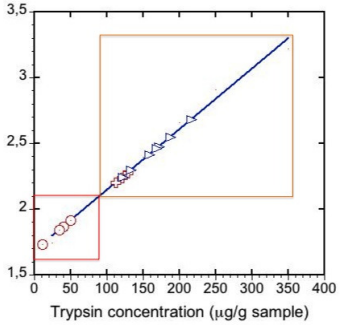

Electrically controllable strong light-matter interactions with graphene.

K.J. Tielrooij[1], L. Orona[2], M. Badioli[1], L. Gaudreau[1], S. Coop[1], Q. Ma[2], G. Navickaite[1], H. de Riedmatten[1], P. Goldner[3], F.J. Garcia de Abajo[1], A. Ferrier[3], P. Jarillo-Herrero[2], and F.H.L. Koppens[1]

[1] ICFO - Institut de Ciéncies Fotoníques, Mediterranean Technology Park, Castelldefels (Barcelona) 08860, Spain;
[2] Department of Physics, Massachusetts Institute of Technology, Cambridge, MA 02139, USA;
[3] Chimie ParisTech, Laboratoire de Chimie de la Matière Condensée de Paris, CNRS-UMR 7574, UPMC Univ Paris 06, 11 rue Pierre et Marie Curie 75005 Paris, France.

klaas-jan.tielrooij@icfo.es

The nanoscale interaction between light emitters and graphene can lead to a plethora of novel applications in fields such as sensing and telecommunications. Here we demonstrate a hybrid device containing graphene and near infrared light emitters that play a very important role in modern telecommunications: Er3+ ions with stimulated emission at ~1530 nm. By changing the Fermi energy of graphene, we demonstrate, for the first time, the unique capability of in-situ tuning of the optical density of states experienced by emitters in near proximity of graphene. In particular, we access three distinct regimes of emitter–graphene coupling: i) the non-radiative coupling regime, ii) the reduced coupling regime, and iii) the plasmon coupling regime. We witness the transition through these regimes by monitoring the lifetime of the emitters and their emission, which are strongly modified by the graphene.

In the first regime, non-radiative coupling leads to energy transfer from the emitter to the graphene sheet, where electron-hole pairs are generated with the same energy as the excited state dipole of the emitter. By increasing the Fermi level in graphene, we suppress almost completely this energy transfer process, and thus the emitter–graphene coupling strength. Therefore, in this second regime the emission and the excited state lifetime approach the same value as for uncoupled emitters. Finally, in the third regime, the very high electron density can give rise to collective excitations (plasmons).

Plasmonic nanoparticle strings: threading nanoparticle chains with light.

Christos Tserkezis[1], Lars O. Herrmann[2], Ventsislav K. Valev[2], Jonathan S. Barnard[3], Setu Kasera[4], Oren A. Scherman[4], Jeremy J. Baumberg[2], and Javier Aizpurua[1]

[1]Donostia International Physics Center and Centro de Física de Materiales CSIC-UPV/EHU, Spain
[2]Nanophotonics Centre, Cavendish Laboratory, University of Cambridge, Cambridge CB3 0HE, U.K.
[3]Department of Materials Science and Metallurgy, Charles Babbage Road, University of Cambridge, U.K.
[4]Melville Laboratory for Polymer Synthesis, Department of Chemistry, Lensfield Road, University of Cambridge, U.K.

christos_tserkezis001@ehu.es

Light-matter interactions in the nanoscale can be efficiently controlled by novel plasmonic materials, opening the path for important techological applications in sensing, optical communications and electronics [1-3]. Several techniques, such as nanolithography and self-assembly, have been developed to fabricate and tailor the optical response of such nanomaterials. A particularly attractive approach for nanofabrication, which has not been much explored yet, consists of using light itself for laser-welding metallic nanoparticles (NPs). Here we demonstrate an efficient way to exploit light for threading gold (Au) NP strings, i.e., chains of Au nanospheres conductively connected via Au threads (cylindrical bridges between NPs) with well-controlled dimensions [4]. These strings can be exploited as the main building blocks in the design of more complex nanostructures, such as active and chiral photonic metamaterials.

The successive steps of fabrication of Au NP strings are shown schematically in Fig. 1a. Au NP clusters are first self-assembled in aqueous solutions using appropriate rigid organic molecular linkers, namely cucurbiturils (CBs), which fix the interparticle gaps with exquisite precision at 0.9 nm [5]. As the self-ssembly procedure evolves in time, disordered and linear NP chains are formed within the clusters. These chains are traced by the emergence of collective plasmonic modes that involve several NPs (Capacitive Chain Plasmons, CCP), strongly redshifted in the spectrum with respect to the individual Au NP plasmonic modes. As the particle chains are formed, the CCP modes eventually dominate the extinction spectra (Fig. 2a). These modes are accompanied by strong near-field enhancement at the interparticle gaps [6,7], as shown in Fig. 2b for a linear chain of six 50-nm Au spheres in water, illuminated by a plane wave with amplitude E0 polarised along the chain axis (taken to be the z axis). The wavelength of these modes and the resulting near-field enhancement are very robust with respect to deviations from linearity of the chains [6,7], thus the presence of the CCP modes is maintained over kinks and turns, facilitating the use of such clusters in practical applications.

Once the CB-assisted self-assemblies have been prepared, the large intragap near-field enhancement can be exploited for threading. Illumination of the clusters with ultrafast lasers, whose wavelength coincides with that of the CCP mode, leads to non-thermal melting of Au at the gaps. In this way, Au threads connecting several particles are formed, to produce a Au NP string (Fig. 1b). The Au threads allow charge transfer within the entire NP strings, leading to the appearance of new modes at wavelengths even more to the infrared of the spectrum, that we name as Threaded Chain Plasmons (TCPs) (Figs. 1c and 2c). These modes are hybrid chain/rod modes, as can bee observed in Fig. 2d for the first two TCP modes. They exhibit a strong antenna-like character, with charge oscillations along the entire string, while large near-field enhancements at the gaps between individual NPs (around the formed Au threads) are

maintained. The nature of these modes becomes even clearer by examining the phase of the z component of the electric field (Fig. 2d) for the first two TCP modes, which has the characteristics of the first and second-order antenna mode, respectively, while phase changes (which imply the presence of surface charges) can be seen at the gaps.

The evolution and the optical properties of the TCP modes depend strongly on the length of the strings and the width of the threads. The latter can be adjusted by controlling the initial nanoparticle size, the laser power and its wavelength, thus providing unique control of the threading procedure. On the other hand, while the threads are not easily accessible by electron microscopy, the excitation of TCP modes acts as proof that threading has indeed taken place. The exact thread widths can then be identified with great precision by comparing experimental and simulated extinction spectra.

In summary, we showed that ultrafast lasers can be used to fabricate Au threads, which connect the individual Au NPs in self-assembled clusters, leading to a new plasmonic unit, namely the Au NP string. Such strings, whose optical response is characterised by hybrid rod/chain plasmonic modes in the infrared, can be controlled with great precision, and may be exploited as building blocks for novel plasmonic materials.

References

[1] J. A. Schuller et al., Nature Mater., 9 (2010) 193.
[2] J. N. Anker et al., Nature Mater., 7 (2008) 442.
[3] Z. Fang and X. Zhu, Adv. Mater., 25 (2013) 3840.
[4] L. O. Herrmann et al., submitted.
[5] R. W. Taylor et al., ACS Nano, 5 (2011) 3878.
[6] R. Esteban et al., Langmuir, 28 (2012) 8881.
[7] C. Tserkezis et al., Part. Part. Syst. Charact., 31 (2014) 152.

Figures

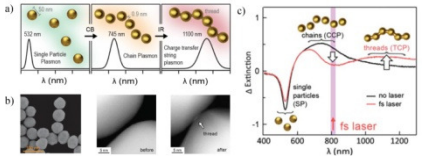

Figure 1: .a) Schematic representation of the self-assembly and nano-threading procedures. At first, Au NPs are assembled into chains by appropriate molecular linkers (CBs), leading to a near-infrared capacitive chain plasmon (CCP) mode. The chains are then illuminated by ultrafast lasers, non-thermal melting of Au takes place at the gaps and Au threads connecting the NPs are formed, resulting in the excitation of threaded chain plasmon (TCP) modes in the infrared that allow charge transfer along the string of particles. b) SEM image of a Au NP string (left) and TEM images of the gap between two NPs before (middle) and after (right) threading. c) Experimental differential extinction spectra before (black curve) and after (red curve) laser illumination.

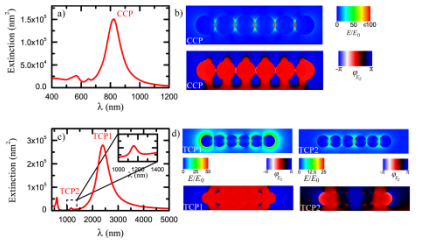

Figure 2: .a) Simulated extinction spectrum of a linear chain of six CB-linked 50-nm Au NPs in water, illuminated by a plane wave polarised along the chain's axis (z axis). b) Contour plots of the amplitude of the electric field, E, normalised to the incident field, E0, and the phase of the z component of the electric field (ϕEz) at the wavelength of the CCP resonance (λ = 820 nm). c) Extinction spectrum of a threaded chain of six 50-nm Au NPs (thread width 12 nm). d) Contour plots of E/E0 and ϕEz at the wavelengths of the two first TCP modes (TCP1: λ = 2200 nm, left contours, and TCP2: λ = 1160 nm, right contours)

Parallel Collective Resonances in Arrays of Gold Nanorods.

Alan Vitrey[1], Lionel Aigouy[2], Patricia Prieto[1], José Miguel García-Martín[1], María U. González[1]

[1]IMM-Instituto de Microelectrónica de Madrid (CNM-CSIC), Isaac Newton 8, 28760 Tres Cantos, Madrid, Spain
[2]Laboratoire de Physique et d'Etude des Matériaux (LPEM), UMR CNRS 8213, Ecole Supérieure de Physique et de Chimie Industrielles (E.S.P.C.I.), 10 Rue Vauquelin, 75231 Paris Cedex 05, France

alan.vitrey@imm.cnm.csic.es

Localized surface plasmon resonances (LSPRs) sustained by metallic nanostructures have been shown to be suitable for various applications such as sensors and SERS because of the sensitivity of their extinction peak to environment modifications and their capability of enhancing the near-field intensity. Several works have pointed out that these properties are improved when the LSPRs couple with diffraction orders in periodic arrays of nanostructures [1-3]. Indeed, this coupling can induce a sharp peak of extinction which is associated to an intense enhancement and delocalization of the near-field. Recent studies have successfully demonstrated the benefit of these resonances named lattice, geometric, or collective resonances to a large range of applications, from the above mentioned SERS and sensing to the enhancement and control of spontaneous and stimulated emission [4-7]. However, these resonances undergo a damping in presence of a difference of optical index between substrate and superstrate, which could lead to their disappearance at glass-air interfaces.

The canonical configuration of these collective resonances consists in coupling the LSPRs with the evanescent diffraction orders travelling orthogonally to the dipolar moment of the nanostructures [1-3].

Recently, we have focused our attention on what we call the parallel coupling configuration, which involves diffraction orders propagating in the direction parallel to the dipole axis. In this work [8], we have analyzed the far- and near-field properties of arrays of gold nanorods (shown schematically in Fig. 1) with different coupling conditions between the LSPRs and the collective resonances depending on their geometrical characteristics. To carry out this investigation, we have performed extinction measurements and Scanning Near-field Optical Microscopy (SNOM). Figure 1 shows the scheme of principle of the SNOM technique we have used. Extinction spectra and SNOM images are compared to FDTD calculations, and a good agreement between experimental and numerical results has been achieved (see Fig. 2a and b for the far- and near-field results respectively). We show that parallel collective resonances can be excited even for a system with a glass-air interface while no major orthogonal coupling is observed, which could indicate a difference of robustness to index heterogeneity between both kinds of lattice resonances. Moreover, it is also shown that parallel resonances give rise to a sharp extinction peak (Fig. 2a) and a delocalization of the near-field (Fig. 2b). The near-field distribution of the parallel resonances differs from that of the orthogonal configuration, since in the first case the field is delocalized vertically whereas in the case of the canonical coupling it occurs between the nanostructures.

References

[1] S. Zou, N. Janel, and G. C. Schatz, J. Chem Phys. 120 (2004) 10871.

[2] F. J. García de Abajo, Rev. Mod. Phys. 79 (2007) 1267.

[3] B. Auguié and W. L. Barnes, Phys. Rev. Lett. 101 (2008) 143902.

[4] P. Offermans, M. C. Schaafsma, S. R. K. Rodriguez, Y. Zhang, M. Crego-Calama, S. H. Brongersma, and J. Gómez Rivas, ACS Nano 5 (2011) 5151.

[5] L. K. Ausman, S. Li, and G. C. Schatz, J. Phys. Chem. C 116 (2012) 17318.

[6] G. Vecchi, V. Giannini, and J. Gómez Rivas, Phys. Rev. Lett. 102 (2009) 146807.

[7] W. Zhou, M. Dridi, J. Y. Suh, C. H. Kim, D. T. Co, M. R. Wasielewski, G. C. Schatz, and T. W. Odom, Nat Nanotechnol. 8 (2013) 506.

[8] A. Vitrey, L. Aigouy, P. Prieto, J.M. García-Martín, and M.U. González, Nano Lett. (2014) doi: 10.1021/nl500238h.

Figures

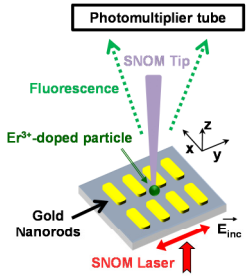

Figure 1: Schematic drawing showing the analyzed system of arrays of Au nanorods on glass and the SNOM configuration employed for the near-field measurements.

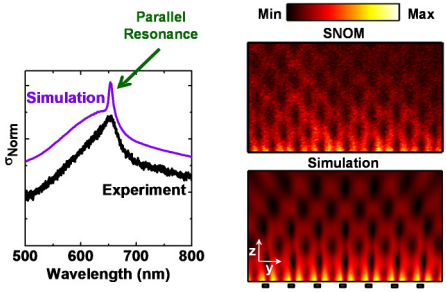

Figure 2: (a) Extinction cross-section spectrum of a Au nanorod array where the parallel diffraction order in air and the LSPR are strongly coupled, showing the presence of a parallel collective resonance. (b) Near-field distribution of this parallel collective resonance, obtained when only 16 periods within the array are illuminated.

Synthesis and biophotonic applications of porous alumina micro and nanoparticles.

E. Xifré-Pérez[1], S. Guaita[2], J. Ferré-Borrull[1], J. Pallarès[1], L. Masana[2] and L.F. Marsal[1]

[1]Departament d'Enginyeria Electrònica, Elèctrica i Automàtica, Universitat Rovira i Virgili, Avda. Països Catalans 26, 43007 Tarragona, Spain.
[2]Unitat de Recerca en Lípids i Arteriosclerosi - IISPV, Universitat Rovira i Virgili, C/ Sant Llorenç, 21, 43201 Reus, Spain.

elisabet.xifre@urv.cat, lluis.marsal@urv.cat

Porous alumina is a very interesting material widely used in the development of optical and electronic devices specially due to its optical characteristics of reflectivity, transmission and its inherent photoluminescence [1,2]. So far porous alumina has been used as a substrate for many different applications such as biosensors, optical devices and as a template for other porous materials [3,4] but its versatility makes of it a suitable material for developing applications where particles of nanometric dimensions are required.

Nanoparticle research is an outstanding field in continuous development that recently has attracted great interest [5,6]. This increasing interest on nanotechnology manifested the necessity for developing materials with stable optical and physical characteristics, a high surface area and ease development in the nanometric range [7]. Porous alumina meets all these requirements and reveals as a potential material in this research field.

In this work we present the synthesis of porous alumina micro and nanoparticles and the analysis of their optical, physical and chemical characteristics. Different microscopic techniques are used for the characterization of the porous alumina particles like optical microscopy (Fig. 1), scanning and transmission electron microscopy (Fig. 2) and confocal microscopy (Fig. 3) together with other analytical techniques like Fourier Transform Infrared Spectrometry, electron backscatter diffraction and X-Ray diffraction. Their optical response is also studied by analyzing their transmission, reflection and photoluminescence spectrum. Besides, biophotonic applications of the porous alumina micro and nanoparticles are proposed here as they are a very stable and biocompatible material allowing an easy modification of its surface with organic components [8]. The nanometric size of the particles allows their absorption by the cells [9] that in addition to the intrinsic photoluminescence of the material makes of porous alumina nanoparticles ideal candidates for developing low-cost label-free specific biomarkers. Also, the controllable porosity of the material makes it suitable for developing drug delivery localized systems [10].

Acknowledgements

This work was supported by the Spanish Ministry of Economy and Competitiveness (MINECO) under grant number TEC2012-34397, and by the Catalan Government under project 2009 SGR 549.

References

[1] K. Huang, L. Pu, Y. Shi, P. Han, R. Zhang, Y.D. Zheng, Appl. Phys. Lett., 89 (2006) 201118.
[2] A. Santos, V.S. Balderrama, M. Alba, P. Formentín, J. Ferré-Borrull, J. Pallarès, and L.F. Marsal, Adv. Mater. 24 (2012) 1050.
[3] G. Macias , L.P. Hernández-Eguía , J. Ferré-Borrull , J. Pallares , and L.F. Marsal, ACS Appl. Mater. Interfaces, 5 (2013) 8093.
[4] K. Choi , S.H. Park , Y.M. Song , Y.T. Lee , C.K. Hwangbo , H. Yang , and H.S. Lee, Adv. Mater. 22 (2010) 3713.
[5] J.M. Kinsella, J.M. Jimenez, R.E. Karmali, P.P. Rush, A.M. Kotamraju, V.R. Gianneschi, N.C. Ruoslahti, E. Stupack, M.J. Sailor, Angew. Chem. Int. Ed., 50 (2011) 12308.
[6] J.-H. Park, G. Von Maltzahn, L.L. Ong, A. Centrone, T.A. Hatton, E. Ruoslahti, S.N. Bhatia, M.J. Sailor, Adv. Mater., 22 (2010) 880.
[7] S. Zhang, C. Ji, Z. Bian, P. Yu, L. Zhang, D. Liu, E. Shi, Y. Shang, H. Peng, Q. Cheng, D. Wang, C. Huang, C. Cao, ACS Nano, 6 (2012) 7191.

[8] I. Mey, C. Steinema, A. Janshoff, J. Mat. Chem., 37 (2012) 19348.
[9] H. Li, Y. Li, J. Jiao, H-M. Hu, Nature Nanotech. 6 (2011) 645.
[10] J. Salonen, L. Laitinen, A.M. Kaukonen, J. Tuura, M. Björkqvist, T. Heikkilä, K. Vähä-Heikkilä, J. Hirvonen, V.-P. Lehto, J. Control. Release, 108 (2005) 362.

Figures

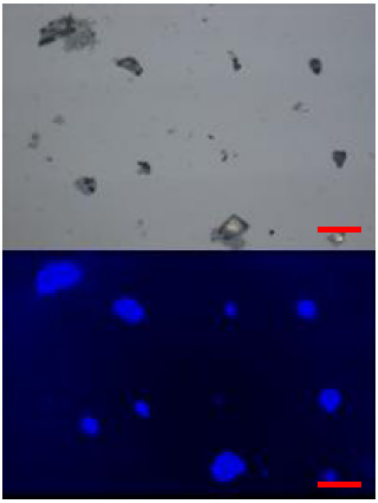

Figure 1: Optical microscope image of micrometric porous alumina particles a) white light b) photoluminescence. Scale bar: 10 um.

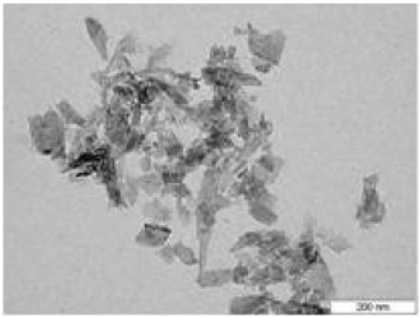

Figure 2: TEM image of nanometric porous alumina particles.

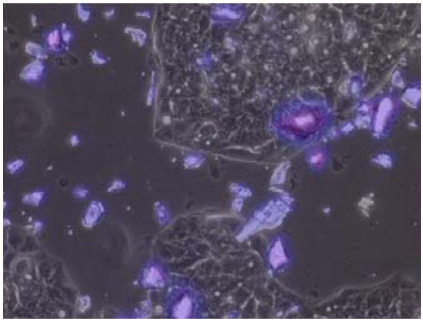

Figure 3: Confocal fluorescence microscopic images of HEPG2 cells incubated with micrometric porous alumina particles.

Few Photon Photonics in waveguides: Continuous frequency conversion in the single photon limit.

David Zueco[1]
E. Sanchez-Burillo[1], J. J. Garcia-Ripoll[2] and L. Martín-Moreno[1]

[1]Instituto de Ciencia de Materiales de Aragon and Departamento de Fisica de la Materia Condensada, CSIC-Universidad de Zaragoza, E-50009, Zaragoza, Spain
[2]Instituto de Física Fundamental, IFF-CSIC, Serrano 113-B, 28006 Madrid, Spain

dzueco@unizar.es

Light-matter interaction is one of the most fascinating topics in physics. Its enhancement using few-level-systems (FLS) in cavities has lead to the rich field of Cavity Quantum Electrodynamics. More recently, it has been realized that enhanced light-matter interaction can be realized in quasi-one-dimensional waveguides, such as dielectric waveguides, superconducting strips, photonic crystal waveguides, plasmonic waveguides, etc. Different types of waveguides may work at different frequency ranges and different physical conditions (like temperature), but they all profit from the confinement of the field and the reduced dimensionality in light propagation.

Several results are known in these one-dimensional quantum-electrodynamics (1DQED) systems, but the large majority of them have been obtained considering one incoming photon, and within the rotating-wave-approximation, valid for small couplings between the photon field and the FLS, which conserves the total number of excitations (be it a photon or an excitation of the FLS). Considering more than one photon (but few) interacting with several qubits new effects are expected due to the finiteness and the photon-photon interactions. However, the theoretical analysis is notoriously difficult and has only been performed for a few cases concerning two and three photons treated.

In this talk we will present our numerical approach, based on the Matrix Product States time evolution, for scattering processes involving few photons (1 -10) through several emitter arrays. Finally, we will present a a novel effect. Whenever the coupling between the emitter and the waveguide is sufficiently strong, a continuous frequency conversion is possible at the single photon level

Edited by

Phantoms Foundation

Alfonso Gómez 17
28037 Madrid – Spain

info@phantomsnet.net
www.phantomsnet.net

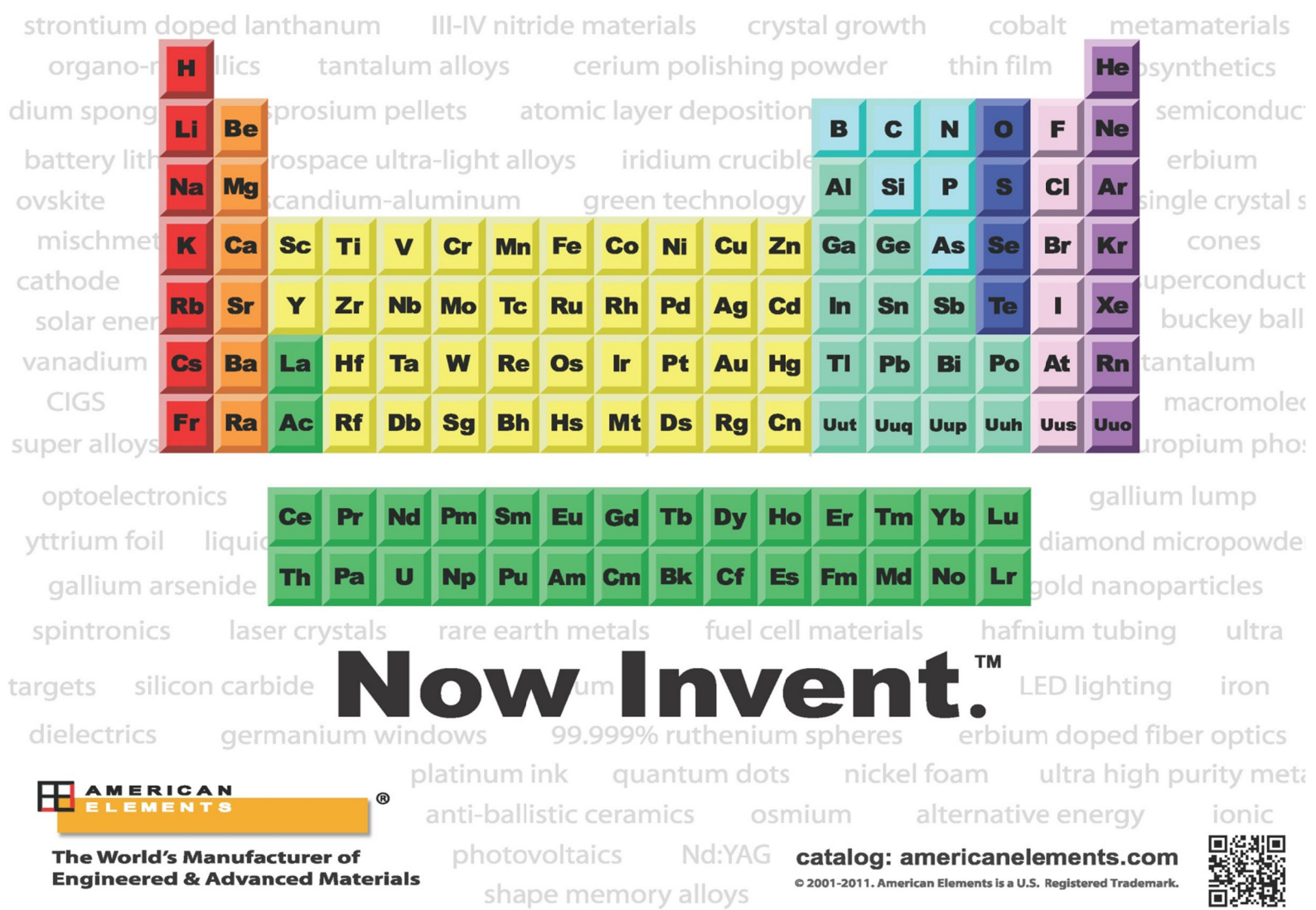

Now Invent.™

AMERICAN ELEMENTS®

The World's Manufacturer of Engineered & Advanced Materials

catalog: americanelements.com

© 2001-2011. American Elements is a U.S. Registered Trademark.